Thesis for the Degree of Doctor of Philosophy

Stable Walking Control of Biped Robot

By
Nguyen Thanh Phuong

Department of Interdisciplinary Program of Mechatronics Engineering
The Graduate School

Pukyong National University

February 2008

Stable Walking Control of Biped Robot

2 족로봇의 안정보행제어

Supervised by
Professor Sang Bong Kim

by
Nguyen Thanh Phuong

A thesis submitted in partial fulfillment of the requirements
for the degree of

Doctor of Philosophy

in Department of Interdisciplinary Program of Mechatronics Engineering, The Graduate School,
Pukyong National University

February 2008

Stable Walking Control of Biped Robot

A dissertation
by
Nguyen Thanh Phuong

Approved as to styles and contents by:

_____

(Chairman) **Yeon Wook Choe**

_____ _____

(Member) **Young Seok Jung** (Member) **Sang Bong Kim**

_____ _____

(Member) **Sea June Oh** (Member) **Young Bok Kim**

February 19, 2008

Acknowledgements

Firstly, I am greatly thankful to my supervisory, Professor Sang Bong Kim, not only for offering his deep and clear guidance in academics, research, and skills but also for enlightening me with the true philosophy of life. He has been more than an advisor to me. His insight, knowledge and advice encouraged and helped me to accomplish my research and finish this thesis.

I would like to thank the members of my thesis committee: Prof. Yeon Wook Choe, Prof. Young Seok Jung, Prof. Sea June Oh and Prof. Young Bok Kim for their considerable helpful comments and suggestions.

I would like to thank Prof. Hak Kyeong Kim for his great helps to complete this thesis.

I would like to thank Prof. Myung Suk Lee in Department of Microbiology for her helps and encouragements.

I am grateful to Dr. Tan Tien Nguyen from Ho Chi Minh City University of Technology for his essential assistances.

I would like to acknowledge and thank all members of CIMEC laboratory, Dr. Tan Tung Phan, Dr. Thien Phuc Tran, Dr. Tan Lam Chung, Dr. Manh Dung Ngo, Dr. Hoang Duy Vo, Mr. Hung Nguyen, Mr. Seong Jin Ma, Mr. Sang Chan Kim, Mr. Ba Da Park, Miss. Hee Suk Lee, Mr. Byoung Yong Kim, Mr. Suk Min Yoon, Mr. Do Kyoung Lee, Mr. Nak Soon Choi, Mr. Dae Won Kim, Mr. Joon Ho Jeong, Mr. Jeong Woo Park, Mr. Kyeong Mok Lee, Chul Han Park, Miss. Yu Mi Park and Miss. Ha Yeon Choi for all scientific discussions and helps.

Thanks are due to all members of Vietnamese Student's Association in Korea, especially Mr. Van Tung Tran, Miss. Ngoc Han Pham, Mr. Xuan Vinh

Nguyen, Mr. Manh Vu Tran and Mr. Van Phuoc Nhan Le for their vigorous support.

I would like to thank Mr. Cao Cuong Ngo, my closest friend, for his exertion to help me in the time I was in Korea.

Finally, there are various thanks to my father, my mother, my father in law, my mother in law, my sisters, my brothers and especially my wife, Mrs. Le Thi Minh Tam, for their love, encouragement and sympathy for me not only in this thesis time but also in the whole of my life.

Nguyen Thanh Phuong

Contents

Stable Walking Control of Biped Robot

Nguyen Thanh Phuong

Department of Interdisciplinary Program of Mechatronics Engineering,
Graduate School, Pukyong National University

Abstract

This thesis presents a stable walking control of 10 degree of freedom biped robot. To control the walking of this 10 DOF biped robot stably, the followings are performed.

Firstly, kinematics model in 3D space of this biped robot is proposed. Under the assumption that the mass of trunk of the biped robot is much larger than the mass of its joints, center of mass (COM) of the biped robot is concentrated at the center of pelvis link. In this case, the biped robot is modeled as 3D inverted pendulum whose base is the foot of the biped robot and its head is the COM of the biped robot.

Secondly, based on the 3D inverted pendulum, dynamics model of the biped robot is proposed. Under the assumption that the COM of the biped robot moves on the horizontal constraint plane, the dynamics equation of the biped robot is separated into two linear equations along x and y axes. These equations are independent each other. Based on the D'Alembert's principle, zero moment point (ZMP) equations of the biped robot with respect to its COM's position and acceleration are expressed. These equations are used to generate stable walking

pattern of the biped robot.

Thirdly, in order to realize the stable walking of the biped robot, the ZMP of the biped robot should exist inside the supported region. A ZMP tracking control system is constructed to track the ZMP of the biped robot to ZMP trajectory reference input which is decided by the footprint of the biped robot. For constructing the ZMP tracking control system, the ZMP equations are rewritten in continuous time strictly proper form. Their input is time derivative of acceleration of the COM, their output is coordinate of the ZMP and their state vector consists of the COM's position, velocity and acceleration. These are called ZMP systems. A continuous time optimal tracking controller and a discrete time optimal tracking controller are designed to control the ZMP of the biped robot to track the ZMP trajectory reference input. From the advantages of the designed discrete time optimal tracking controller in the practical system compared with the designed continuous time optimal tracking controller, this controller is chosen to control the ZMP tracking control systems. The ZMP of the biped robot depends on its COM's coordinate. The COM's coordinate and the ZMP of the biped robot are chosen as state variable and output, respectively. When the ZMP of the biped robot is controlled to track the ZMP trajectory reference input, a trajectory of the COM is generated as stable walking pattern of the biped robot. Furthermore, since the ZMP trajectory reference input is chosen inside stable region of the biped robot, walking of the biped robot is stable. The effectiveness of the designed optimal tracking controllers are proven by simulation results.

Fourthly, based on the stable walking pattern of the biped robot, a walking control method of the biped robot is proposed. From the trajectory of the COM of the biped robot and trajectory reference input of the swinging leg, inverse kinematics solved by solid geometry method is used to compute the angles of joints of the biped robot which are used as references of joint's angles of the biped

robot. Because the references of the joint's angles of the biped robot are computed from the stable walking pattern of the biped robot, the walking of the biped robot is stable if the joint's angles of the biped robot are controlled to track those references. The simulation results show that the walking of the biped robot controlled by proposed walking control method is stable.

Fifthly, because each rotating joint of the biped robot is driven by one DC motor, the motion of the biped robot depends on the motion of DC motors at joints. An optimal tracking control of each DC motor is constructed to track angle of rotor of the DC motor to its angle reference. To realize the discrete time optimal tracking controller, the information of all state variables of the DC motor is needed. However, all state variables are not accessible in practical systems. Furthermore, in the case of the system that all state variables are accessible, the hardware configuration of this system becomes complex and the cost to implement this system is very high because sensors to measure the information of all state variables are needed. To solve this problem, a discrete time full-order state observer is designed to estimate the states of the DC motor. The feedback gain matrix of the designed observer is obtained by pole assignment method using Ackermann formulation with observability matrix. A controller designed based on the information of the state variables obtained from the designed discrete time full-order state observer is also presented. The simulation results of the designed controller based on the discrete time full-order state observer are compared with those of the previous discrete time PID controller using forward-rectangular integration to show the effectiveness of the designed controller.

Finally, the stable walking control method of the biped robot is implemented by simple hardware using PIC18F4431 and dsPIC30F6014. The dsPIC30F6014 is used as master unit and PIC18F4431 is used as slave unit. The master unit and slave units communicate each other via I2C communication. The master unit

receives data of trajectory of COM generated by personal computer and data of circular trajectory of swinging foot once from personal computer via RS-232 communication. These data are stored in EEPROM of the master unit. Based on the data stored in EPPROM, the master unit is used to solve the inverse kinematics problem to obtain angles of joints of the biped robot at the k^{th} sample time. These angles are sent to the slaves as reference angle. The slaves control angles of the DC motors to track the reference angles. The experimental results on the CIMEC-1 biped robot developed for this thesis are shown to prove the effectiveness of the proposed walking control method.

Keywords: Discrete Time Optimal Control, Discrete Time Observer, ZMP Tracking Control System, Biped Robot, Walking Control.

List of Figures

Chapter 1: Introduction

Chapter 2: Mathematic model of the biped robot

Chapter 3: Walking pattern generation

Chapter 4: Walking control of biped robot

Chapter 5: Optimal tracking control for motion of the biped robot and experiment results

List of Tables

Chapter 3: Walking pattern generation

Chapter 4: Walking control of biped robot

Chapter 5: Optimal tracking control for motion of the biped robot and experiment results

Nomenclatures

Variables	Descriptions	Units
m_b	mass of the ankle joint of the right leg	[kg]
m_1	mass of the knee joint of the right leg	[kg]
m_2	mass of the hip joint of the right leg	[kg]
m_c	mass of center of pelvis link	[kg]
m_3	mass of the hip joint of the left leg	[kg]
m_4	mass of the knee joint of the left leg	[kg]
m_e	mass of the ankle joint of the left leg	[kg]
m	total mass of the biped robot	[kg]
l_1	length of lower link of the right leg	[m]
l_2	length of upper link of the right leg	[m]
l_3	length of pelvis link	[m]
l_4	length of upper link of the left leg	[m]
l_5	length of lower link of the left leg	[m]
r	length of inverted pendulum	[m]
z_{cd}	height of center of mass	[m]
b	length of foot	[m]
a	width of foot	[m]
θ_1	ankle joint angle of right leg in frontal plane	[deg]
θ_2	ankle joint angle of right leg in sagittal plane	[deg]
θ_3	knee joint angle of right leg in frontal plane	[deg]
θ_4	hip joint angle of right leg in sagittal plane	[deg]
θ_5	hip joint angle of right leg in frontal plane	[deg]
θ_6	Hip joint angle of left leg in sagittal plane	[deg]
θ_7	hip joint angle of left leg in frontal plane	[deg]
θ_8	knee joint angle of left leg in frontal plane	[deg]
θ_9	ankle joint angle of left leg in sagittal plane	[deg]

θ_{l0}	ankle joint angle of right leg in frontal plane	[deg]
θ_r	angle between inverted pendulum and $0x_az_a$ plane	[deg]
θ_P	angle between inverted pendulum and $0y_az_a$ plane	[deg]
Σ_w	world coordinate system	
Σ_a	coordinate system with the origin taken on ankle joint of right leg	
Σ_h	coordinate system with the origin taken on the center of pelvis link	
Σ_f	coordinate system with the origin taken on ankle joint of left leg	
(x_b, y_b, z_b)	coordinate of the ankle joint of the right leg	
(x_1,y_1,z_1)	coordinate of the knee joint of the right leg	
(x_2,y_2,z_2)	coordinate of the hip joint of the right leg	
(x_c,y_c,z_c)	coordinate of the center of pelvis link	
(x_3,y_3,z_3)	coordinate of the knee joint of the left leg	
(x_4,y_4,z_4)	coordinate of the hip joint of the left leg	
(x_e, y_e, z_e)	coordinate of the ankle joint of the left leg	
$(x_{com}, y_{com}, z_{com})$	coordinate of the center of mass	
(x_{zmp}, y_{zmp})	coordinate of the zero moment point	
(x_{ca}, y_{ca}, z_{ca})	coordinate of the center of mass of biped robot in Σ_a	
(x_{eh}, y_{eh}, z_{eh})	coordinate of the ankle joint of swinging leg of biped robot in Σ_h	
$\boldsymbol{J}, \boldsymbol{J_c}$	Cost function	
$\boldsymbol{v_{cp}}$	normal vector of constraint plane	
τ_r	torque associated with θ_r	[Nm]
τ_P	torque associated with θ_P	[Nm]
f	force associated with r	[N]
g	the gravity acceleration	$[m/s^2]$
u_x, u_y	input of ZMP system	$[m/s^3]$
T	sampling time	[sec]
$\boldsymbol{M}$	controllability matrix of continuous time ZMP system	
$\boldsymbol{M_d}$	controllability matrix of discrete time ZMP system	

$\boldsymbol{O_d}$	observability matrix of discrete time ZMP system	
$\boldsymbol{A}$, $\boldsymbol{B}$, $\boldsymbol{C}$	coefficient matrix of continuous time ZMP system	
$\boldsymbol{A_d}$, $\boldsymbol{B_d}$, $\boldsymbol{C_d}$	coefficient matrix of discrete time system	
$\boldsymbol{\Phi}$, $\boldsymbol{\theta}$, $\boldsymbol{C}$	coefficient matrix of discrete time ZMP system	
$\boldsymbol{x_x}$	state vector of ZMP system along x axis	
$\boldsymbol{x_y}$	state vector of ZMP system along y axis	
$\boldsymbol{r}$	reference input vector	
$\boldsymbol{e}$	error between reference input and output	
$\boldsymbol{\Delta x}$	incremental of state vector	
$\boldsymbol{\Delta r}$	incremental of reference input vector	
$\boldsymbol{\Delta u}$	incremental of control law	
J	cost function	
$\boldsymbol{Q}$, $\boldsymbol{Q_c}$	semi-positive definite matrix	
$\boldsymbol{R}$, $\boldsymbol{R_c}$	positive definite matrix	
$\boldsymbol{P}$, $\boldsymbol{P_c}$	positive definite matrix	
$\boldsymbol{P_1}$	positive definite matrix	
$\boldsymbol{K_1}$	feedback matrix gain	
$\boldsymbol{K_2}$	feed forward matrix gain	
$\boldsymbol{u}$, $\boldsymbol{u_c}$	control law	
K_e	back EMF constant of DC motor	[Vs/rad]
K_t	torque constant of DC motor	[Nm/A]
R	armature resistance of DC motor	[Ω]
J_m	moment of inertia of DC motor	[kgm^2]
L	inductance of DC motor	[H]
θ	rotation angle of the rotor of motor	[rad]
b	friction coefficient of the DC motor	[Nms]
V	source voltage	[V]
K	electromotive force constant	[Nm/A]
$\boldsymbol{L}$	feedback gain matrix	
$\boldsymbol{O_m}$	observability matrix of discrete time of DC motor	

$\hat{\boldsymbol{x}}_m$	state vector of observer
$\boldsymbol{x}_m$	state vector of DC motor
$\tilde{\boldsymbol{x}}_m$	estimated error state vector
$\boldsymbol{\Phi}_m$, $\boldsymbol{\theta}_m$, $\boldsymbol{C}_m$	coefficient matrix of discrete time of DC motor
k_i, k_p, k_d	proportional, derivative and integral gain of PID controller

Chapter 1: Introduction

This chapter begins with a quick look at animals that stand or walk on two-legged. Next, human locomotion is also discussed. The background and motivation of the biped robot is also introduced. The final section of this chapter deals with outline of this thesis and summary of contributions.

1.1 Legged Locomotion:

The control of locomotion in legged robots requires consideration of two problems:

- ✓Stability control to ensure maintenance of a vertical posture.
- ✓Motion control to allow forward motion at various speeds.

Animals with six or more legs have guaranteed static stability, for example, the ability to stand in stable posture. The stability of four-legged animals depends on the location of their center of gravity as soon as they lift one leg off the ground. Clearly, static stability is even more difficult to ensure in a two-legged creature.

Human beings are not the only creatures capable of locomotion on two legs. Marsupials such as Kangaroo, Opossum, etc hop on two legs, but they use their tails for static stability. Dinosaurs also used their tails to keep their balance during bipedal locomotion. Birds have only two legs, and they move on the ground either by hopping or by walking. The bird's stability is maintained by the forward-backward

distribution of its body weight because there is some compensation for the forward position of the head by the position of the tail. Furthermore, birds have active control systems that enable them to maintain static stability even when they perch on relatively small support surfaces such as tree branches. It is very evident that a bird moves its head and tail forward-backward when the bird walks. Many quadrupeds are capable of moving for short distances on their hind legs, but this is not their normal mode of locomotion. Even insects such as cockroaches are capable of running on two legs for short distances. Nevertheless, the creatures apparently evolved for primary locomotion on two legs are some of the great apes and human beings.

In view of the previous comments on static stability, the followings should be evident.

- ✓Human beings must place their center of mass between their feet to ensure lateral stability
- ✓Some form of active control is required to maintain forward-backward stability.

It is also evident that the design and construction of two-legged robots are more difficult than design and construction of robots with four or more legs. The static stability problem for the biped robots is usually solved with one of the following two ways. In toy walking machines, it is common to have very large feet to ensure static stability. In other biped robots, active control is used; that is, sensors are employed to measure the deviation of the robot's posture compared with the vertical axis. Based on information obtained from sensors, controller sends

appropriate compensating signals to actuators. During locomotion, the support forces of the legs, momentum, and inertial forces are considered to produce dynamic stability of the biped robot.

1.2 The Nature of Human Walking:

Human walking is a surprisingly complex process, and requires the coordinated activity of a lot of muscles in the lower limbs and in the trunk. Stable locomotion of human requires a periodic motion of the legs, which produce a series of strides resulting in a normal free gait velocity of approximately 80 m/min for adults on a smooth level surface. Normal people can increase and decrease their normal walking speed by about 50% of the normal velocity. Increase of velocity of more than 50% of the normal velocity is either uncomfortable or lead to running, whereas decrease of velocity by 50% of normal walking velocity disrupts the walking rhythm [20]. During locomotion, each leg can be in one of two states: *stance* and *swinging*. During stance, the foot is in contact with the ground and the center of mass (COM) of body moves forward over the contacted foot on the ground, while the opposite leg swings forward as illustrated in Fig. 1.1. Stance begins when the heel touches the ground at the end of swinging, and stance ends when the toes leave the ground. Stance consists of two phases: *single-limb stance* when one foot is on the ground and *double-limb stance* when both feet are on the ground. Double-limb stance occurs both at the beginning of a gait cycle and at middle gait cycle, when the foot that has been in swinging state contacts the floor.

It is evident from Fig. 1.1 that normal walking involves coordinated motion at the hip, knee and ankle. None of these joints are simple pin or hinge joints. Furthermore, muscles attach at difference points along the rigid skeletal supporting structure and

often perform more than one function. Some muscles cross more than one joint. This complex architecture makes mathematical modeling and analysis extremely difficult.

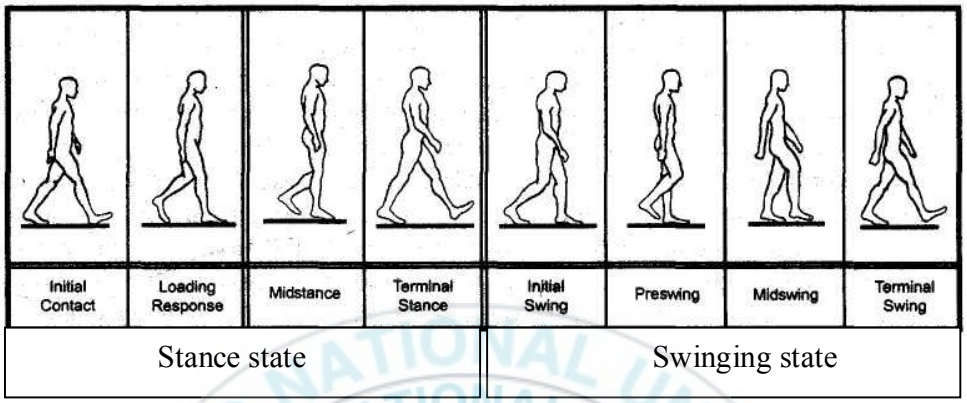

Fig. 1.1: Stages of human walking.

Energy consumption in normal walking increases linearly with velocity. Moreover, a large fraction of the energy expended during walking is required for the vertical motion of the COM of body, and a relatively smaller fraction of the energy is required for forward propulsion at normal walking velocity [20]. Thus, on the flat road, human beings can walk longer distance than on the slope road. Upon the beginning of swinging leg, the foot rotates about an approximately horizontal axis through the ankle. Thus, this effectively shortens the leg and allows forward swinging without bending of the trunk or dragging of the foot on the ground. In addition, the pelvis can have both lateral and anterior tilt. The combination of these two motions allows smooth forward progression with minimal vertical displacement of the body center of gravity.

The rotation of the foot about the ankle joint is a major contributor to stable walking. Upward and downward movements of the foot about this axis are known as *plantar-flexion* when the toes move downward with respect to the ankle and *dorsiflexion* when they move upward. Dorsiflexion allows the toes to land off the ground during swinging, whereas plantar-flexion produces forward motion. These two motions effectively shorten and lengthen the leg during walking. Thus, this produces the upward and downward movement of the body's COM. The importance of this mechanism becomes clear when we observe the handicapped. Their toes of swinging leg cannot land off the ground because the neurons fail in controlling these motions. The motions of the handicapped can frequently be overcome through electrical stimulation of the dorsiflexor muscles in the lower leg at the beginning of swinging.

1.3 The Biped Robot Stability Problem:

The stability problems in biped robot during standing, walking and running are different, respectively. As indicated previously, during stable stance, the projection of the COM of the body lies between the feet. Thus, this provides lateral balance. However, in the forward-backward plane, the body is statically unstable, and human beings sway their body back and forth. In order that a robot keeps its static stability to stand in a stable posture, at least three legs are needed. Stance in a stable posture of robot can be obtained with two legs only when the feet of robot are very large in comparison to those of human beings. Walking and running are statically unstable. To prevent the body from falling forward while the robot is moving, the robot must satisfy the condition for *dynamic stability* that sum of inertial, frictional, and gravitational forces is equal to zero. To maintain a stable vertical posture, many robots have been provided with sensors to measure joint angles in the legs and reaction forces at the feet.

Appropriate feedback controllers can then be used to return the robot to a vertical posture if the robot starts to lean in one direction or another. Clearly, this is an attempt to imitate the posture control system in human beings.

Dynamic stability during walking or running requires the actual measurement of the trunk angular acceleration, velocity and position with respect to the ground. For human beings, these measurements are obtained using the semicircular canals and the otolith organ in the head. To obtain such information in biped robots, it is necessary to equip biped robots with gyroscopes to obtain the angular velocities in each axis, or in some cases, biped robots is equipped with a complete platforms that provide accelerometers as well as gyroscopes in all three rotational axes. The latter are expensive but have been used in recent biped robots such as the Honda P-3 robot [17] and the MIT M-2 [22].

1.4 Control of Leg Movements During Walking:

According to anthropomorphism, legs are complex nonlinear systems with many degrees of freedom. To produce an appropriate sequence of joint angles to allow walking, several approaches have been taken:

- *Simple oscillator control*: If the legs are sufficiently simple and have few degrees of freedom, their movements can be controlled by treating them as oscillators to produce a stable periodic walking sequence.
- *Direct kinematics*: If the legs of biped robots are sufficiently similar to human legs, it is possible to measure and record the information of the hip, knee, and ankle joint movements in human walkers under various circumstances using a lot of sensors. The recorded data of movements in human walkers is used to control the

corresponding joints in the robot. This approach was taken in the design of the early Honda P-2 and P-3 robots.

- *Inverse kinematics*: The inverse kinematics is used to compute the angle of joints based on the desired sequence of footprints and the motion of the body.

1.5 Overview of Biped Robot and Humanoid Robot:

1.5.1 Early biped robots:

Early biped robots relied on large feet and very slow walking for static balance. One of the first dynamic walking bipeds was built by Miura and Shimoyama in1984. They considered the body of biped robot as an inverted pendulum during the single-limb supported phase. Another very interesting early implementation was done by McGeer in 1990 who introduced the idea *of passive dynamic walking:* A totally passive-legged structure developed by McGeer was able to walk stably downward on inclined plane.

The late Ichiro Kato was a pioneer in mobile robotics. He demonstrated a biped robot known as WL-104R during the Tokyo World's Fair in 1984, where it walked several kilometers [2, 26]. It weighed 40 kg and had 10 degrees of freedom which are driven by hydraulic power. The WL-104R robot relied on large feet for static stability. The WL-104R robot's stance phase was quite long, but during walking, the robot tipped forward when the foot swung forward. Then, when the swinging foot is contacted on the ground, the robot kept equilibrium by quickly transferring the weight to the swinging foot. This robot's gait is *quasi-dynamic* because the robot kept its stability passively after each step without any active control mechanisms. The WL-104R robot was modeled as an inverted pendulum.

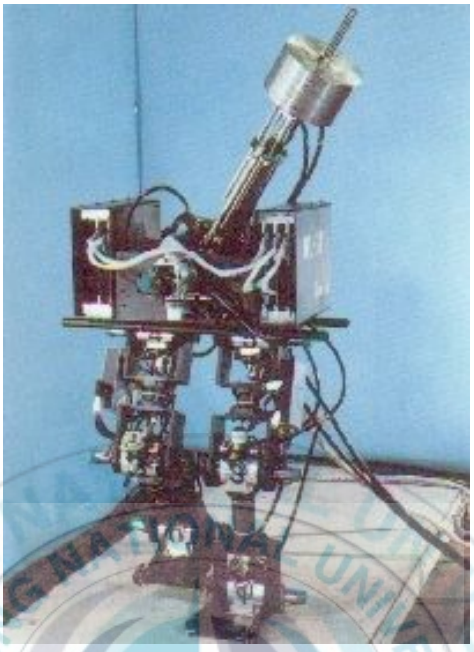

Fig. 1.2: WL-104R.

1.5.2 Walking legs:

Several biped robots constructed during the 1980s and 1990s were basically with two legs and only a single link for the torso and no head or arms. The emphasis in these projects was the study of gait control. These robots were constructed in the laboratories of Hemami [32], Zheng [23], and Gruver [6]. The SD-2 biped robot developed by Y. F. Zheng, et al. is shown in Fig. 1.3. This robot consists mainly of two legs with joints at the hips and ankles. The robot has no knees, but the hip and ankle joints have two degrees of freedom. It allows motion in both the frontal and sagittal planes. The feet have a flat bottom equipped with force sensors, enabling the system to be

compensated for an unbalanced position and retain static stability. The torso is rigid. This 8-dof robot was able to adjust its own parameters, so it could walk on inclined surfaces.

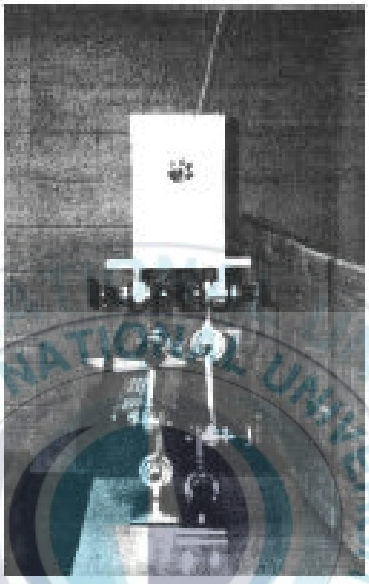

Fig. 1.3: SD-2 biped robot.

1.5.3 Elvis robot:

Elvis is the oldest of the humanoid robot. Elvis was developed in 1998. In 1999, Elvis was equipped with a new head, torso and legs. Elvis took its first autonomous steps in 2000. Elvis has 23 degrees of freedom: 6 in each leg, 4 in each arm, one in the torso and 2 in the neck. Three independent sensory systems provide visual information, pressure and acceleration information.

Fig. 1.4: Elvis robot.

1.5.4 Tron – X robot:

The giant blue skinned servo-pneumatic robot Tron-X robot was developed by the German company Festo to demonstrate their skill at air powered machines. Tron-X was constructed by 200 cylinders calibrated carefully. Tron-X can walk like human gait. Tron-X was displayed at the Fraunhofer Institute for Production Technology and Automation station during the CeBIT 2006 in Hanover, Germany. In its presentation, Tron-X demonstrated its ability not only to analyze human

gestures using 3-D camera sensors and then accurately reproduce the human gestures but also to effectively imitate people's standing.

Fig. 1.5: Tron-X robot.

1.5.5 HRP robot:

The HRP robot was initially developed as part of a five-year project launched by the Ministry of Economy, Trade and Industry (METI) in 1998. The project goal was to develop a first-generation robot that could work in human environments and use human tools.

Fig. 1.6: HRP robot.

At least three different proto-type HRP's had been created before the project was completed in 2003: the HRP-1S, HRP-2P and the HRP-2. The HRP-2 has a new 3D vision system, named as Versatile Volumetric Vision (VVV) which replaced the common single head mounted camera with four high precision color cameras. With VVV system, HRP-2 can have an expanded field of view with greater accuracy. Along with the VVV system enhancements, laser-based distance measuring equipment was installed into the robot's head. This allows HRP-2 to build a two-dimensional map of its environment for comparison with the VVV system's visual

input, so it can easily avoid obstacles. The narrow design of the legs allows one leg to be put in front of the other. The HRP could walk on a narrow plank or through very narrow spaces. It uses two 1GHz onboard computers for control, and has three visual sensors.

1.5.6 ASIMO robot:

ASIMO (Advanced Step in Innovative Mobility) robot is humanoid robot developed by Honda Company in 2000. In 2004, Honda introduced an updated version of ASIMO. Along with an improved body design and a longer lasting battery (1 hour), ASIMO could run nearly 3 kilometers per hour. ASIMO accomplished this by means of a new hip joint, which could sway its torso while ASIMO was moving. In addition, the 2004 ASIMO had one thumb and four fingers allowing it to grasp objects with. ASIMO not only can distinguish between people and obstacles but also can recognize voices, faces and hand gestures. ASIMO can also deliver coffee, relay messages, push carts, navigate stairs, get up on its own, communicate with people by voice, and run about 6 kilometers per hour.

Fig. 1.7: ASIMO robot.

1.5.7 HUBO robot:

The Korea Advanced Institute of Science and Technology (KAIST) researched and developed humanoid robot named as HUBO. The fist prototype KHR-1 without a head or arms was developed in 2003, and was followed by KHR-2 in 2004. HUBO with voice recognition and special abilities as well as with sophisticated vision was developed in January of 2005. Two eyes of the HUBO can move independently. At the 2005 Asia-Pacific Economic Cooperation (APEC) convention, a HUBO robot with Albert Einstein's head was displayed.

Fig. 1.8: HUBO robot.

1.6 Background and Motivation of Biped Robot:

Research on humanoid robots and biped locomotion is currently one of the most exciting topics in the field of robotics, and there exist many ongoing projects. Although some of those works have already demonstrated very reliable dynamic biped walking, it is still important to understand the theoretical background of the biped robot [43]. The biped robot performs its locomotion relatively to ground while it is keeping its balance and not falling down. Since there is no base link fixed on the ground or the base, the gait planning and control of the biped robot is very important but difficult. Up so far, numerious approaches have been proposed. The common methods are to locate zero moment point (ZMP) within stable region to protect the biped robot from falling down [7].

In the recent years, a great amount of scientific and engineering research has been devoted to the development of legged robots that are able to produce gait patterns similar to human beings. Towards this objective, many scientific papers have been published. Sunil, et al. proposed motion control of a novel planar biped with nearly linear dynamics [44]. They introduced a biped robot whose model is nearly linear. The motion control for following trajectory used nonlinear control method. J. H. Park proposed impedance control for biped robot locomotion [19]. Both legs of the biped robot are controlled by the impedance control. The desired impedance at the hip and the swinging foot is specified. Qiang, et al. introduced sensory reflex control for humanoid walking [39]. The walking controller of the robot consists of a feedforward dynamic pattern and a feedback sensory reflex. H. K. Lum, et al. presented gait planning and control of the biped robot [15]. The biped robot has no feet, and locomotion of the biped robot is constrained within the sagittal plane. A robust variable structure control law for the biped robot is also proposed. H. Hirukawa, et al. introduced HPR-2, a human-size humanoid robot that can walk, lie down and get up [16]. K. Mitobe, et al. studied a new control method for walking robots based on angular momentum [25]. An efficient algorithm for controlling the angular momentum of walking robots through the manipulation of the ZMP was presented.

This thesis presents a stable walking control of 10 degrees of freedom (DOF) biped robot and develops this biped robot with stable and human-like walking using simple hardware configuration. Kinematics model and dynamic models of the biped robot are presented. The dynamic model of the biped robot is realized by using the 3D inverted pendulum model. Based on the dynamic model of the biped robot, a zero

moment point (ZMP) tracking control system is constructed to generate 3D walking pattern of the biped robot which guarantees that the ZMP of the biped robot is located inside supported region. A continuous time optimal tracking controller and a discrete time optimal tracking controller are designed to control the ZMP tracking control system. From the advantages of the designed discrete time optimal tracking controller in the practical system compared with the designed continuous time optimal tracking controller, this controller is chosen to control the ZMP tracking control systems. By the ZMP tracking control system, a trajectory of center of mass (COM) of the biped robot can be obtained. A method to solve inverse kinematics of the biped robot based on the solid geometry is proposed. From the trajectory of COM and the trajectory of the ankle of swinging leg, the angle of each joint of the biped robot is obtained by solving inverse kinematics. The motion control of the biped robot problem is to track the angle of DC motors at joints of the biped robot.

1.7 Outline of the Thesis and Summary of Contributions:

This thesis consists of six chapters. The content and summary of contribution in each chapter is summarized as follows:

Chapter 1: Introduction

In this chapter, background and motivation of the biped robot is described. The outline of content and summary of contribution of this thesis is given.

Chapter 2: Mathematic Model of the Biped Robot

This chapter presents the kinematics and dynamic models of the biped robot. Based on the solid geometry, the kinematics equations are

presented. These equations are used to establish the dynamic model of the biped robot is approximated by a simple 3D inverted pendulum. This chapter provides fundamental knowledge that will be used in chapter 3.

Chapter 3: Walking Pattern Generation

In this chapter, the relationship between ZMP and stability of the biped robot is discussed. Based on the dynamic model of the biped robot, a walking pattern is generated by using the ZMP tracking control system. A continuous time optimal tracking controller and a discrete time optimal tracking controller are designed by using optimal control theory. From the advantages of the designed discrete time optimal tracking controller in the practical system compared with the designed continuous time optimal tracking controller, this controller is chosen to control the ZMP tracking control systems. Furthermore, simulation results are also presented to show the effectiveness of the designed controllers.

Chapter 4: Walking Control of the Biped Robot

In this chapter, a simple control method of the biped robot is proposed. Based on the trajectory of the COM which is generated by the ZMP tracking control system, the inverse kinematics using solid geometry is solved to obtain the angle of joints. The walking control of the biped is to track the angle of DC motors at joints of the biped robot. The

simulation results are presented to show the effectiveness of the proposed control method.

Chapter 5: Optimal Tracking Control for the Motion of the Biped Robot and Experiment results

This chapter presents a discrete time optimal tracking control of DC motor. A discrete time close loop observer is designed to estimate state variables. Based on the information of the state variables obtained by the discrete time close loop observer, the discrete time optimal tracking controller introduced in chapter 3 is applied to control the DC motor. A traditional discrete time PID controller using forward-rectangular integration is designed to compare with the discrete time optimal tracking controller. Furthermore, simulation results are presented to show the effectiveness of the designed controllers. Hardware developed to implement the designed controller is presented. Experimental results of the motion control of the biped robot are also presented to demonstrate performance of the developed biped robot.

Chapter 6: Conclusions and Future Work

Some conclusions are made and some ideas are presented for future work.

Chapter 2: Mathematic Model of Biped Robot

2.1 Kinematics model of biped robot:

A 10 DOF biped robot developed in this thesis is considered as shown in Fig. 2.1. It is assumed that the biped robot is supported by right leg and swung by left leg.

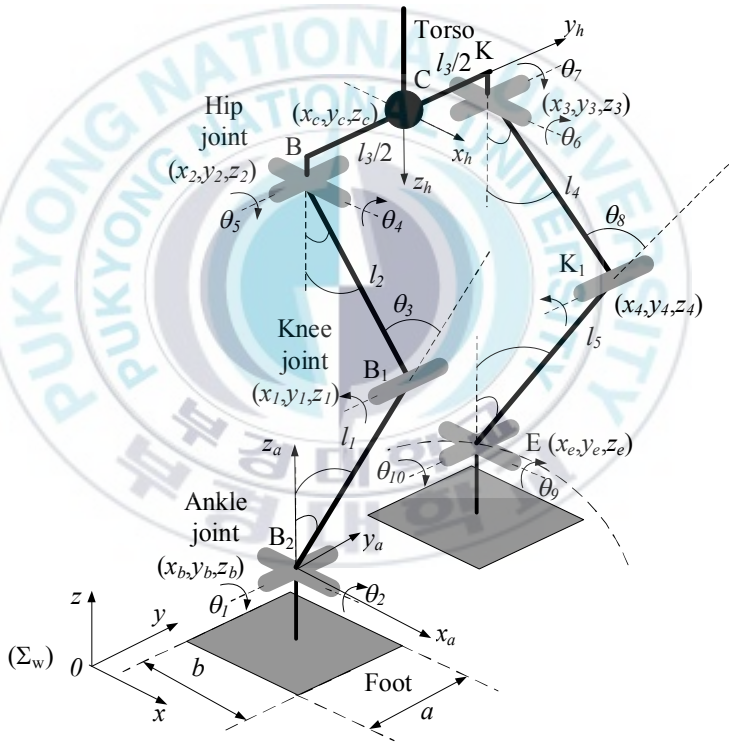

Fig. 2.1: Configuration of 10 DOF biped robot model.

In Fig. 2.1, l_1 and l_5 are length of the lower links of the right leg and the left leg, l_2 and l_4 are length of the upper links of the right leg and the left leg, l_3 is length of the pelvis link, (x_b, y_b, z_b) and (x_e, y_e, z_e) are coordinates of the ankle joints B_2 and E, (x_1, y_1, z_1) and (x_4, y_4, z_4) are coordinates of the knee joints B_1 and K_1, (x_2, y_2, z_2) and (x_3, y_3, z_3) are coordinates of the hip joints B and K, and (x_c, y_c, z_c) is coordinate of the center of the pelvis link C.

The biped robot consists of five links that are one torso, two links in each leg with upper link and lower link, and two feet. The two legs of the biped robot are connected with the torso via two DOF rotating hip joints. The hip joints can rotate the legs in the angles θ_5 for the left leg and θ_7 for the right leg on sagittal plane, and in the angles θ_4 for the left leg and θ_6 for the right leg on frontal plane. The upper links are connected with the lower links via one DOF rotating knee joints which can rotate only on the sagittal plane. The right knee joint can rotate the lower link and the upper link of the right leg in angle θ_3, and the left knee joint can rotate the lower link and the upper link of the left leg in angle θ_8. The lower links are connected with the feet via two DOF ankle joints. The ankle joints can rotate the feet in angle θ_1 for the left leg and θ_{10} for the right leg on the sigattal plane, and in angle θ_2 for the left leg and θ_9 for the right leg on the in frontal plane. All the rotating joints are considered to be friction free and each one is driven by one DC motor.

It is assumed that the soles of the biped robot do not slip. In the world coordinate system Σ_w which the origin is set on the ground, the positions of all joints and the center of the pelvis link can be expressed as follows:

❖ Coordinate of the knee joint of the right leg (x_1,y_1,z_1) is given as

$$x_1 = x_b + l_1 \sin\theta_1$$

$$y_1 = y_b + l_1 \sin\theta_2$$

$$z_1 = z_b + l_1 \cos\theta_1 \cos\theta_2$$

❖ Coordinate of the hip joint of the right leg (x_2,y_2,z_2) is obtained as

$$x_2 = x_1 - l_2 \sin(\theta_3 - \theta_1)$$

$$y_2 = y_1 + l_2 \cos(\theta_3 - \theta_1)\sin\theta_2$$

$$z_2 = z_1 + l_2 \cos(\theta_3 - \theta_1)\cos\theta_2$$

❖ Coordinate of the center of the pelvis link (x_c,y_c,z_c) is given as

$$x_c = x_2 = x_b + l_1 \sin\theta_1 - l_2 \sin(\theta_3 - \theta_1)$$

$$y_c = y_2 + \frac{l_3}{2}\cos(\theta_2 + \theta_4) = y_b + l_1 \sin\theta_2 + l_2 \cos(\theta_3 - \theta_1)\sin\theta_2 + \frac{l_3}{2}\cos(\theta_2 + \theta_4)$$

$$z_c = z_2 - \frac{l_3}{2}\sin(\theta_2 + \theta_4) = z_b + l_1 \cos\theta_1 \cos\theta_2 + l_2 \cos(\theta_3 - \theta_1)\cos\theta_2 - \frac{l_3}{2}\sin(\theta_2 + \theta_4)$$

❖ Coordinate of the hip joint of the left leg (x_3,y_3,z_3) is expressed as

$$x_3 = x_c$$

$$y_3 = y_c + \frac{l_3}{2}\cos(\theta_2 + \theta_4)$$

$$z_3 = z_c - \frac{l_3}{2}\sin(\theta_2 + \theta_4)$$

❖ Coordinate of the knee joint of the left leg (x_4,y_4,z_4) is given as

$$x_4 = x_3 + l_4 \sin\theta_7$$

$$y_4 = y_3 + l_4 \sin\theta_6$$

$$z_4 = z_3 - l_4 \cos\theta_6 \cos\theta_7$$

❖ Coordinate of the ankle joint of the left leg (x_e,y_e,z_e) is expressed as

$$x_e = x_4 - l_5 \sin(\theta_8 - \theta_7)$$

$$y_e = y_4 - l_5 \cos(\theta_8 - \theta_7)\sin\theta_6$$

$$z_e = z_4 - l_5 \cos(\theta_8 - \theta_7)\cos\theta_6$$

From the above equations, the positions of the center of the pelvis link and the ankle joint of the swinging leg can be rewritten as:

$$x_c = x_b + l_1 \sin\theta_1 - l_2 \sin(\theta_3 - \theta_1) \tag{2.1}$$

$$y_c = y_b + l_1 \sin\theta_2 + l_2 \cos(\theta_3 - \theta_1)\sin\theta_2 + \frac{l_3}{2}\cos(\theta_2 + \theta_4) \tag{2.2}$$

$$z_c = z_b + l_1 \cos\theta_1 \cos\theta_2 + l_2 \cos(\theta_3 - \theta_1)\cos\theta_2 - \frac{l_3}{2}\sin(\theta_2 + \theta_4) \tag{2.3}$$

$$x_e = x_b + l_1 \sin\theta_1 - l_2 \sin(\theta_3 - \theta_1) + l_4 \sin\theta_7 - l_5 \sin(\theta_8 - \theta_7) \tag{2.4}$$

$$\begin{aligned} y_e = {} & y_b + l_1 \sin\theta_2 + l_2 \cos(\theta_3 - \theta_1)\sin\theta_2 + l_3 \cos(\theta_2 + \theta_4) \\ & + l_4 \sin\theta_6 - l_5 \cos(\theta_8 - \theta_7)\sin\theta_6 \end{aligned} \tag{2.5}$$

$$z_e = z_b + l_1 \cos\theta_1 \cos\theta_2 + l_2 \cos(\theta_3 - \theta_1)\sin\theta_2 - l_3 \sin(\theta_2 + \theta_4) - l_4 \cos\theta_6 \cos\theta_7 - l_5 \cos(\theta_8 - \theta_7)\cos\theta_6 \quad (2.6)$$

In choosing Cartesian coordinate Σ_a, which the origin is taken on the ankle joint, position of the center of the pelvis link is expressed as follows:

$$x_{ca} = l_1 \sin\theta_1 - l_2 \sin(\theta_3 - \theta_1) \quad (2.7)$$

$$y_{ca} = l_1 \sin\theta_2 + l_2 \cos(\theta_3 - \theta_1)\sin\theta_2 + \frac{l_3}{2}\cos(\theta_2 + \theta_4) \quad (2.8)$$

$$z_{ca} = l_1 \cos\theta_1 \cos\theta_2 + l_2 \cos(\theta_3 - \theta_1)\cos\theta_2 - \frac{l_3}{2}\sin(\theta_2 + \theta_4) \quad (2.9)$$

where x_{ca}, y_{ca} and z_{ca} are position of the center of the pelvis link in the coordinate system Σ_a.

Derivative of Eqs. (2.7)~(2.9) are

$$\dot{x}_{ca} = l_1\dot{\theta}_1 \cos\theta_1 - l_2(\dot{\theta}_3 - \dot{\theta}_1)\cos(\theta_3 - \theta_1) \quad (2.10)$$

$$\dot{y}_{ca} = l_1\dot{\theta}_2 \cos\theta_2 - l_2(\dot{\theta}_3 - \dot{\theta}_1)\sin(\theta_3 - \theta_1)\sin\theta_2 + l_2\dot{\theta}_2 \cos(\theta_3 - \theta_1)\cos\theta_2 - \frac{l_3}{2}(\dot{\theta}_2 + \dot{\theta}_4)\sin(\theta_2 + \theta_4) \quad (2.11)$$

$$\dot{z}_{ca} = -l_1\dot{\theta}_1 \sin\theta_1 \cos\theta_2 - l_1\dot{\theta}_2 \cos\theta_1 \sin\theta_2 - l_2(\dot{\theta}_3 - \dot{\theta}_1)\sin(\theta_3 - \theta_1)\cos\theta_2 - l_2\dot{\theta}_2 \cos(\theta_3 - \theta_1)\sin\theta_2 - \frac{l_3}{2}(\dot{\theta}_2 + \dot{\theta}_4)\cos(\theta_2 + \theta_4) \quad (2.12)$$

Similarly, position of the ankle joint of the swinging leg is expressed in the coordinate system Σ_h as:

$$x_{eh} = l_4 \sin\theta_7 - l_5 \sin(\theta_8 - \theta_7) \tag{2.13}$$

$$y_{eh} = \frac{l_3}{2} + l_4 \sin\theta_6 - l_5 \cos(\theta_8 - \theta_7)\sin\theta_6 \tag{2.14}$$

$$z_{eh} = l_4 \cos\theta_6 \cos\theta_7 + l_5 \cos(\theta_8 - \theta_7)\cos\theta_6 \tag{2.15}$$

The velocity of the ankle joint can be obtained as:

$$\dot{x}_{eh} = l_4\dot{\theta}_7 \cos\theta_7 - l_5(\dot{\theta}_8 - \dot{\theta}_7)\cos(\theta_8 - \theta_7) \tag{2.16}$$

$$\begin{aligned}\dot{y}_{eh} = {} & l_4\dot{\theta}_6 \cos\theta_6 + l_5(\dot{\theta}_8 - \dot{\theta}_7)\sin(\theta_8 - \theta_7)\sin\theta_6 \\ & - l_5\dot{\theta}_6 \cos(\theta_8 - \theta_7)\cos\theta_6\end{aligned} \tag{2.17}$$

$$\begin{aligned}\dot{z}_{eh} = {} & -l_4\dot{\theta}_6 \sin\theta_6 \cos\theta_7 - l_4\dot{\theta}_7 \cos\theta_6 \sin\theta_7 \\ & - l_5(\dot{\theta}_8 - \dot{\theta}_7)\sin(\theta_8 - \theta_7)\cos\theta_6 - l_5\dot{\theta}_6 \cos(\theta_8 - \theta_7)\sin\theta_6\end{aligned} \tag{2.18}$$

It is assumed that and the center of mass of each link concentrates at the tip of the link.

The center of mass of the biped robot can be obtained as follows:

$$x_{com} = \frac{m_b x_b + m_1 x_1 + m_2 x_2 + m_c x_c + m_3 x_3 + m_4 x_4 + m_e x_e}{m_b + m_1 + m_2 + m_c + m_3 + m_4 + m_e} \tag{2.19}$$

$$y_{com} = \frac{m_b y_b + m_1 y_1 + m_2 y_2 + m_c y_c + m_3 y_3 + m_4 y_4 + m_e y_e}{m_b + m_1 + m_2 + m_c + m_3 + m_4 + m_e} \tag{2.20}$$

$$z_{com} = \frac{m_b z_b + m_1 z_1 + m_2 z_2 + m_c z_c + m_3 z_3 + m_4 z_4 + m_e z_e}{m_b + m_1 + m_2 + m_c + m_3 + m_4 + m_e} \tag{2.21}$$

where

m_b is mass of the ankle joint of the right leg B_2,

m_1 is mass of the knee joint of the right leg B_1,

m_2 is mass of the hip joint of the right leg B,

m_c is mass of the center of the pelvis link C,

m_3 is mass of the hip joint of the left leg K,

m_4 is mass of the knee joint of the left leg K_1, and

m_e is mass of the ankle joint of the left leg E,

It is assumed that the mass of links of legs is negligible compared with mass of the trunk. Eqs. (2.19)~(2.21) can be rewritten as follows:

$$x_{com} = x_c \tag{2.22}$$

$$y_{com} = y_c \tag{2.23}$$

$$z_{com} = z_c \tag{2.24}$$

This means that the center of mass (COM) is concentrated at the center of the pelvis link.

2.2 Dynamic model of biped robot:

When the biped robot is supported by one leg, the dynamics of the biped robot can be approximated by a simple 3D inverted pendulum whose base is the foot of the biped robot and its head is COM of the biped robot as shown in Fig. 2.2. The length of the inverted pendulum r is able to be expanded or contracted. The position of the

COM of the inverted pendulum C(x_{ca}, y_{ca}, z_{ca}) in the Cartesian coordinate can be uniquely specified by $\boldsymbol{q} = [\theta_r, \theta_p, r]^T$ in the polar coordinate as follows [42]:

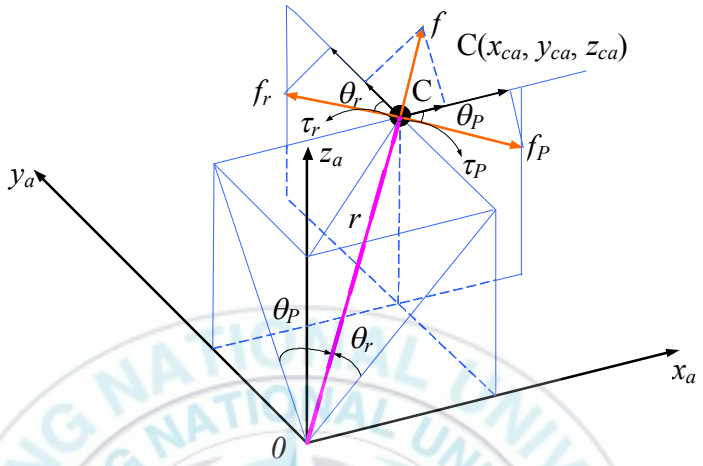

Fig. 2.2: Three dimension (3D) inverted pendulum.

$$x_{ca} = r\sin\theta_p \equiv rS_p \tag{2.25}$$

$$y_{ca} = -r\sin\theta_r \equiv -rS_r \tag{2.26}$$

$$z_{ca} = r\sqrt{1-\sin^2\theta_r - \sin^2\theta_p} \equiv rD \tag{2.27}$$

where $S_r \equiv \sin\theta_r$, $S_p \equiv \sin\theta_p$, $C_p \equiv \cos\theta_p$, $C_r \equiv \cos\theta_r$, and $D \equiv \sqrt{1-\sin^2\theta_p - \sin^2\theta_r}$.

$[\tau_r, \tau_p, f]^T$ are defined as the actuator torques and force associated with the variables $[\theta_r, \theta_p, r]^T$. The Lagrangian of the 3D inverted pendulum is

$$L = \frac{1}{2} m(\dot{x}_{ca}^2 + \dot{y}_{ca}^2 + \dot{z}_{ca}^2) - mgz_{ca} \tag{2.28}$$

where m is the total mass of the biped robot, and g is the gravitational acceleration.

Based on the Largange's equation, the dynamics of the 3D inverted pendulum can be obtained in the Cartesian coordinate as follows:

$$m\begin{bmatrix} \ddot{x}_{ca} \\ \ddot{y}_{ca} \\ \ddot{z}_{ca} \end{bmatrix} = \begin{bmatrix} -\frac{S_r S_p}{rC_r} & \frac{C_p}{r} & S_p \\ -\frac{C_r}{r} & \frac{S_r S_p}{rC_p} & -S_r \\ -\frac{S_r D}{rC_r} & -\frac{S_p D}{rC_p} & D \end{bmatrix} \begin{bmatrix} \tau_r \\ \tau_p \\ f \end{bmatrix} + \begin{bmatrix} 0 \\ 0 \\ -mg \end{bmatrix} \tag{2.29}$$

The proof of Eq. (2.29) is in Appendix A.

Eq. (2.29) can be rewritten as

$$m\begin{bmatrix} \ddot{x}_{ca} \\ \ddot{y}_{ca} \\ \ddot{z}_{ca} \end{bmatrix} = \left(\boldsymbol{J}^T\right)^{-1} \begin{bmatrix} \tau_r \\ \tau_p \\ f \end{bmatrix} + \begin{bmatrix} 0 \\ 0 \\ -mg \end{bmatrix}. \tag{2.30}$$

where $\boldsymbol{J}$ is Jacobian matrix which is expressed as

$$\boldsymbol{J} = \frac{\partial \boldsymbol{p}}{\partial \boldsymbol{q}} = \begin{bmatrix} 0 & rC_p & S_p \\ -rC_r & 0 & -S_r \\ -\frac{rC_r S_r}{D} & -\frac{rC_p S_p}{D} & D \end{bmatrix}. \tag{2.31}$$

Multiplying $\boldsymbol{J}^T$ on the left of both side of Eq. (2.30) yeilds

$$m\begin{bmatrix} 0 & -rC_r & -\dfrac{rC_rS_r}{D} \\ rC_p & 0 & -\dfrac{rC_pS_p}{D} \\ S_p & -S_r & D \end{bmatrix}\begin{bmatrix} \ddot{x}_{ca} \\ \ddot{y}_{ca} \\ \ddot{z}_{ca} \end{bmatrix} = \begin{bmatrix} \tau_r \\ \tau_p \\ f \end{bmatrix} - mg\begin{bmatrix} -\dfrac{rC_rS_r}{D} \\ -\dfrac{rC_pS_p}{D} \\ D \end{bmatrix} \tag{2.32}$$

Multiplying the first row of the Eq. (2.32) by D/C_r yields

$$m\left(-rD\ddot{y}_{ca} - rS_r\ddot{z}_{ca}\right) = \frac{D}{C_r}\tau_r + mgrS_r . \tag{2.33}$$

Substituting Eqs. (2.26)~(2.27) into Eq. (2.33), the dynamics equation of the inverted pendulum along y_a axis can be obtained as

$$m\left(-z_{ca}\ddot{y}_{ca} + y_{ca}\ddot{z}_{ca}\right) = \tau_x - mgy_{ca} . \tag{2.34}$$

where $\tau_x \equiv \dfrac{D}{C_r}\tau_r$ is the torque around x_a axis.

Using similar procedure, the dynamics equation of the inverted pendulum along x_a axis can be derived from the second row of the Eq. (2.32) as

$$m\left(z_{ca}\ddot{x}_{ca} - x_{ca}\ddot{z}_{ca}\right) = \tau_y + mgx_{ca} \tag{2.35}$$

where $\tau_y \equiv \dfrac{D}{C_p}\tau_p$ is the torque around y_a axis.

There are many classes of moving pattern of the inverted pendulum. For selecting one of them, a constraint is applied to limit the motion of the inverted pendulum. That is, the motions of the COM of the inverted pendulum are constrained on the

plane whose normal vector $\boldsymbol{v}_{cp}$ is $[k_x, k_y, -1]^T$ and z_a intersection is z_{cd} as shown in Fig. 2.3.

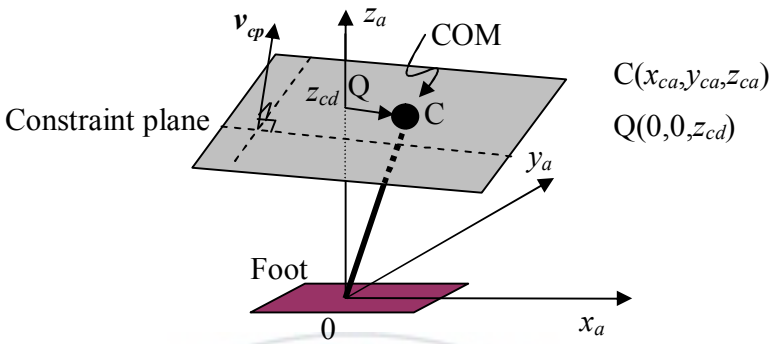

Fig. 2.3: Motion of inverted pendulum on constraint plane.

It is assumed that the constraint plane intersects the z_a axis at Q(0,0,z_{cd}) as shown in Fig. 2.3. Because C(x_{ca},y_{ca},z_{ca}) is located on the constraint plane, vector $\boldsymbol{v}_{cp}$ is perpendicular to vector $\overrightarrow{QC}$. It means that the following is satisfied.

$$\overrightarrow{QC} \cdot \boldsymbol{v}_{cp} = 0 \tag{2.36}$$

Eq. (2.36) can be rewritten as

$$k_x x_{ca} + k_y y_{ca} - (z_{ca} - z_{cd}) = 0 \tag{2.37}$$

By re-arranging Eq. (2.37), the constraint condition of the motion of the COM of the inverted pendulum is expressed as

$$z_{ca} = k_x x_{ca} + k_y y_{ca} + z_{cd} \tag{2.38}$$

where k_x, k_y and z_{cd} are constants.

When biped robot walks on a rugged terrain, the normal vector of the constraint plane should be perpendicular to the slope of the ground, and z_a intersection z_{cd} in the coordinate system Σ_a is set as distance between the COM and the ground.

The second order derivative of Eq. (2.38) is

$$\ddot{z}_{ca} = k_x \ddot{x}_{ca} + k_y \ddot{y}_{ca} . \tag{2.39}$$

Substituting Eqs. (2.38)~(2.39) into Eqs. (2.34)~(2.35), the equation of motion of the 3D inverted pendulum under the constraint condition (2.38) can be expressed as

$$\ddot{y}_{ca} = \frac{g}{z_{cd}} y_{ca} - \frac{k_x}{z_{cd}} \left(x_{ca} \ddot{y}_{ca} - \ddot{x}_{ca} y_{ca} \right) - \frac{1}{m z_{cd}} \tau_x \tag{2.40}$$

$$\ddot{x}_{ca} = \frac{g}{z_{cd}} x_{ca} + \frac{k_y}{z_{cd}} \left(x_{ca} \ddot{y}_{ca} - \ddot{x}_{ca} y_{ca} \right) + \frac{1}{m z_{cd}} \tau_y . \tag{2.41}$$

It is assumed that the biped robot walks on the flat floor with the horizontal plane. In this case, k_x and k_y are set to zero. It means that the COM of the inverted pendulum moves on the horizontal plane which has height $z_{ca} = z_{cd}$ as shown in Fig. 2.4.

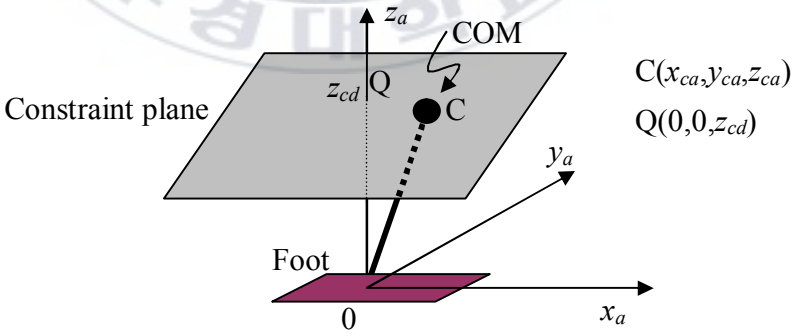

Fig. 2.4: Motion of inverted pendulum on horizontal constraint plane.

Eqs. (2.40)~(2.41) can be rewritten as:

$$\ddot{y}_{ca} = \frac{g}{z_{cd}} y_{ca} - \frac{1}{mz_{cd}} \tau_x \tag{2.42}$$

$$\ddot{x}_{ca} = \frac{g}{z_{cd}} x_{ca} + \frac{1}{mz_{cd}} \tau_y . \tag{2.43}$$

When the COM of the inverted pendulum moves on the horizontal plane, the dynamic equations along the x_a axis and y_a axis are independent each other and can be rewritten as linear differential equations [42].

(x_{zmp}, y_{zmp}) is defined as location of zero moment point (ZMP) on the floor as shown in Fig. 2.5.

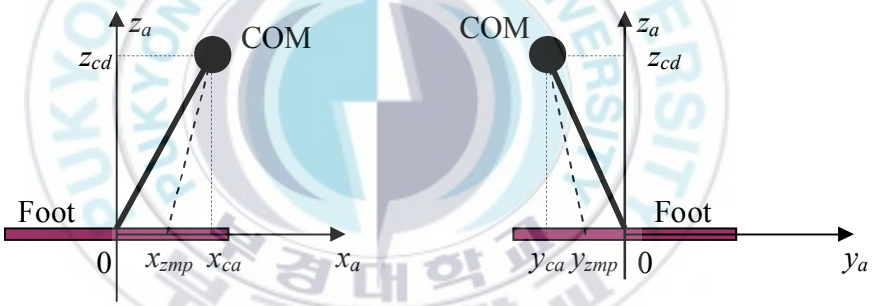

Fig. 2.5: ZMP of inverted pendulum.

(x_{ca},y_{ca},z_{ca}) is projection of the COM in the coordinate system Σ_a.

The ZMP is a point where the net support torques from floor about x_a axis and y_a axis are zero. From D'Alembert's principle, the ZMP of the inverted pendulum under the constraint that the COM of the inverted pendulum moves on the horizontal plane can be expressed as

$$x_{zmp} = x_{ca} - \frac{z_{cd}}{g}\ddot{x}_{ca} \tag{2.44}$$

$$y_{zmp} = y_{ca} - \frac{z_{cd}}{g}\ddot{y}_{ca}\,. \tag{2.45}$$

Eq. (2.44) shows that position of the ZMP along x_a axis is linear differential equation and it depends only on the position of the COM along x_a axis. Similarly, position of the ZMP along y_a axis does not depend on the position of the COM along x_a axis, but it depends only on the position of the COM along y_a axis.

When the biped robot moves with slow speed, Eqs. (2.44)~(2.45) can be approximated as Eqs. (2.46)~(2.47). It is shown that coordinate of the ZMP is projection of the COM.

$$x_{zmp} = x_{ca} \tag{2.46}$$

$$y_{zmp} = y_{ca}\,. \tag{2.47}$$

Since there are no actions torques that cause the biped robot to fall down at the ZMP, the ZMP is very important for walking robot and generally used as dynamic criterion for gait planning and control. During the walking of robot, the ZMP is located inside of the footprint of supported foot or inside the supported polygon.

Chapter 3: Walking Pattern Generation

3.1 ZMP and Stable Walking of Biped Robot:

As well known, the ZMP is defined as the point on the ground about which the sum of all moments of active forces is equal to zero. If the ZMP is inside the supported polygon, the biped robot is stable. Otherwise, the biped robot is unstable. The supported polygon is called the stable region. Minimum distance between the ZMP and the boundary of the stable region is called the stability margin [38]. When biped robot is supported by one leg, the supported polygon is boundary of footprint as dashed line shown in Fig. 3.1.a. When the biped robot is supported by two legs, the supported polygon is solid line shown in Fig. 3.1.b.

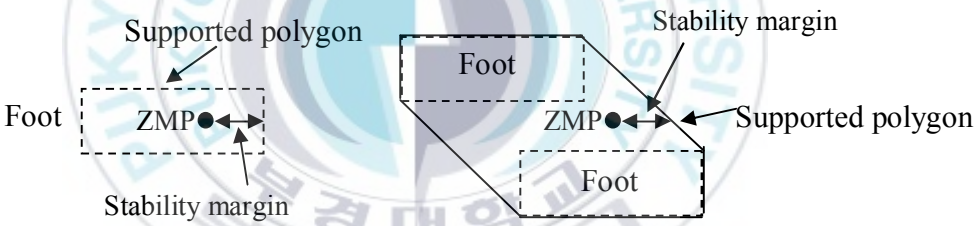

(a) One-leg supported phase (b) Two-leg supported phase

Fig. 3.1: Supported polygon.

The ZMP is very important for the stable walking of the biped robot. The ZMP is used as dynamic criterion for gait planning and control. Since feet of the biped robot are not fixed on the ground, it causes the biped robot to fall down at the ZMP. The relationship between the ZMP and the walking stability of the biped robot can be generalized as follows:

1 During the walking and standing of the biped robot, the ZMP must be inside the supported polygon.

2 The biped robot keeps its dynamic balance and the stable waking when the ZMP is inside the supported polygon as shown in Fig. 3.2.a.

3 When the ZMP is on the boundary of the supported polygon as shown in Fig. 3.2.b, the biped robot falls down or has the trend of falling down. In this case, the dynamic balance of the biped robot cannot be kept.

4 When the ZMP is outside of the supported polygon, the biped robot falls down. In this case, the dynamic balance of the biped robot cannot be kept.

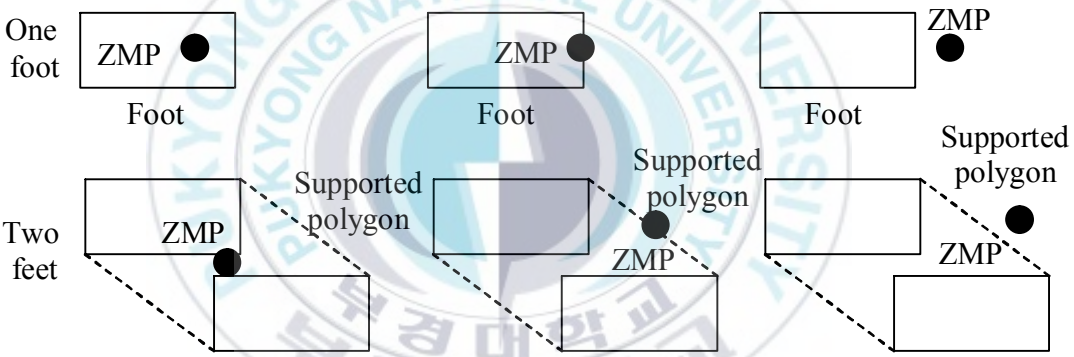

(a) ZMP inside (b) ZMP on the boundary (b) ZMP outside

Fig. 3.2: Position of ZMP with respect to stable region.

3.2 Walking Pattern Generation:

The objective of controlling the biped robot is to realize a stable walking or running. The stable walking or running of the biped robot depends on walking pattern. The walking pattern generation is used to generate a trajectory for COM of

the biped robot. For the stable walking or running of the biped robot, the walking pattern should satisfy the condition that the ZMP of the biped robot always exists inside the stable region. Since position of the COM of the biped robot has the close relationship with position of the ZMP as shown in Eqs. (2.44)~(2.45), a trajectory of the COM can be obtained from the trajectory of the ZMP. Based on the sequence of the desired footprint and period time of each step of the biped robot, a reference trajectory of the ZMP can be specified. Fig. 3.3 illustrates the footprint and the rectangular ZMP reference trajectory of the biped robot to guarantee stable gait. The period time of one step T_w is equal to 16 seconds. The ZMP reference trajectories versus time obtained from the rectangular ZMP reference trajectory and T_w are shown in Fig. 3.4. During one-leg supported phase, the ZMP of the biped robot is followed in x direction as segments t_2, t_4, t_6, t_8, t_{10}. When the biped robot is supported by two legs, the ZMP of the biped robot is followed in y direction as segments t_1, t_3, t_5, t_7, t_9. The stability margin is chosen to be 10 [cm] for y direction and 2.5 [cm] for x direction.

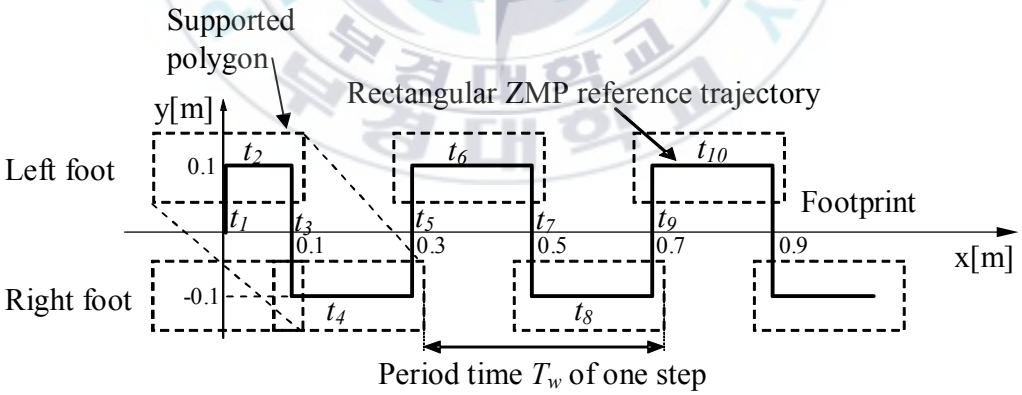

Fig. 3.3: Footprint and reference trajectory of ZMP.

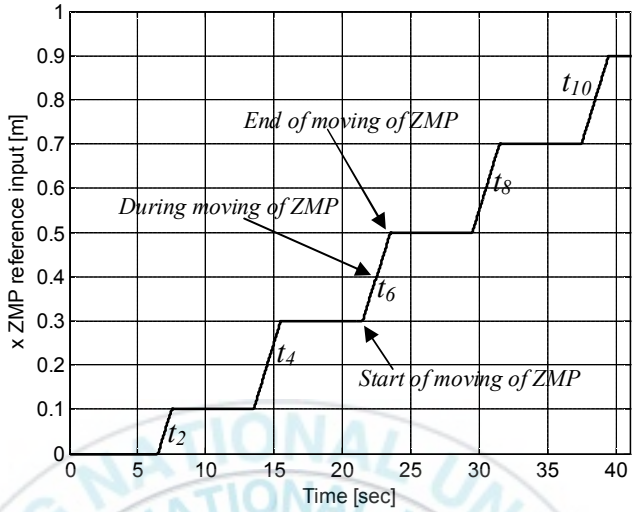

(a) *x* ZMP reference input versus time.

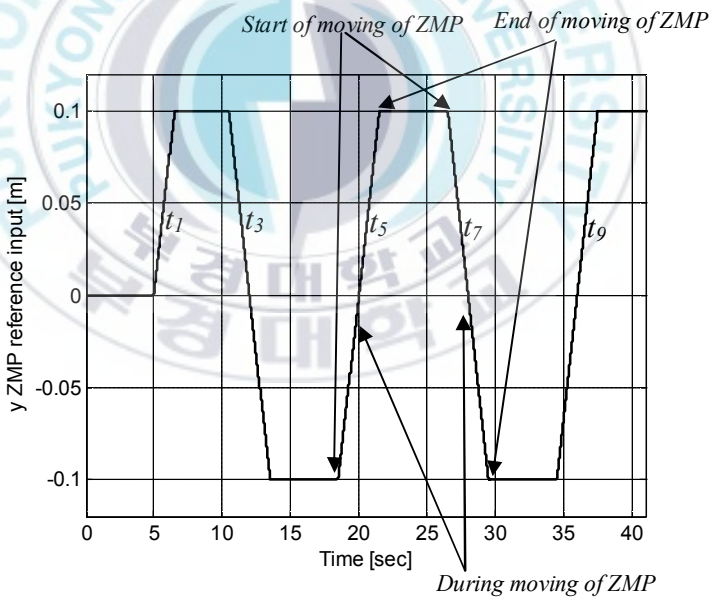

(b) *y* ZMP reference input versus time.

Fig. 3.4: Rectangular ZMP reference input trajectory versus time.

3.3 Walking Pattern Generation Based on Tracking Control of ZMP:

When a biped robot is modeled as a 3D inverted pendulum which is moved on horizontal plane, the ZMP's position of the biped robot is expressed by linear independent equations along x_a and y_a directions which are shown as Eqs. (2.44)~(2.45).

$u_x = \dddot{x}_{ca}$ is defined as the time derivative of the horizontal acceleration along x_a direction of the COM, and $u_y = \dddot{y}_{ca}$ is defined as time derivative of the horizontal acceleration along y_a direction of the COM. u_x and u_y are introduced as inputs. Eqs. (2.44)~(2.45) can be rewritten in strictly proper form as follows [16]:

$$\underbrace{\begin{bmatrix} \dot{x}_{ca} \\ \ddot{x}_{ca} \\ \dddot{x}_{ca} \end{bmatrix}}_{\dot{x}_x(t)} = \underbrace{\begin{bmatrix} 0 & 1 & 0 \\ 0 & 0 & 1 \\ 0 & 0 & 0 \end{bmatrix}}_{A} \underbrace{\begin{bmatrix} x_{ca} \\ \dot{x}_{ca} \\ \ddot{x}_{ca} \end{bmatrix}}_{x_x(t)} + \underbrace{\begin{bmatrix} 0 \\ 0 \\ 1 \end{bmatrix}}_{B} u_x,$$

$$x_{zmp} = \underbrace{\begin{bmatrix} 1 & 0 & -\dfrac{z_{cd}}{g} \end{bmatrix}}_{C} \underbrace{\begin{bmatrix} x_{ca} \\ \dot{x}_{ca} \\ \ddot{x}_{ca} \end{bmatrix}}_{x_x(t)}, \tag{3.1}$$

$$\underbrace{\begin{bmatrix} \dot{y}_{ca} \\ \ddot{y}_{ca} \\ \dddot{y}_{ca} \end{bmatrix}}_{\dot{x}_y(t)} = \underbrace{\begin{bmatrix} 0 & 1 & 0 \\ 0 & 0 & 1 \\ 0 & 0 & 0 \end{bmatrix}}_{A} \underbrace{\begin{bmatrix} y_{ca} \\ \dot{y}_{ca} \\ \ddot{y}_{ca} \end{bmatrix}}_{x_y(t)} + \underbrace{\begin{bmatrix} 0 \\ 0 \\ 1 \end{bmatrix}}_{B} u_y,$$

$$y_{zmp} = \underbrace{\begin{bmatrix} 1 & 0 & -\dfrac{z_{cd}}{g} \end{bmatrix}}_{C} \underbrace{\begin{bmatrix} y_{ca} \\ \dot{y}_{ca} \\ \ddot{y}_{ca} \end{bmatrix}}_{x_y(t)}. \tag{3.2}$$

where position of the ZMP along x_a axis, x_{zmp}, is output of the continuous time system (3.1), position of the ZMP along y_a axis, y_{zmp}, is output of the continuous time system (3.2), x_{ca} and y_{ca} are position of the COM with respect to x_a and y_a axes, and $\dot{x}_{ca}$, $\ddot{x}_{ca}$, $\dot{y}_{ca}$, $\ddot{y}_{ca}$ are horizontal velocity and acceleration with respect to x_a and y_a directions, respectively. The continuous time systems (3.1) and (3.2) are controllable because those are expressed as controllable canonical form. The continuous time systems (3.1) and (3.2) are observable because observability matrix $\boldsymbol{O_c}$ has full rank.

$$\boldsymbol{O}_c = \begin{bmatrix} \boldsymbol{C} \\ \boldsymbol{CA} \\ \boldsymbol{CA^2} \end{bmatrix} = \begin{bmatrix} 1 & 0 & -\frac{z_{cd}}{g} \\ 0 & 1 & 0 \\ 0 & 0 & 1 \end{bmatrix} \tag{3.3}$$

The continuous time systems (3.1) and (3.2) can be generalized in the form as follows:

$$\begin{aligned} \dot{\boldsymbol{x}} &= \boldsymbol{A}\boldsymbol{x} + \boldsymbol{B}u_c \\ y &= \boldsymbol{C}\boldsymbol{x} \end{aligned} \tag{3.4}$$

The continuous time systems (3.1) and (3.2) can be discretized by using zero-order-hold with sampling time T as follows [5]:

$$\begin{aligned} \boldsymbol{x}_x[(k+1)] &= \boldsymbol{\Phi}(T)\boldsymbol{x}_x(k) + \boldsymbol{\theta}(T)u_x(k) \\ x_{zmp}(k) &= \boldsymbol{C}\boldsymbol{x}_x(k) \end{aligned} \tag{3.5}$$

$$\begin{aligned} \boldsymbol{x}_y[(k+1)] &= \boldsymbol{\Phi}(T)\boldsymbol{x}_y(k) + \boldsymbol{\theta}(T)u_y(k) \\ y_{zmp}(k) &= \boldsymbol{C}\boldsymbol{x}_y(k) \end{aligned} \tag{3.6}$$

where $\boldsymbol{x}_x(k) \equiv [x(kT) \quad \dot{x}(kT) \quad \ddot{x}(kT)]^T$ and $\boldsymbol{x}_y(k) \equiv [y(kT) \quad \dot{y}(kT) \quad \ddot{y}(kT)]^T$ are states vectors, $u_x(k) \equiv u_x(kT)$ and $u_y(k) \equiv u_y(kT)$ are input signals, and $x_{zmp}(k) \equiv x_{zmp}(kT)$ and $y_{zmp}(k) \equiv y_{zmp}(kT)$ are outputs.

$$\boldsymbol{\Phi}(T) = e^{\boldsymbol{A}T} = \boldsymbol{I} + \boldsymbol{A}T + \frac{1}{2!}\boldsymbol{A}^2T^2 + \frac{1}{3!}\boldsymbol{A}^3T^3 + \cdots = \begin{bmatrix} 1 & T & T^2/2 \\ 0 & 1 & T \\ 0 & 0 & 1 \end{bmatrix} \tag{3.7}$$

$$\boldsymbol{\theta}(T) = \int_0^T \boldsymbol{\Phi}(T-\tau)\boldsymbol{B}d\tau \tag{3.8}$$

Substituting $\boldsymbol{\Phi}(T-\tau)$ into Eq. (3.8), $\boldsymbol{\theta}(T)$ can be obtained as

$$\boldsymbol{\theta}(T) = \int_0^T \begin{bmatrix} 1 & T-\tau & (T-\tau)^2/2 \\ 0 & 1 & T-\tau \\ 0 & 0 & 1 \end{bmatrix} \begin{bmatrix} 0 \\ 0 \\ 1 \end{bmatrix} d\tau = \begin{bmatrix} T^3/6 \\ T^2/2 \\ T \end{bmatrix}. \tag{3.9}$$

The controllability matrix of the discrete time systems (3.5) and (3.6) is expressed as

$$\boldsymbol{M}_d = [\boldsymbol{\theta} \quad \boldsymbol{\Phi}\boldsymbol{\theta} \quad \boldsymbol{\Phi}^2\boldsymbol{\theta}] = \begin{bmatrix} T^3/6 & 7T^3/6 & 19T^3/6 \\ T^2/2 & 3T^2/2 & 5T^2/2 \\ T & T & T \end{bmatrix} \tag{3.10}$$

When T is not equal to zero, the controllability matrix of the discrete time systems have full rank. The discrete time systems are controllable and stabilizable [5].

Similarly, the discrete time systems (3.5) and (3.6) are observable and detectable because the following observability matrix $\boldsymbol{O}_d$ of them has full rank [5].

$$\boldsymbol{O}_d = \begin{bmatrix} \boldsymbol{C} \\ \boldsymbol{C\Phi} \\ \boldsymbol{C\Phi}^2 \end{bmatrix} = \begin{bmatrix} 1 & 0 & -\frac{z_{cd}}{g} \\ 1 & T & \frac{T^2}{2} - \frac{z_{cd}}{g} \\ 1 & 2T & 2T^2 - \frac{z_{cd}}{g} \end{bmatrix} \tag{3.11}$$

The discrete time systems (3.5) and (3.6) can be generalized in the form as follows:

$$\begin{aligned} \boldsymbol{x}[(k+1)] &= \boldsymbol{A}_d \boldsymbol{x}(k) + \boldsymbol{B}_d \boldsymbol{u}(k) \\ \boldsymbol{y}(k) &= \boldsymbol{C}_d \boldsymbol{x}(k) \end{aligned} \tag{3.12}$$

3.4 Controller Design for ZMP Tracking Control:

Instead of solving the differential Eqs. (2.44)~(2.45), position of the COM can be obtained by constructing a controller to track the ZMP as the output of Eqs. (3.1)~(3.2) or Eqs. (3.5)~(3.6). The block diagram of the ZMP tracking control systems are shown in Fig. 3.5. When x_{zmp} and y_{zmp} are controlled to track the ZMP reference trajectory, the COM trajectory can be obtained from state variables x_{ca} and y_{ca} of Eqs. (3.1)~(3.2) or Eqs. (3.5)~(3.6).

According to this pattern, the walking or running of the biped robot are stable.

By constructing the ZMP tracking control systems, the walking pattern generation problem turns into designing a tracking controller to track the ZMP reference trajectory [16].

To control the ZMP output of the systems in Fig. 3.5 to track the ZMP reference trajectory, many types of controllers can be applied. In this chapter, a continuous time optimal tracking controller and a discrete time optimal tracking controller utilizing the future values of the ZMP reference trajectory are designed to control the systems (3.1) and (3.2) or (3.5) and (3.6) to track the ZMP reference trajectory.

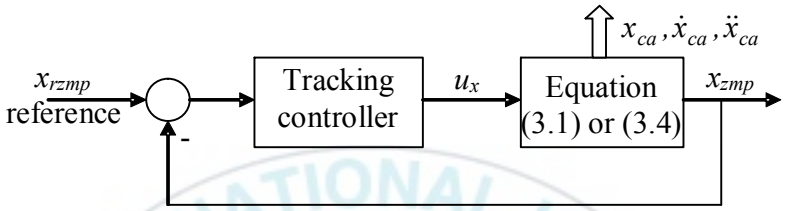

(a) ZMP tracking control system along x_a axis

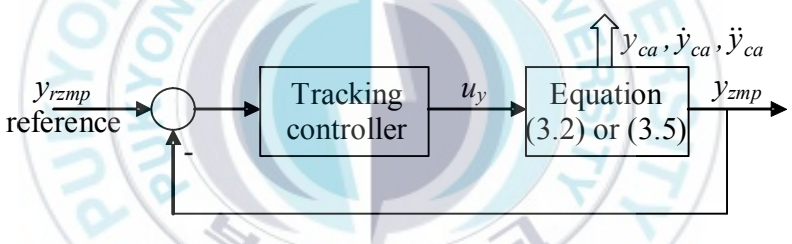

(b) ZMP tracking control system along y_a axis

Fig. 3.5: ZMP tracking control system.

3.4.1 Continuous time optimal tracking controller design:

A linear time invariant system is considered as

$$\begin{aligned} \dot{\boldsymbol{x}} &= \boldsymbol{A}\boldsymbol{x} + \boldsymbol{B}u_c \\ y &= \boldsymbol{C}\boldsymbol{x} \end{aligned} \tag{3.13}$$

where $\boldsymbol{x} \in \Re^{n\times 1}$ is state vector of system, $u_c \in \Re$ is input signal, $y \in \Re$ is output, $\boldsymbol{A} \in \Re^{n\times n}$, $\boldsymbol{B} \in \Re^{n\times 1}$ and $\boldsymbol{C} \in \Re^{1\times n}$.

The continuous time system is assumed to be controllable and observable. The objective for designing this controller is to stabilize the closed loop system and to track the controlled output of this system to the reference input.

An error signal between the reference input $r(t)$ and the output of the continuous time system $y(t)$ is defined as follows:

$$e(t) = r(t) - y(t) \tag{3.14}$$

The objective of the control system is to regulate the error signal $e(t)$ equal to zero when time goes to infinity.

Because the ZMP reference trajectory has segments as ramp function so that the designed controller has to track the output of this system to the ramp reference input signal. When the output of this system is controlled to track the ramp reference input signal, it also tracks the step reference input signal. The reference signal is assumed to be ramp function.

The first order and second order derivatives of the error signal are expressed as follows:

$$\dot{e}(t) = \dot{r}(t) - \dot{y}(t) = \dot{r}(t) - \boldsymbol{C}\dot{\boldsymbol{x}} \tag{3.15}$$

$$\ddot{e}(t) = -\boldsymbol{C}\ddot{\boldsymbol{x}} \tag{3.16}$$

From the second order derivative of the first row of (3.13), (3.15) and (3.16), the augmented system is obtained as follows:

$$\underbrace{\frac{d}{dt}\begin{bmatrix}\ddot{\boldsymbol{x}}\\ \dot{e}\\ e\end{bmatrix}}_{\dot{X}_a}=\underbrace{\begin{bmatrix}\boldsymbol{A} & \boldsymbol{0}_{n\times 1} & \boldsymbol{0}_{n\times 1}\\ -\boldsymbol{C} & 0 & 0\\ 0 & 1 & 0\end{bmatrix}}_{A_a}\underbrace{\begin{bmatrix}\ddot{\boldsymbol{x}}\\ \dot{e}\\ e\end{bmatrix}}_{X_a}+\underbrace{\begin{bmatrix}\boldsymbol{B}\\ 0\\ 0\end{bmatrix}}_{B_a}w \tag{3.17}$$

where $w=\dddot{u}_c$ is defined as new input signal.

A scalar cost function of the quadratic form is chosen as

$$J_c=\int_0^\infty\left(\boldsymbol{X}_a^T\boldsymbol{Q}_c\boldsymbol{X}_a+R_c w^2\right)dt \tag{3.18}$$

where $\boldsymbol{Q}_c=\left[\begin{array}{c|c}\boldsymbol{0}_{(n+1)\times(n+1)} & \boldsymbol{0}_{(n+1)\times 1}\\ \hline \boldsymbol{0}_{1\times(n+1)} & Q_{ec}\end{array}\right]\in\Re^{(n+2)\times(n+2)}$ is symmetric semi-positive definite matrix, $R_c\in\Re$ and $Q_{ec}\in\Re$ are positive scalar.

The control signal w that minimizes the cost function (3.18) of the system (3.17) can be obtained as

$$w=\dddot{u}_c=-\boldsymbol{K}_c\boldsymbol{X}_a=\boldsymbol{K}_{1c}\ddot{\boldsymbol{x}}+K_{2c}\dot{e}+K_{3c}e \tag{3.19}$$

where $\boldsymbol{K}_c=\begin{bmatrix}-\boldsymbol{K}_{1c} & -K_{2c} & -K_{3c}\end{bmatrix}=R_c^{-1}\boldsymbol{B}^T\boldsymbol{P}_c$ and $\boldsymbol{P}_c\in\Re^{(n+2)\times(n+2)}$ is solution of the following Ricatti equation with symmetric positive definite matrix.

$$\boldsymbol{A}_a^T\boldsymbol{P}_c+\boldsymbol{P}_c\boldsymbol{A}_a-\boldsymbol{P}_c\boldsymbol{B}_a R_c^{-1}\boldsymbol{B}_a^T\boldsymbol{P}_c+\boldsymbol{Q}_c=0 \tag{3.20}$$

When the initial conditions are $u_c(0)=0$, $\dot{u}_c(0)=0$, $\boldsymbol{x}(0)=0$ and $\dot{\boldsymbol{x}}(0)=0$, Eq. (3.19) yields

$$u_c(t) = \boldsymbol{K}_{1c}\boldsymbol{x}(t) + K_{2c}\int_0^t e(t)dt + K_{3c}\int_0^t\left(\int_0^t e(t)dt\right)dt \tag{3.21}$$

Block diagram of the closed loop optimal tracking control system is shown as follows:

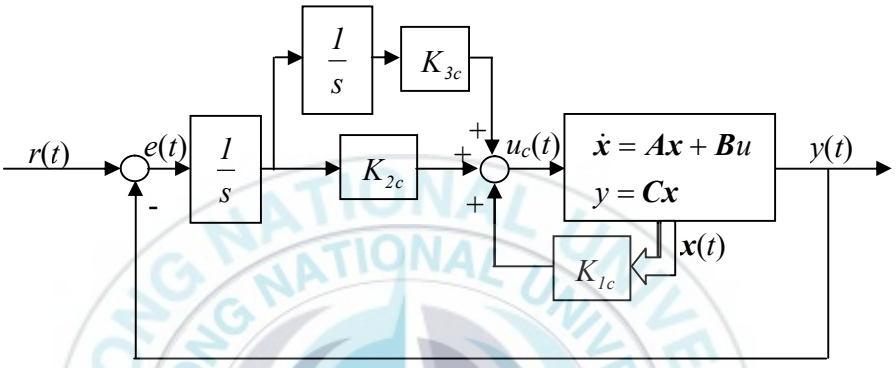

Fig. 3.6: Block diagram of the continuous time closed loop optimal tracking control system.

3.4.2 Discrete time optimal tracking controller design:

A time invariant discrete time system is considered as follows:

$$\begin{aligned}\boldsymbol{x}[(k+1)] &= \boldsymbol{A}_d\boldsymbol{x}(k) + \boldsymbol{B}_d\boldsymbol{u}(k)\\ \boldsymbol{y}(k) &= \boldsymbol{C}_d\boldsymbol{x}(k)\end{aligned} \tag{3.22}$$

where $\boldsymbol{x}(k) \in \Re^{n\times 1}$ is $n\times 1$ state vector, $\boldsymbol{y}(k) \in \Re^{m\times 1}$ is $m\times 1$ output vector, $\boldsymbol{u}(k) \in \Re^{r\times 1}$ is $r\times 1$ control input vector, and $\boldsymbol{A_d} \in \Re^{n\times n}$, $\boldsymbol{B_d} \in \Re^{n\times r}$, $\boldsymbol{C_d} \in \Re^{m\times n}$ are matrices with corresponding dimensions.

An error signal $\boldsymbol{e}(k) \in \Re^{m\times 1}$ is defined as the difference between the reference input $\boldsymbol{r}(k) \in \Re^{m\times 1}$ and the output of the discrete time system $\boldsymbol{y}(k)$ as follows:

$$\boldsymbol{e}(k) = \boldsymbol{r}(k) - \boldsymbol{y}(k) \tag{3.23}$$

It is denoted that the incremental control input is $\Delta\boldsymbol{u}(k) = \boldsymbol{u}(k) - \boldsymbol{u}(k-1)$ and the incremental state is $\Delta\boldsymbol{x}(k) = \boldsymbol{x}(k) - \boldsymbol{x}(k-1)$. If the discrete time system (3.22) is controllable and observable, it can be rewritten in the increment as follows:

$$\begin{aligned} \Delta\boldsymbol{x}[(k+1)] &= \boldsymbol{A}_d \Delta\boldsymbol{x}(k) + \boldsymbol{B}_d \Delta\boldsymbol{u}(k) \\ \boldsymbol{y}(k) &= \boldsymbol{C}_d \boldsymbol{x}(k) \end{aligned} \tag{3.24}$$

The error at the $k+1^{th}$ sample time can be obtained from Eq. (3.23) as

$$\boldsymbol{e}(k+1) = \boldsymbol{r}(k+1) - \boldsymbol{y}(k+1). \tag{3.25}$$

Subtracting Eq. (3.23) from Eq. (3.25) yields

$$\boldsymbol{e}(k+1) - \boldsymbol{e}(k) = \boldsymbol{r}(k+1) - \boldsymbol{r}(k) - \boldsymbol{y}(k+1) + \boldsymbol{y}(k). \tag{3.26}$$

Substituting Eq. (3.24) into Eq. (3.26) can be reduced as

$$\boldsymbol{e}(k+1) = \boldsymbol{e}(k) + \Delta\boldsymbol{r}(k+1) - \boldsymbol{C}_d \boldsymbol{A}_d \Delta\boldsymbol{x}(k) - \boldsymbol{C}_d \boldsymbol{B}_d \Delta\boldsymbol{u}(k). \tag{3.27}$$

where $\Delta\boldsymbol{r}(k+1) = \boldsymbol{r}(k+1) - \boldsymbol{r}(k) \in \Re^{m\times 1}$

From the first row of Eq. (3.24) and Eq. (3.27), the error system can be obtained as

$$\underbrace{\begin{bmatrix} \boldsymbol{e}(k+1) \\ \Delta\boldsymbol{x}(k+1) \end{bmatrix}}_{\boldsymbol{X}(k+1)} = \underbrace{\begin{bmatrix} \boldsymbol{I}_m & -\boldsymbol{C}_d \boldsymbol{A}_d \\ \boldsymbol{0}_{nxm} & \boldsymbol{A}_d \end{bmatrix}}_{\boldsymbol{A}_E} \underbrace{\begin{bmatrix} \boldsymbol{e}(k) \\ \Delta\boldsymbol{x}(k) \end{bmatrix}}_{\boldsymbol{X}(k)} + \underbrace{\begin{bmatrix} \boldsymbol{I}_m \\ \boldsymbol{0}_{nxm} \end{bmatrix}}_{\boldsymbol{G}_R} \Delta\boldsymbol{r}(k+1) + \underbrace{\begin{bmatrix} -\boldsymbol{C}_d \boldsymbol{B}_d \\ \boldsymbol{B}_d \end{bmatrix}}_{\boldsymbol{G}} \Delta\boldsymbol{u}(k) \tag{3.28}$$

where $\boldsymbol{X}(k) \in \Re^{(m+n)\times 1}$, $\boldsymbol{A_E} \in \Re^{(m+n)\times(m+n)}$, $\boldsymbol{G_R} \in \Re^{(m+n)\times m}$ and $\boldsymbol{G} \in \Re^{(m+n)\times r}$.

It is assumed that at each time *k*, the reference input of the error system (3.28) can be known for the *N* future values as well as the present and the past values are available.

A scalar cost function of the quadratic form is chosen as

$$J = \sum_{k=0}^{\infty} \left[\boldsymbol{X}^{T}(k)\, \boldsymbol{Q}\, \boldsymbol{X}(k) + \Delta \boldsymbol{u}^{T}(k)\, \boldsymbol{R}\, \Delta \boldsymbol{u}(k) \right] \tag{3.29}$$

where $\boldsymbol{Q} = \begin{bmatrix} \boldsymbol{Q_e} & \boldsymbol{0_{m\times n}} \\ \boldsymbol{0_{n\times m}} & \boldsymbol{0_{n\times n}} \end{bmatrix} \in \Re^{(m+n)\times(m+n)}$ is semi-positive definite matrix, $\boldsymbol{Q_e} \in \Re^{m\times m}$, and $\boldsymbol{R} \in \Re^{r\times r}$ are positive definite matrix.

It is assumed that the *N* future values of the reference input $\boldsymbol{r}(k+1), \boldsymbol{r}(k+2), \cdots, \boldsymbol{r}(k+N)$ can be utilized. The future values of the reference input beyond time $(k+N)$ are approximated by $\boldsymbol{r}(k+N)$. It means that the following is satisfied.

$$\Delta \boldsymbol{r}(k+i) = 0 \qquad (i = N+1, N+2, \ldots). \tag{3.30}$$

$\boldsymbol{X_R}(k) = \begin{bmatrix} \Delta \boldsymbol{r}(k+1) \\ \Delta \boldsymbol{r}(k+2) \\ \vdots \\ \Delta \boldsymbol{r}(k+N) \end{bmatrix} \in \Re^{Nm\times 1}$ is defined as a future reference input incremental vector depending on the *N* incremental future values of the reference input.

The augmented error system which contains future values of the reference input is obtained as

$$\begin{bmatrix} \boldsymbol{X}(k+1) \\ \boldsymbol{X}_R(k+1) \end{bmatrix} = \begin{bmatrix} \boldsymbol{A_E} & \boldsymbol{G_{PR}} \\ \boldsymbol{0}_{(Nm)\times(n+m)} & \boldsymbol{A_R} \end{bmatrix} \begin{bmatrix} \boldsymbol{X}(k) \\ \boldsymbol{X}_R(k) \end{bmatrix} + \begin{bmatrix} \boldsymbol{G} \\ \boldsymbol{0}_{(Nm)\times r} \end{bmatrix} \Delta\boldsymbol{u}(k). \tag{3.31}$$

where $\boldsymbol{G}_{PR} = \begin{bmatrix} \boldsymbol{G_R} & \boldsymbol{0}_{(m+n)\times m} & \cdots & \boldsymbol{0}_{(m+n)\times m} \end{bmatrix} \in \Re^{(m+n)\times(Nm)}$, and

$$\boldsymbol{A_R} = \begin{bmatrix} \boldsymbol{0_m} & \boldsymbol{I_m} & \boldsymbol{0_m} & \cdots & \boldsymbol{0_m} \\ \vdots & & \ddots & \ddots & \vdots \\ \vdots & & & \ddots & \boldsymbol{0_m} \\ \vdots & & & & \boldsymbol{I_m} \\ \boldsymbol{0_m} & \cdots & \cdots & \cdots & \boldsymbol{0_m} \end{bmatrix} \in \Re^{(Nm)\times(Nm)}$$

The cost function (3.29) can be rewritten as

$$J = \sum_{k=0}^{\infty} \left\{ \begin{bmatrix} \boldsymbol{X}^T(k) & \boldsymbol{X}_R^T(k) \end{bmatrix} \begin{bmatrix} \boldsymbol{Q} & \boldsymbol{0}_{(n+m)\times(Nm)} \\ \boldsymbol{0}_{(Nm)\times(n+m)} & \boldsymbol{0}_{(Nm)\times(Nm)} \end{bmatrix} \begin{bmatrix} \boldsymbol{X}(k) \\ \boldsymbol{X}_R(k) \end{bmatrix} + \Delta\boldsymbol{u}^T(k)\boldsymbol{R}\Delta\boldsymbol{u}(k) \right\} \tag{3.32}$$

The optimal control signal $\Delta\boldsymbol{u}(k)$ that minimizes the cost function (3.32) of the system (3.31) can be obtained as [5]

$$\Delta\boldsymbol{u}(k) = -\left[\boldsymbol{R} + \begin{bmatrix} \boldsymbol{G^T} & \boldsymbol{0}_{(Nm)\times r} \end{bmatrix} \boldsymbol{P} \begin{bmatrix} \boldsymbol{G} \\ \boldsymbol{0}_{(Nm)\times r} \end{bmatrix} \right]^{-1} \begin{bmatrix} \boldsymbol{G^T} & \boldsymbol{0}_{(Nm)\times r} \end{bmatrix} \boldsymbol{P} \begin{bmatrix} \boldsymbol{A_E} & \boldsymbol{G_{PR}} \\ \boldsymbol{0}_{(Nm)\times(n+m)} & \boldsymbol{A_R} \end{bmatrix} \begin{bmatrix} \boldsymbol{X}(k) \\ \boldsymbol{X}_R(k) \end{bmatrix} \tag{3.33}$$

where $\boldsymbol{P}$ is semi-positive definite matrix. It is solution of the following algebraic Ricatti equation [5].

$$
\begin{aligned}
\boldsymbol{P} = &\begin{bmatrix} \boldsymbol{Q} & \boldsymbol{0}_{(n+m)\times(Nm)} \\ \boldsymbol{0}_{(Nm)\times(n+m)} & \boldsymbol{0}_{(Nm)\times(Nm)} \end{bmatrix} + \begin{bmatrix} \boldsymbol{A_E} & \boldsymbol{G_{PR}} \\ \boldsymbol{0}_{(Nm)\times(n+m)} & \boldsymbol{A_R} \end{bmatrix}^T \boldsymbol{P} \begin{bmatrix} \boldsymbol{A_E} & \boldsymbol{G_{PR}} \\ \boldsymbol{0}_{(Nm)\times(n+m)} & \boldsymbol{A_R} \end{bmatrix} \\
&- \begin{bmatrix} \boldsymbol{A_E} & \boldsymbol{G_{PR}} \\ \boldsymbol{0}_{(Nm)\times(n+m)} & \boldsymbol{A_R} \end{bmatrix}^T \boldsymbol{P} \begin{bmatrix} \boldsymbol{G} \\ \boldsymbol{0}_{(Nm)\times r} \end{bmatrix} \left(\boldsymbol{R} + \begin{bmatrix} \boldsymbol{G} \\ \boldsymbol{0}_{(Nm)\times r} \end{bmatrix}^T \boldsymbol{P} \begin{bmatrix} \boldsymbol{G} \\ \boldsymbol{0}_{(Nm)\times r} \end{bmatrix} \right)^{-1} \\
&\times \begin{bmatrix} \boldsymbol{G} \\ \boldsymbol{0}_{(Nm)\times r} \end{bmatrix}^T \boldsymbol{P} \begin{bmatrix} \boldsymbol{A_E} & \boldsymbol{G_{PR}} \\ \boldsymbol{0}_{(Nm)\times(n+m)} & \boldsymbol{A_R} \end{bmatrix}
\end{aligned} \tag{3.34}
$$

$\boldsymbol{P}$ can be partitioned as follows:

$$
\boldsymbol{P} = \begin{bmatrix} \boldsymbol{P_1} & \boldsymbol{W} \\ \boldsymbol{W^T} & \boldsymbol{P_2} \end{bmatrix} \in \Re^{(m+n+Nm)\times(m+n+Nm)}. \tag{3.35}
$$

where $\boldsymbol{P_1} \in \Re^{(n+m)\times(n+m)}$, $\boldsymbol{P_2} \in \Re^{(Nm)\times(Nm)}$ and $\boldsymbol{W} \in \Re^{(n+m)\times(Nm)}$

Substituting Eq. (3.35) into Eq. (3.34) yields

$$
\boldsymbol{P_1} = \boldsymbol{Q} + \boldsymbol{A_E^T P_1 A_E} - \boldsymbol{A_E^T P_1 G}\left[\boldsymbol{R} + \boldsymbol{G^T P_1 G}\right]^{-1} \boldsymbol{G^T P_1 A_E} \tag{3.36}
$$

$$
\boldsymbol{W} = \boldsymbol{A_E^T}\left(\boldsymbol{I} - \boldsymbol{P_1 G}\left(\boldsymbol{R} + \boldsymbol{G^T P_1 G}\right)^{-1} \boldsymbol{G^T}\right)\left(\boldsymbol{P_1 G_{PR}} + \boldsymbol{W A_R}\right) \tag{3.37}
$$

The optimal control signal $\Delta\boldsymbol{u}(k)$ becomes

$$
\begin{aligned}
\Delta\boldsymbol{u}(k) &= -\left[\boldsymbol{R} + \boldsymbol{G^T P_1 G}\right]^{-1}\left[\boldsymbol{G^T P_1 A_E} \quad \boldsymbol{G^T}\left(\boldsymbol{P_1 G_{PR}} + \boldsymbol{W A_R}\right)\right] \begin{bmatrix} \boldsymbol{X}(k) \\ \boldsymbol{X_R}(k) \end{bmatrix} \\
&= -\left[\boldsymbol{R} + \boldsymbol{G^T P_1 G}\right]^{-1} \boldsymbol{G^T P_1 A_E X}(k) \\
&\quad -\left[\boldsymbol{R} + \boldsymbol{G^T P_1 G}\right]^{-1} \boldsymbol{G^T}\left(\boldsymbol{P_1 G_{PR}} + \boldsymbol{W A_R}\right)\boldsymbol{X_R}(k)
\end{aligned} \tag{3.38}
$$

$\boldsymbol{K_1} = \begin{bmatrix} \boldsymbol{K_{1e}} & \boldsymbol{K_{1x}} \end{bmatrix} = -\left[\boldsymbol{R} + \boldsymbol{G^T P_1 G}\right]^{-1} \boldsymbol{G^T P_1 A_E} \in \Re^{r\times(m+n)}$ is defined as feedback gain matrix and $\boldsymbol{K_2} = -\left[\boldsymbol{R} + \boldsymbol{G^T P_1 G}\right]^{-1} \boldsymbol{G^T}\left(\boldsymbol{P_1 G_{PR}} + \boldsymbol{W A_R}\right) \in \Re^{r\times mN}$ is defined as feed forward matrix. Eq. (3.38) can be expressed into

$$\Delta \boldsymbol{u}(k) = \begin{bmatrix} \boldsymbol{K}_1 & \boldsymbol{K}_2 \end{bmatrix} \begin{bmatrix} \boldsymbol{X}(k) \\ \boldsymbol{X}_R(k) \end{bmatrix} = \boldsymbol{K}_1 \boldsymbol{X}(k) + \boldsymbol{K}_2 \boldsymbol{X}_R(k) \tag{3.39}$$

Corresponding with the N future values of the reference input, $\boldsymbol{W}$ and feed forward matrix $\boldsymbol{K}_2$ can be rewritten as

$$\boldsymbol{W} = \begin{bmatrix} \boldsymbol{W}(1) & \boldsymbol{W}(2) & \cdots & \boldsymbol{W}(N) \end{bmatrix} \tag{3.40}$$

$$\boldsymbol{K}_2 = \begin{bmatrix} \boldsymbol{K}_2(1) & \boldsymbol{K}_2(2) & \cdots & \boldsymbol{K}_2(N) \end{bmatrix} \tag{3.41}$$

where $\boldsymbol{W}(i) \in \Re^{(n+m)\times m}, i = 1,2\ldots,N$; $\boldsymbol{K}_2(i) \in \Re^{r\times m}, i = 1,2\ldots,N$

Using $\boldsymbol{G_{PR}}$ and $\boldsymbol{A_R}$ defined in Eq. (3.31) and Eq. (3.40), the feedback gain matrix $\boldsymbol{K_2}$ is re-expressed as

$$\begin{aligned} \boldsymbol{K}_2 &= -\left[\boldsymbol{R} + \boldsymbol{G}^T \boldsymbol{P}_1 \boldsymbol{G}\right]^{-1} \boldsymbol{G}^T \\ &\quad \times \left\{ \boldsymbol{P}_1 \left[\boldsymbol{G}_R \quad \boldsymbol{0}_{(n+m)\times m} \quad \cdots \quad \boldsymbol{0}_{(n+m)\times m} \right] + \begin{bmatrix} \boldsymbol{W}(1) & \boldsymbol{W}(2) & \cdots & \boldsymbol{W}(N) \end{bmatrix} \boldsymbol{A}_R \right\} \\ &= -\left[\boldsymbol{R} + \boldsymbol{G}^T \boldsymbol{P}_1 \boldsymbol{G}\right]^{-1} \boldsymbol{G}^T \\ &\quad \times \left\{ \boldsymbol{P}_1 \left[\boldsymbol{G}_R \quad \boldsymbol{0}_{(n+m)\times m} \quad \cdots \quad \boldsymbol{0}_{(n+m)\times m} \right] + \begin{bmatrix} \boldsymbol{0} & \boldsymbol{W}(1) & \cdots & \boldsymbol{W}(N-1) \end{bmatrix} \right\} \end{aligned} \tag{3.42}$$

From $\boldsymbol{G_{PR}}$ and $\boldsymbol{A_R}$ defined in Eq. (3.31) and Eq. (3.40), Eq. (3.37) becomes

$$\begin{aligned} &\begin{bmatrix} \boldsymbol{W}(1) & \boldsymbol{W}(2) & \cdots & \boldsymbol{W}(N) \end{bmatrix} = \boldsymbol{A}_E^T \left[\boldsymbol{I} - \boldsymbol{P}_1 \boldsymbol{G} \left(\boldsymbol{R} + \boldsymbol{G}^T \boldsymbol{P}_1 \boldsymbol{G} \right)^{-1} \boldsymbol{G}^T \right] \\ &\times \left\{ \boldsymbol{P}_1 \left[\boldsymbol{G}_R \quad \boldsymbol{0}_{(n+m)\times m} \quad \cdots \quad \boldsymbol{0}_{(n+m)\times m} \right] + \left[\boldsymbol{0}_{(n+m)\times m} \quad \boldsymbol{W}(1) \quad \cdots \quad \boldsymbol{W}(N-1) \right] \right\} \end{aligned} \tag{3.43}$$

It is defined that $\boldsymbol{F} = \boldsymbol{A}_E^T \left(\boldsymbol{I} - \boldsymbol{P}_1 \boldsymbol{G} \left(\boldsymbol{R} + \boldsymbol{G}^T \boldsymbol{P}_1 \boldsymbol{G} \right)^{-1} \boldsymbol{G}^T \right)$.

Eq. (3.43) yields

$$
\begin{aligned}
&\boldsymbol{W}(1) = \boldsymbol{F}\boldsymbol{P}_1\boldsymbol{G}_R \\
&\boldsymbol{W}(2) = F\boldsymbol{W}(1) = \boldsymbol{F}^2\boldsymbol{P}_1\boldsymbol{G}_R \\
&\vdots \\
&\boldsymbol{W}(N-1) = \boldsymbol{F}\boldsymbol{W}(N-2) = \boldsymbol{F}^{N-1}\boldsymbol{P}_1\boldsymbol{G}_R \\
&\boldsymbol{W}(N) = \boldsymbol{F}\boldsymbol{W}(N-1) = \boldsymbol{F}^{N}\boldsymbol{P}_1\boldsymbol{G}_R
\end{aligned}
\tag{3.44}
$$

From Eq. (3.41) and (3.42), $\boldsymbol{K}_2(i),\ i = 1,2,\ldots,N$, can be obtained as

$$
\begin{aligned}
&\boldsymbol{K}_2(1) = -\left[\boldsymbol{R} + \boldsymbol{G}^T\boldsymbol{P}_1\boldsymbol{G}\right]^{-1}\boldsymbol{G}^T\boldsymbol{P}_1\boldsymbol{G}_R \\
&\boldsymbol{K}_2(2) = -\left[\boldsymbol{R} + \boldsymbol{G}^T\boldsymbol{P}_1\boldsymbol{G}\right]^{-1}\boldsymbol{G}^T\boldsymbol{W}(1) = -\left[\boldsymbol{R} + \boldsymbol{G}^T\boldsymbol{P}_1\boldsymbol{G}\right]^{-1}\boldsymbol{G}^T\boldsymbol{F}\boldsymbol{P}_1\boldsymbol{G}_R \\
&\boldsymbol{K}_2(3) = -\left[\boldsymbol{R} + \boldsymbol{G}^T\boldsymbol{P}_1\boldsymbol{G}\right]^{-1}\boldsymbol{G}^T\boldsymbol{W}(2) = -\left[\boldsymbol{R} + \boldsymbol{G}^T\boldsymbol{P}_1\boldsymbol{G}\right]^{-1}\boldsymbol{G}^T\boldsymbol{F}^2\boldsymbol{P}_1\boldsymbol{G}_R \\
&\vdots \\
&\boldsymbol{K}_2(N-1) = -\left[\boldsymbol{R} + \boldsymbol{G}^T\boldsymbol{P}_1\boldsymbol{G}\right]^{-1}\boldsymbol{G}^T\boldsymbol{F}^{N-2}\boldsymbol{P}_1\boldsymbol{G}_R \\
&\boldsymbol{K}_2(N) = -\left[\boldsymbol{R} + \boldsymbol{G}^T\boldsymbol{P}_1\boldsymbol{G}\right]^{-1}\boldsymbol{G}^T\boldsymbol{F}^{N-1}\boldsymbol{P}_1\boldsymbol{G}_R
\end{aligned}
\tag{3.45}
$$

Eq. (3.39) can be rewritten as

$$
\Delta\boldsymbol{u}(k) = \boldsymbol{K}_{1e}\boldsymbol{e}(k) + \boldsymbol{K}_{1x}\Delta\boldsymbol{x}(k) + \sum_{i=1}^{N}\boldsymbol{K}_2(i)\Delta\boldsymbol{r}(k+i) \tag{3.46}
$$

By taking the initial values as zero and integrating both side of Eq. (3.46), the control law $\boldsymbol{u}(k)$ can be obtained as

$$
\boldsymbol{u}(k) = \boldsymbol{K}_{1e}\frac{z}{z-1}\boldsymbol{e}(k) + \boldsymbol{K}_{1x}\boldsymbol{x}(k) + \sum_{i=1}^{N}\boldsymbol{K}_2(i)\,\boldsymbol{r}(k+i) \tag{3.47}
$$

The block diagram of the closed loop control system using the discrete time optimal tracking controller utilizing the future values of the reference input is shown in Fig. 3.7

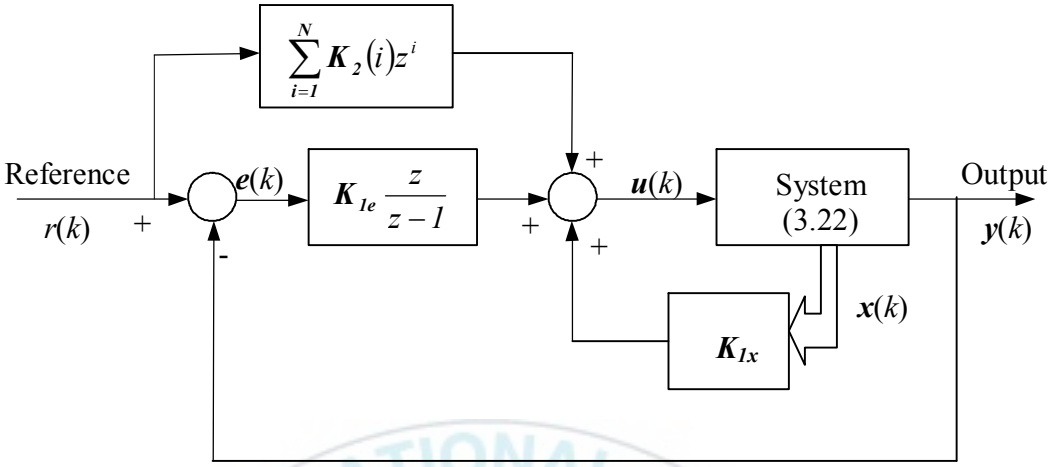

Fig. 3.7: Closed loop control system using the discrete time optimal tracking controller.

3.5 Numerical Simulation Results and Discussion:

The values of the system's parameters used in the simulation are given in Table 3.1. The reference input signals shown in Fig. 3.4 corresponding with the footprints shown in Fig. 3.3 are used in the simulation.

Table 3.1 Numerical values of the system's parameters

Parameters	Values	Units
Period time of one step T_w	16	sec
Width of foot	0.2	m
Length of foot	0.25	m
Distance between center of feet	0.3	m
Height of COM z_{cd}	0.6	m
Gravitational acceleration g	10	m/s^2
Step length	0.2	m

3.5.1 Simulation results of ZMP system using continuous time optimal tracking controller:

The continuous time systems (3.1) and (3.2) are controlled by the designed controller (3.21). The gain matrices of the optimal controller of the form (3.21) are calculated as shown in Table 3.2 for $R_c = 1$ and $Q_{ec} = 10^5$, 10^8, 10^{10} and 10^{12}.

Table 3.2 The gain matrices of the optimal tracking controller

Q_{ec}	$-K_{1c}$			K_{2c}	K_{3c}
10^5	198.98	74.142	10.621	254.75	316.23
10^8	2379.6	616.67	23.312	6898.7	10000
10^{10}	15848	3713.3	42.387	56299	100000
10^{12}	125690	28452	82.266	501370	1000000

The simulation results of the control system depending on Q_{ec} are shown in Figs. 3.8~3.31.

Corresponding with different Q_{ec}, Figs. 3.9, 3.15, 3.21 and 3.27 and Figs. 3.12, 3.18, 3.24 and 3.30 show the control signal inputs u_x and u_y of the x and y ZMP tracking control systems. As shown in these figures, the control signal inputs u_x and u_y of the x and y ZMP tracking control systems are bounded.

Figs. 3.10, 3.16, 3.22 and 3.28 and Figs. 3.13, 3.19, 3.25 and 3.31 illustrate the error signals between the reference input and the output of the x and y ZMP tracking control systems. As shown in these figures, the error occurs at singular points of the reference input and the absolute value of the error increases to the maximum value and then decreases to zero. The maximum values of the absolute value of the error are created by the maximum value of the undercut and the overshoot of the output of the x and y ZMP tracking control systems. When Q_{ec} is increased, the maximum value of the absolute value of the error is decreased.

The reference input, the ZMP output and the position of the COM of the x ZMP and y ZMP tracking control systems are presented in Figs. 3.8, 3.14, 3.20 and 3.26 and Figs. 3.11, 3.17, 3.23 and 3.29. In Figs. 3.8 and 3.11 corresponding with $Q_{ec} = 10^5$, the undercut of the output of the ZMP tracking control system is small but the maximum overshoot of the output of the ZMP tracking control system is about 5 [cm] for the x ZMP tracking control system and about 5 [cm] for the y ZMP tracking control system. The tracking performance of the output of the ZMP tracking control system to the ramp segments of the reference input is not good. In Figs. 3.14 and 3.17, the tracking performance of the output of the x and y ZMP tracking control systems to the ramp segments of the reference input is better in the case of $Q_{ec} = 10^8$ than in the case of $Q_{ec} = 10^5$. The maximum overshoot of the output of the ZMP tracking control system is smaller in the case of $Q_{ec} = 10^8$ than in the case of $Q_{ec} = 10^5$. However, the undercut of the output of the ZMP tracking control system is bigger in the case of $Q_{ec} = 10^8$ than in the case of $Q_{ec} = 10^5$. In Figs. 3.20, 3.23, 3.26 and 3.29, the maximum overshoot of the output of the ZMP tracking control system is smaller in the case of $Q_{ec} = 10^{10}$ and $Q_{ec} = 10^{12}$ than in the case of $Q_{ec} = 10^8$, and the tracking performance of the output of the ZMP tracking control system to the ramp segments of the reference input is faster and better in the case of $Q_{ec} = 10^{10}$ and $Q_{ec} = 10^{12}$ than in the case of $Q_{ec} = 10^8$. However, the undercut of the output of the ZMP tracking control system is bigger in the case of $Q_{ec} = 10^{10}$ and $Q_{ec} = 10^{12}$ than in the case of $Q_{ec} = 10^8$. In Figs. 3.20, 3.23, 3.26 and 3.29, the characteristics as the undercut, the maximum overshoot of the output of the ZMP tracking control system and tracking performance of the output of the ZMP tracking control system to the ramp segments of the reference input have little change when the Q_{ec} is larger than 10^{10}. To control for this system, the $Q_{ec} = 10^{10}$ is chosen.

❖ **simulation results with $Q_{ec} = 10^5$:**

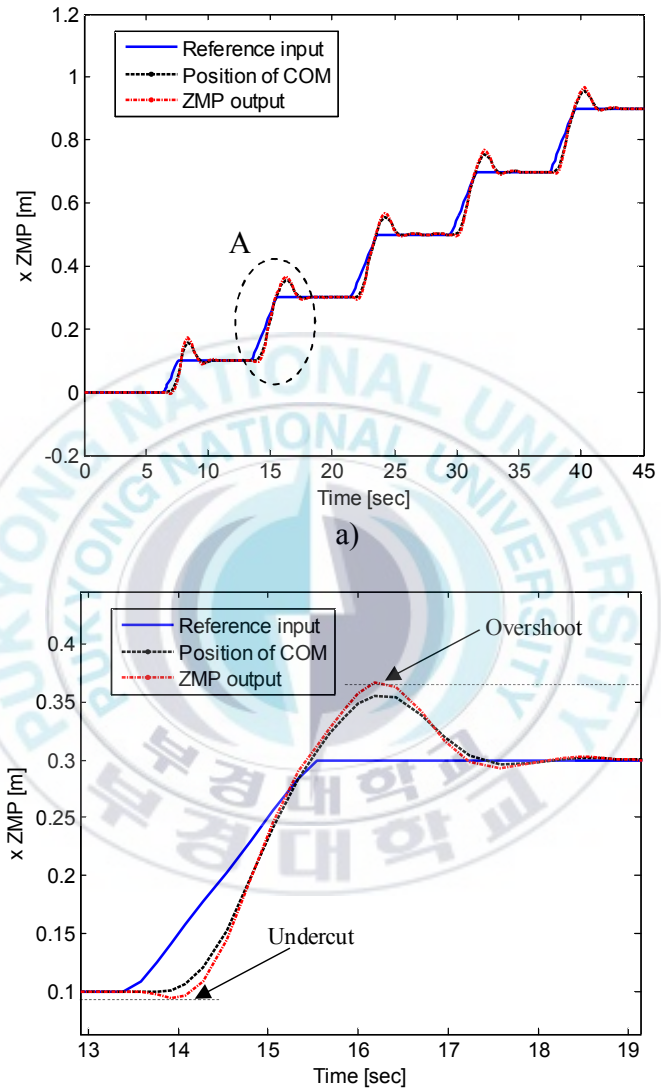

Fig. 3.8: *x* ZMP reference input, *x* ZMP output and position of COM.

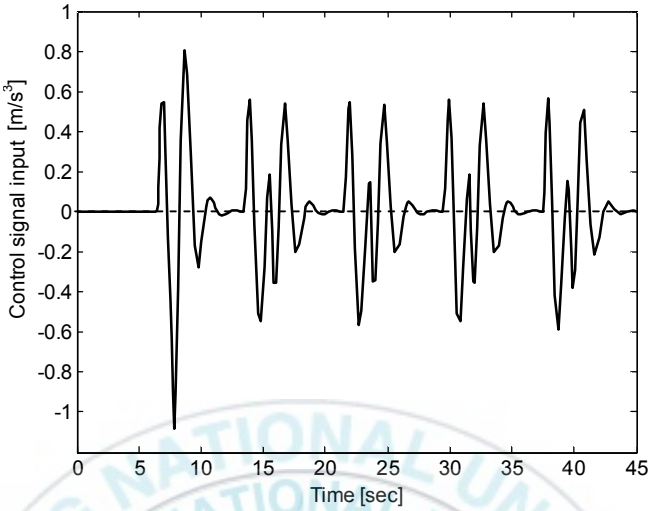

Fig. 3.9: Control signal input u_x.

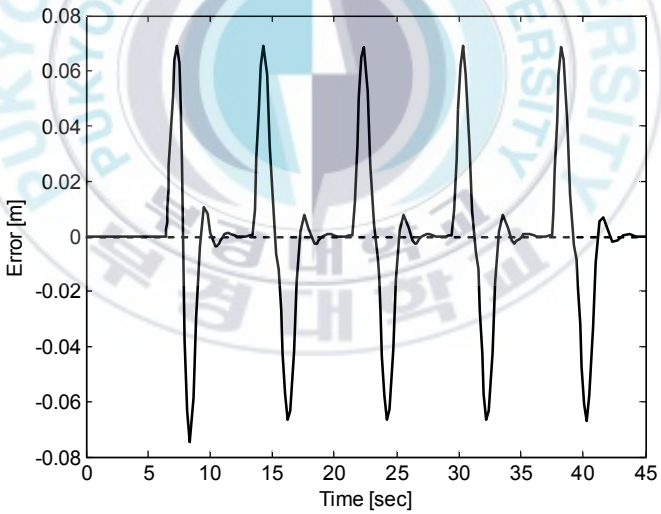

Fig. 3.10: *x* ZMP position error.

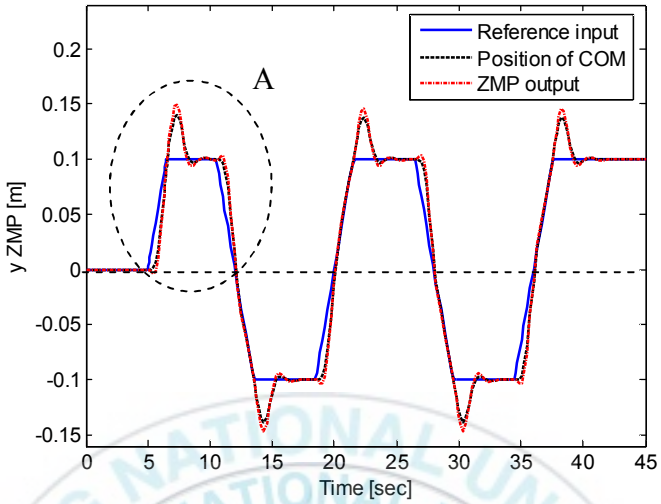

a)

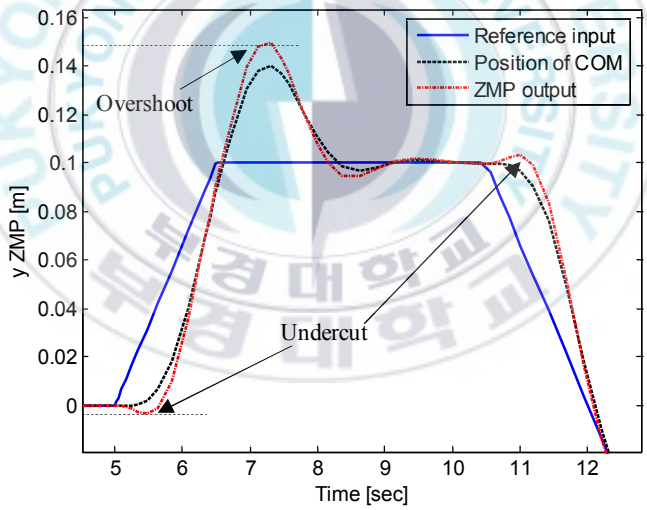

b) A region.

Fig. 3.11: *y* ZMP reference input, *y* ZMP output and position of COM.

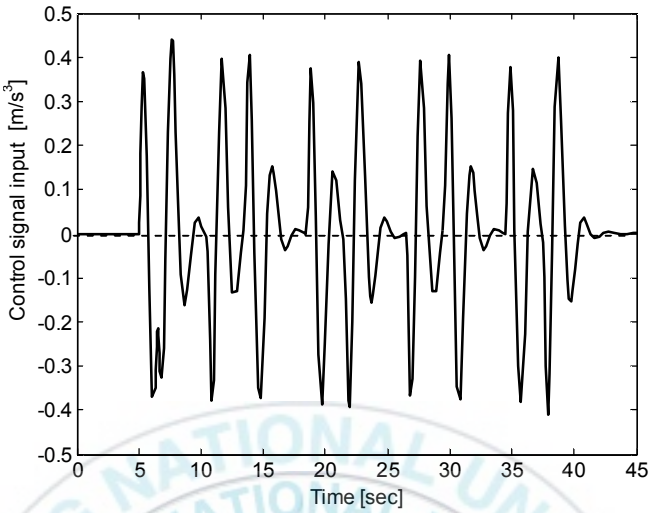

Fig. 3.12: Control signal input u_y.

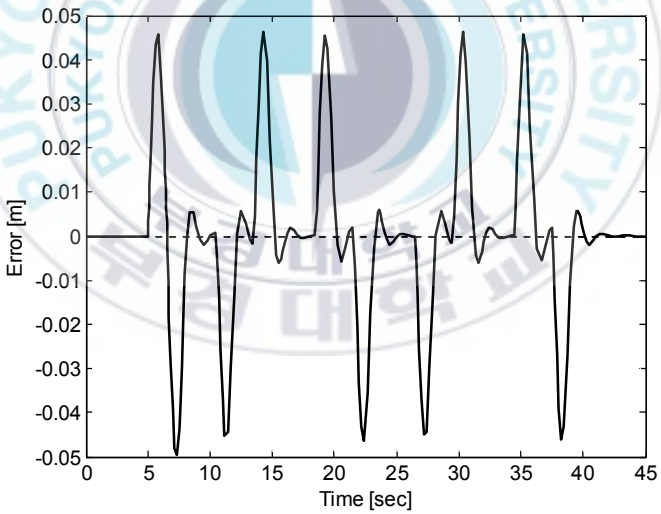

Fig. 3.13: *y* ZMP position error.

❖ **simulation results with $Q_{ec} = 10^8$:**

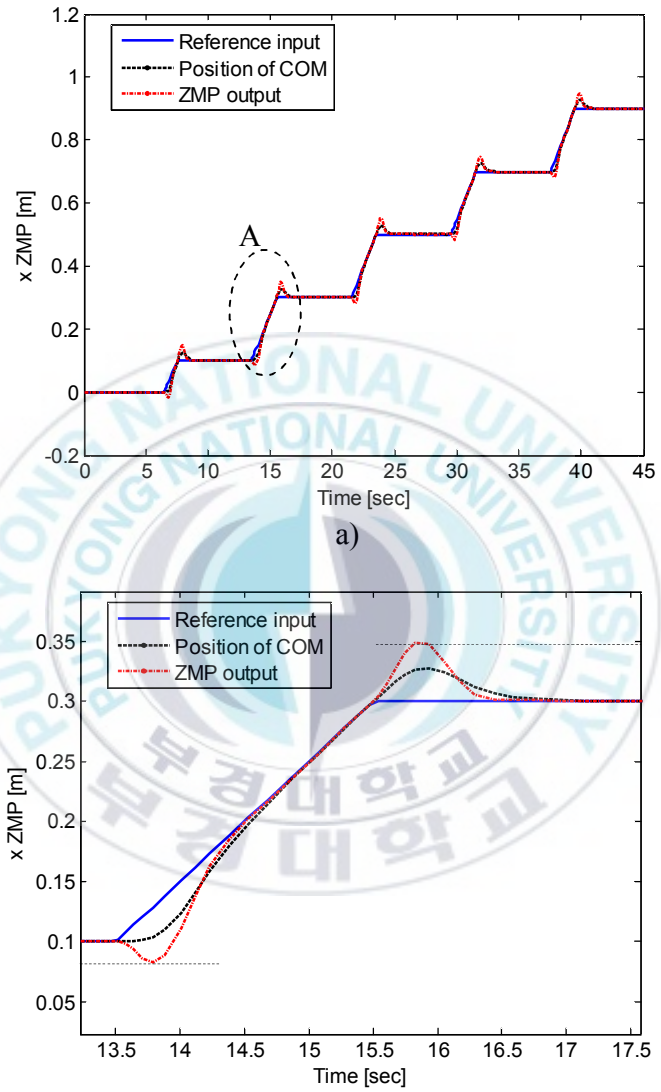

b) A region.

Fig. 3.14: *x* ZMP reference input, *x* ZMP output and position of COM.

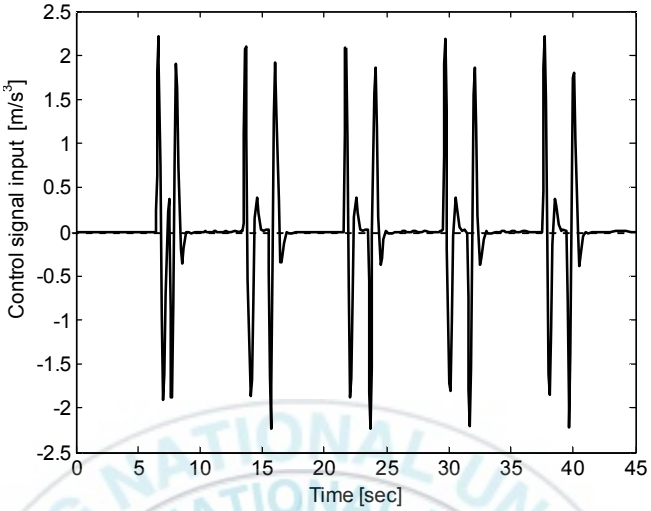

Fig. 3.15: Control signal input u_x.

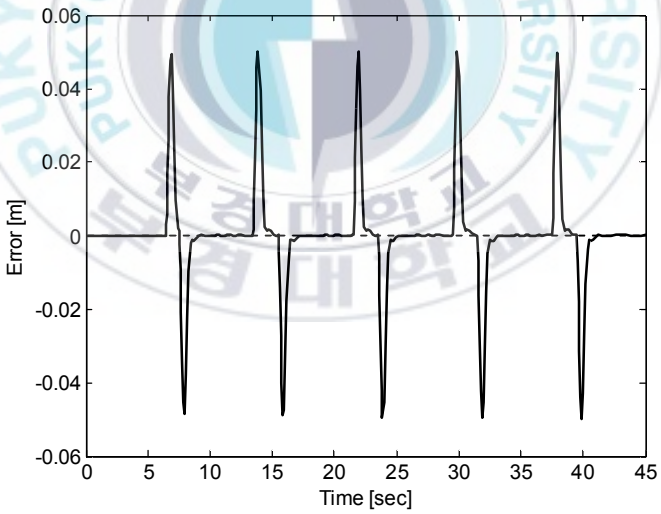

Fig. 3.16: *x* ZMP position error.

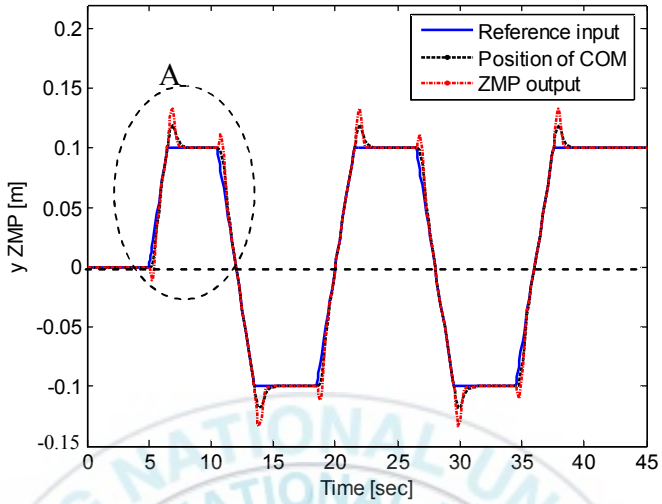

a)

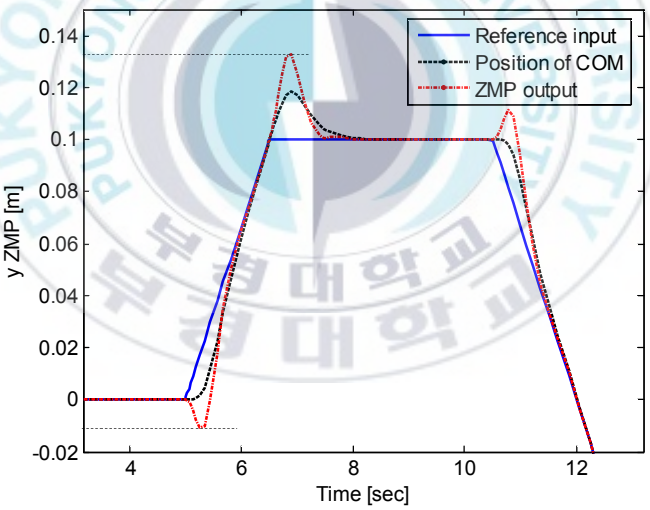

b) A region.

Fig. 3.17: *y* ZMP reference input, *y* ZMP output and position of COM.

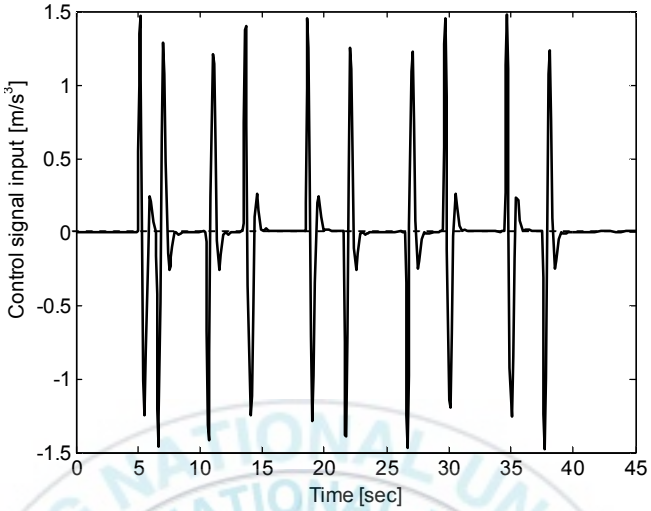

Fig. 3.18: Control signal input u_y.

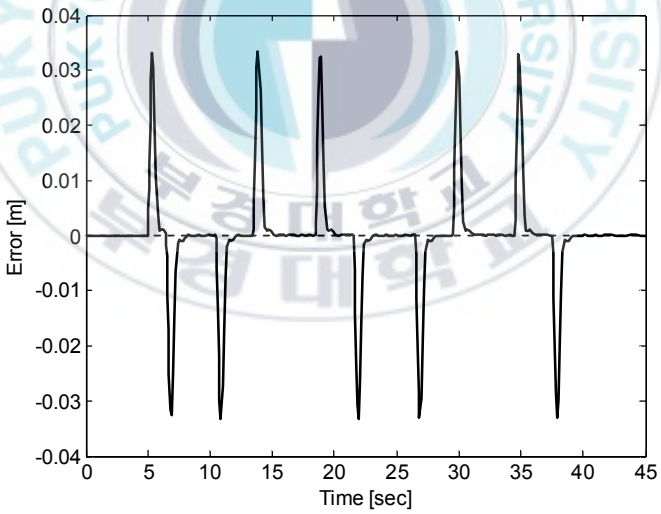

Fig. 3.19: *y* ZMP position error .

❖ **simulation results with $Q_{ec} = 10^{10}$:**

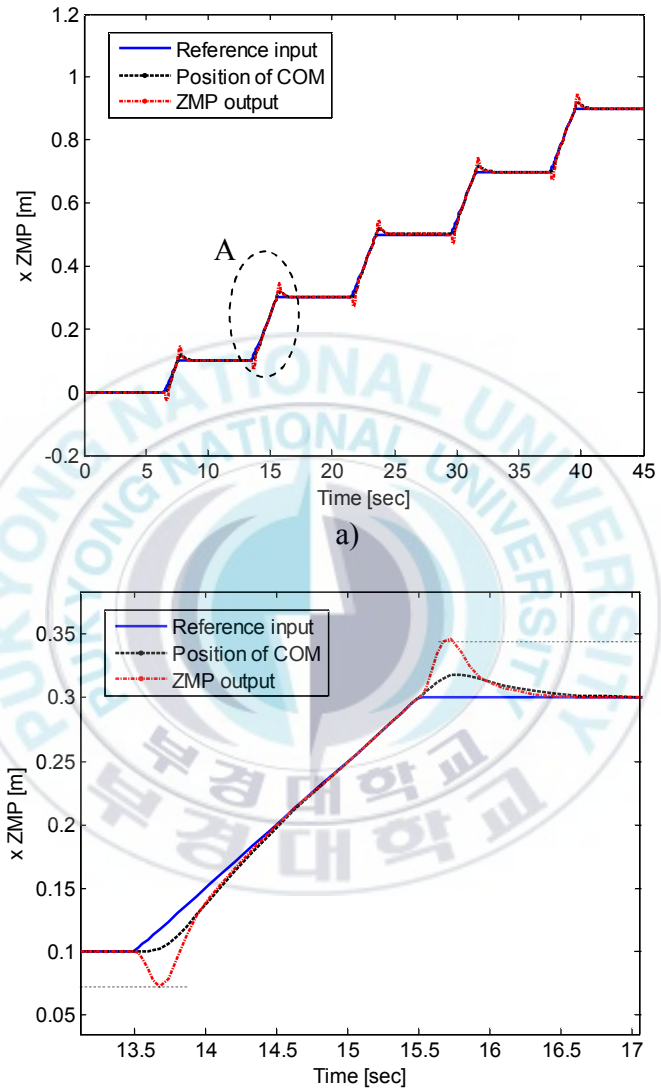

b) A region.

Fig. 3.20: *x* ZMP reference input, *x* ZMP output and position of COM.

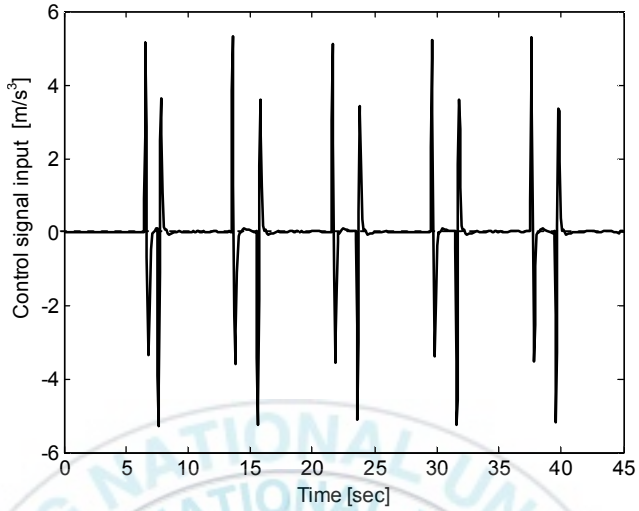

Fig. 3.21: Control signal input u_x.

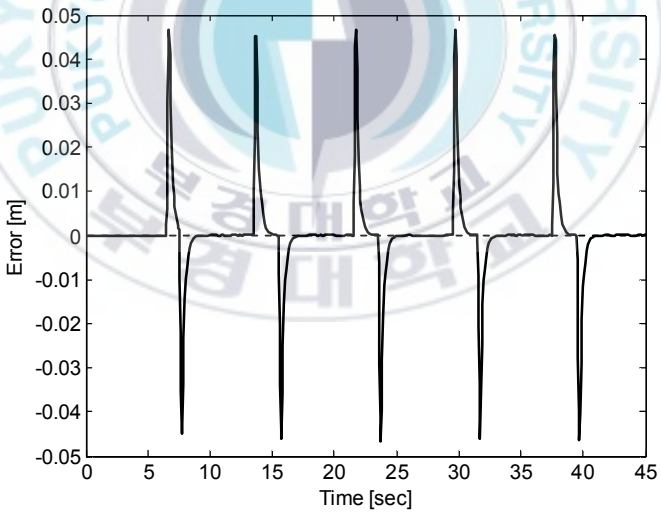

Fig. 3.22: *x* ZMP position error.

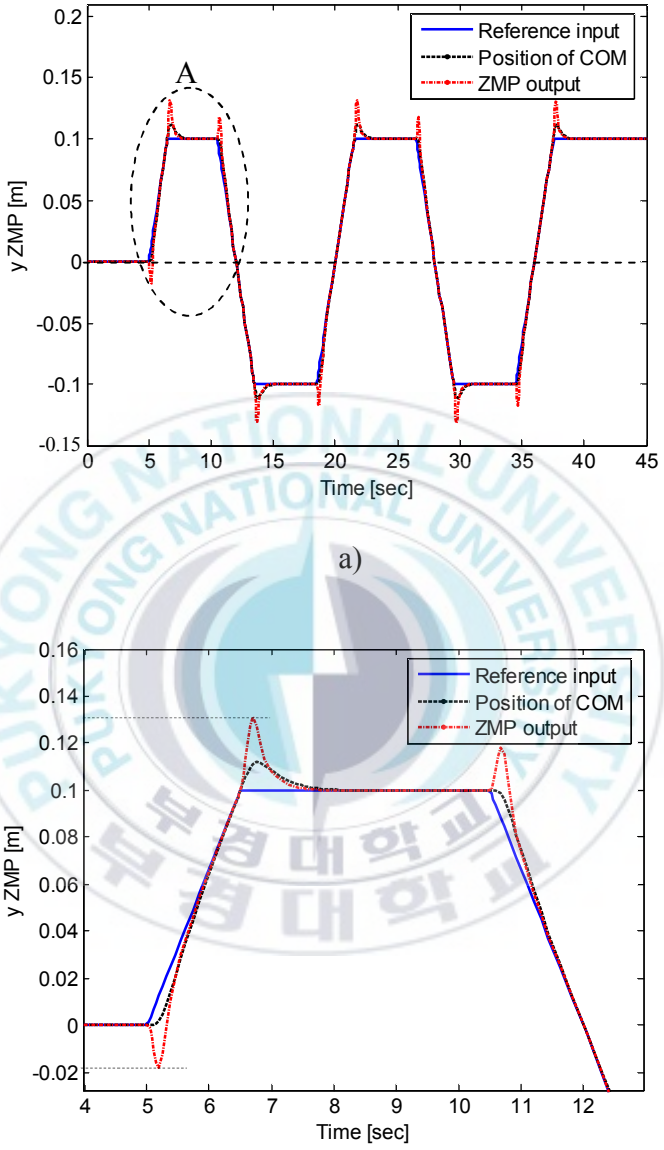

b) A region

Fig. 3.23: *y* ZMP reference input, *y* ZMP output and position of COM.

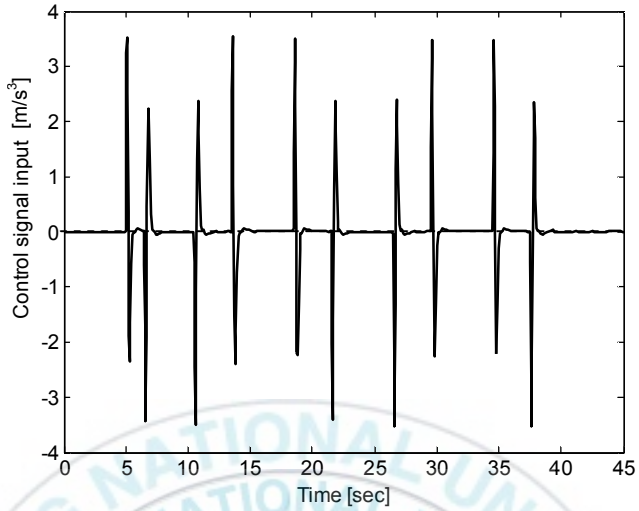

Fig. 3.24: Control signal input u_y.

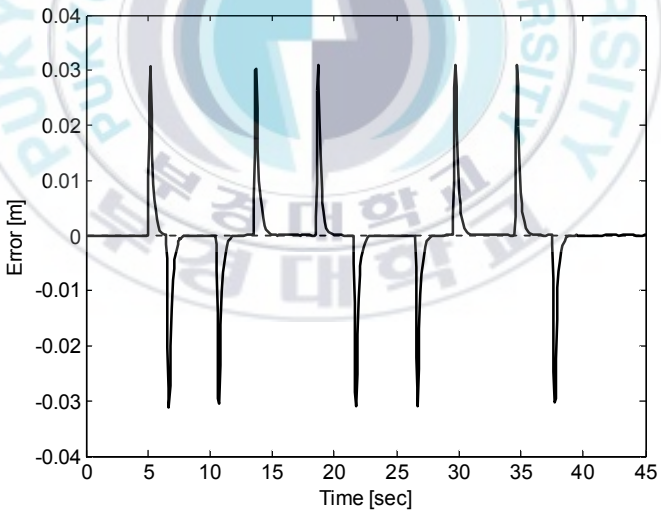

Fig. 3.25: *y* ZMP position error.

❖ **simulation results with $Q_{ec} = 10^{12}$:**

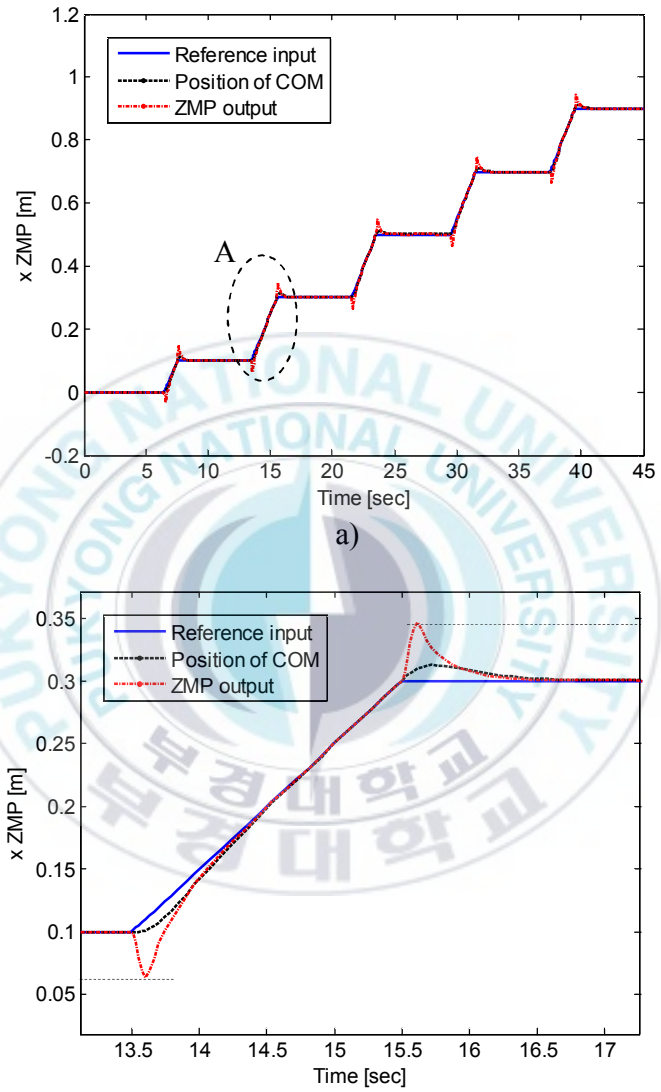

b) A region.

Fig. 3.26: *x* ZMP reference input, *x* ZMP output and position of COM.

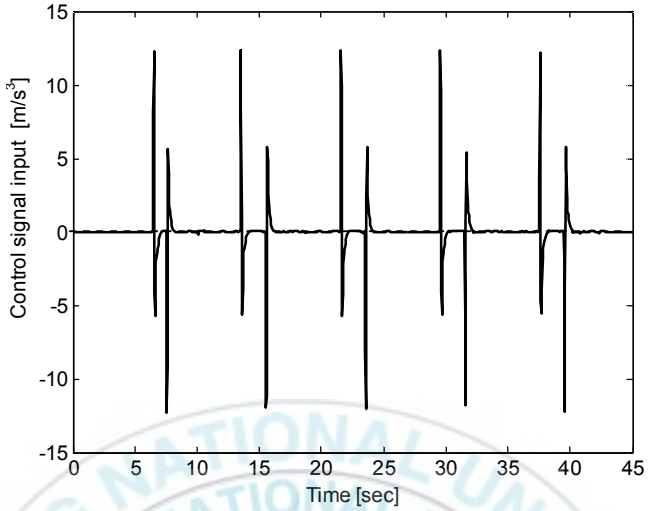

Fig. 3.27: Control signal input u_x.

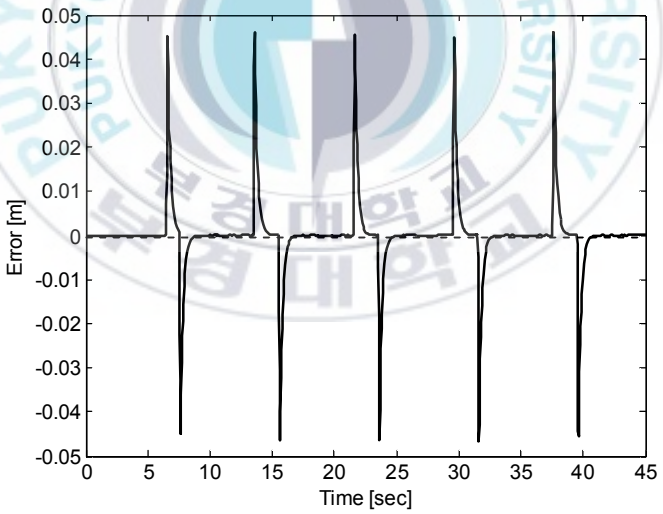

Fig. 3.28: *x* ZMP position error.

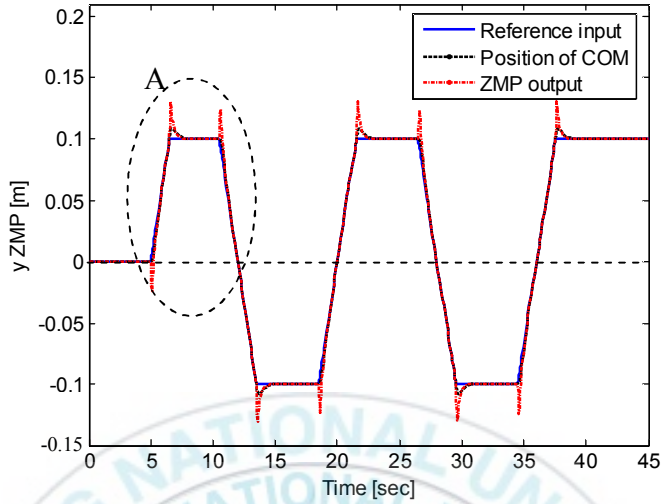

a)

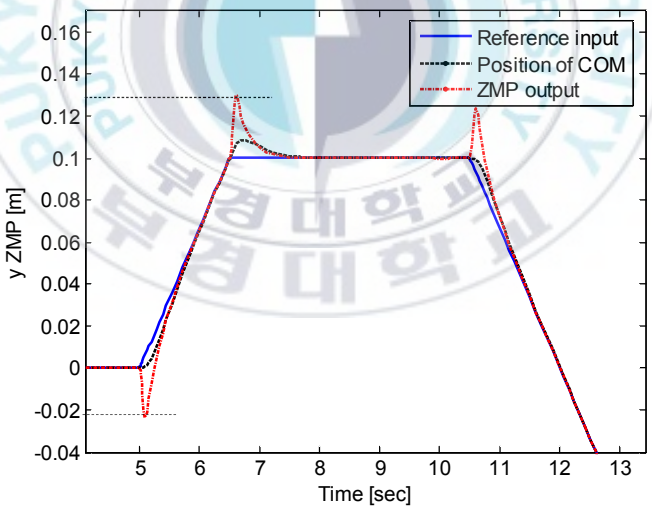

b) A region.

Fig. 3.29: *y* ZMP reference input, *y* ZMP output and position of COM.

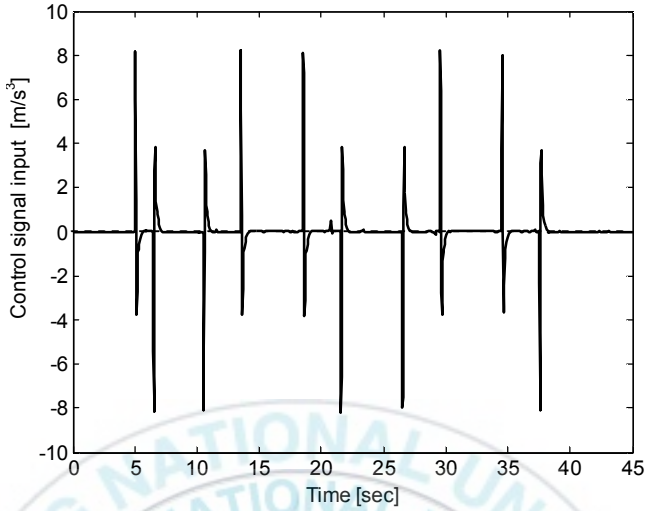

Fig. 3.30: Control signal input u_y.

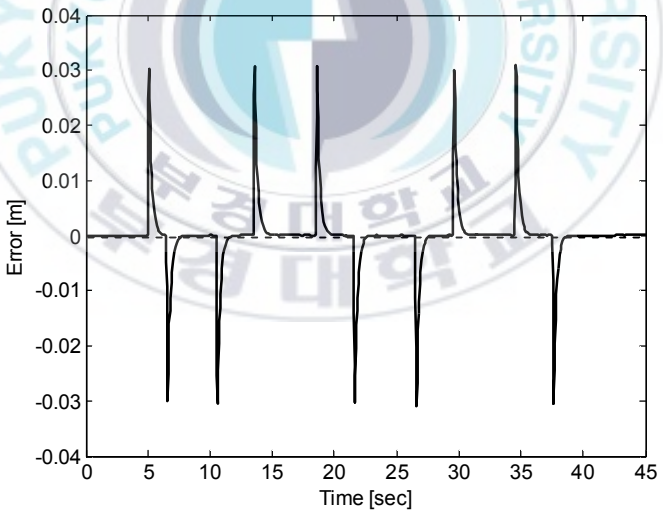

Fig. 3.31: *y* ZMP position error.

3.5.2 Simulation results of ZMP system using discrete time optimal tracking controller:

The discrete time systems (3.5) and (3.6) are considered to be sampled with sampling time T = 1 [ms]. By taking $\boldsymbol{A_d} = \boldsymbol{\Phi}(T)\big|_{T=0.001sec}$, $\boldsymbol{B_d} = \boldsymbol{\theta}(T)\big|_{T=0.001sec}$ and $\boldsymbol{C_d} = \boldsymbol{C}$, the systems (3.5) and (3.6) become

$$\begin{aligned} \boldsymbol{x_x}[(k+1)] &= \boldsymbol{A_d}\boldsymbol{x_x}(k) + \boldsymbol{B_d}u_x(k) \\ x_{zmp}(k) &= \boldsymbol{C_d}\boldsymbol{x_x}(k) \end{aligned} \tag{3.48}$$

$$\begin{aligned} \boldsymbol{x_y}[(k+1)] &= \boldsymbol{A_d}\boldsymbol{x_y}(k) + \boldsymbol{B_d}u_y(k) \\ y_{zmp}(k) &= \boldsymbol{C_d}\boldsymbol{x_y}(k) \end{aligned} \tag{3.49}$$

where $\boldsymbol{A_d} = \begin{bmatrix} 1 & 0.001 & 0.0000005 \\ 0 & 1 & 0.001 \\ 0 & 0 & 1 \end{bmatrix}$ $\boldsymbol{B_d} = [0.0000000001667 \quad 0.0000005 \quad 1]^T$

$\boldsymbol{C_d} = [1 \quad 0 \quad -0.05]$

By choosing $R = 1$, $\boldsymbol{Q} = \left[\begin{array}{c|c} 0.12 & \boldsymbol{0}_{1\times3} \\ \hline \boldsymbol{0}_{3\times1} & \boldsymbol{0}_{3\times3} \end{array}\right]$ and using digital optimal control toolbox of Matlab, $\boldsymbol{K_{1x}}$ and K_{1e} can be obtained as $-\boldsymbol{K_{1x}} = [144.6 \quad 33.096 \quad 0.21025]$ and K_{1e} = 0.3142. The feed-forward gain K_2 depending on the number of the future values of the reference input illustrate in Fig. 3.32. It is shown that the feed-forward gain $\boldsymbol{K_2}$ converges to zero when the number of the future values N is larger than 1000.

The controller (3.47) is rewritten as follows:

$$u_x(k) = \boldsymbol{K}_{1e}\frac{z}{z-1}e_x(k) + \boldsymbol{K_{1x}}\boldsymbol{x}_x(k) + \sum_{i=1}^{N}\boldsymbol{K_2}(i)\,r_x(k+i) \tag{3.50}$$

$$u_y(k) = \boldsymbol{K}_{1e}\frac{z}{z-1}e_y(k) + \boldsymbol{K_{1x}}\boldsymbol{x}_y(k) + \sum_{i=1}^{N}\boldsymbol{K_2}(i)\,r_y(k+i) \tag{3.51}$$

where $e_x(k) = r_x(k) - x_{zmp}(k)$ and $e_y(k) = r_y(k) - y_{zmp}(k)$

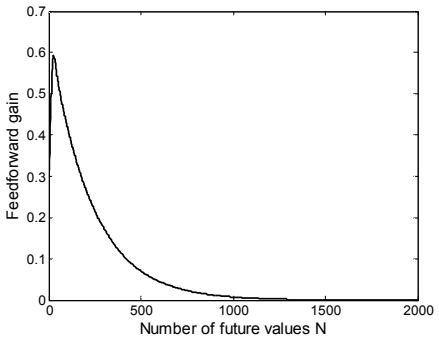

Fig. 3.32: Relation between feed-forward gain K_2 and N.

The simulation results of the discrete time systems based on reference input in Fig. 3.4 with the different values of N are presented as shown in Figs. 3.33~3.62.

Figs. 3.34, 3.40, 3.46, 3.52 and 3.58 and Figs. 3.37, 3.43, 3.49, 3.55 and 3.61 present the control signal inputs u_x and u_y corresponding with the number of the future values of the reference input of the x and y ZMP tracking control system controlled by the designed optimal discrete time tracking controller. As shown in these figures, all control signal inputs u_x and u_y are bounded.

Figs. 3.35, 3.41, 3.47, 3.53 and 3.59 and Figs. 3.38, 3.44, 3.50, 3.56 and 3.62 illustrate the error between the reference inputs and the outputs of the x and y ZMP tracking control systems controlled by the designed optimal discrete time tracking controller. As shown in these figures, when the reference inputs are not changed, the errors converge to zero. The errors occur at singular points and in the ramp segments of the reference input when N is smaller than 1000. However, when N is larger than 1000, the errors appear only at the singular point of the reference input and have negative values. This means that the outputs of the x and y ZMP tracking control systems have very small overshoot and undercut as shown in Figs 3.59 and 3.62.

These figures show that the maximum errors at singular point of the reference are about 0.3 [mm] and 0.2 [mm] for the x and y ZMP tracking control systems. In Figs. 3.35, 3.41, 3.47, 3.53 and 3.59 and Figs. 3.38, 3.44, 3.50, 3.56 and 3.62, the maximum value of the error is decreased when N is increased.

Figs. 3.33, 3.39, 3.45, 3.51 and 3.57 and Figs. 3.36, 3.42, 3.48, 3.54 and 3.60 present the reference inputs, the ZMP outputs and positions of the COM of the x and y ZMP optimal tracking control system corresponding with the different values of the future value N. As shown in these figures, when the number of the future values of the reference input is smaller than 1000, the tracking performance of the outputs of the x ZMP and y ZMP tracking control systems to the ramp segments of the reference inputs is not good. The outputs of the x ZMP and y ZMP tracking control systems do not converge to the ramp segments of the reference inputs. The outputs of the x ZMP and y ZMP tracking control systems have no overshoot but have small undercut. When the number of the future values of the reference input is larger than 1000, the good tracking performance of the x ZMP and y ZMP tracking control systems to the ramp segments of the reference inputs is shown. The outputs of the x ZMP and y ZMP tracking control systems converge to the ramp segments of the reference inputs and have no undercut and overshoot. However, if the number of the future values of the reference input is too large, the calculating time is long. The number of the future values of the reference input should be chosen to satisfy the short calculating time and the good tracking performance. As shown in Fig. 3.32, the future values of the reference input have no influence on the controller because $\boldsymbol{K_2}$ converges to zero when the number of the future values of the reference input is larger than 1000. To control for discrete time systems (3.48) and (3.49), $N = 1200$ is chosen.

❖ **Simulation results with** $N = 0$**:**

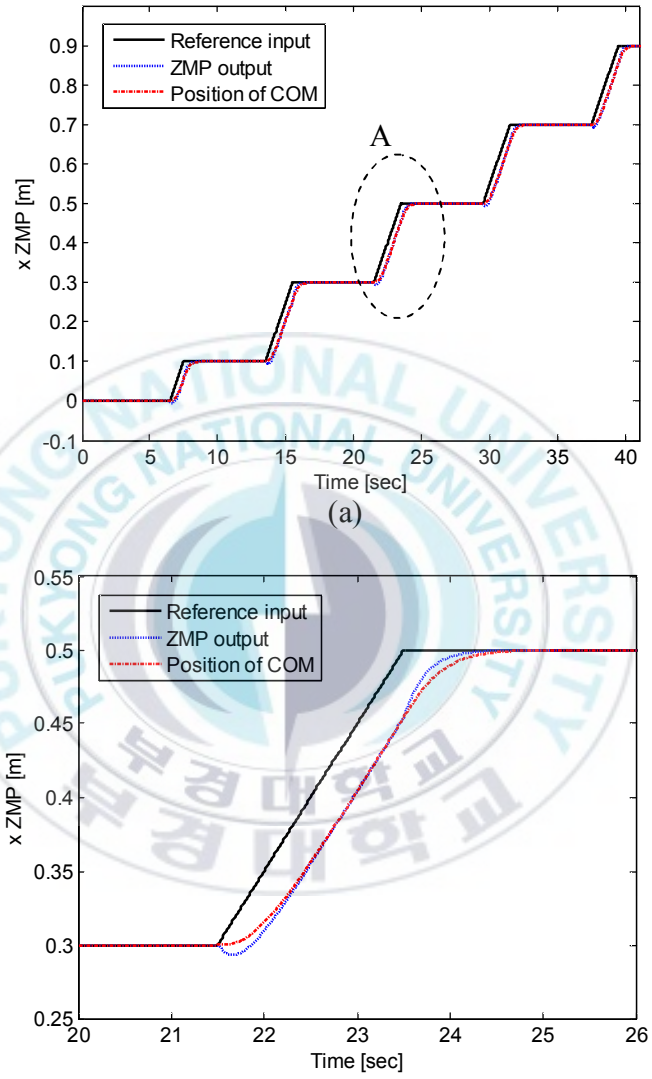

(a)

(b) A region.

Fig. 3.33: *x* ZMP reference input, *x* ZMP output and position of COM.

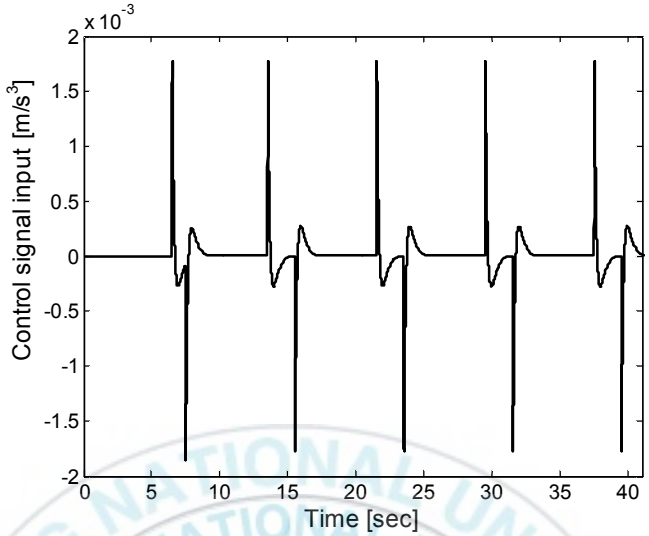

Fig. 3.34: Control signal input u_x.

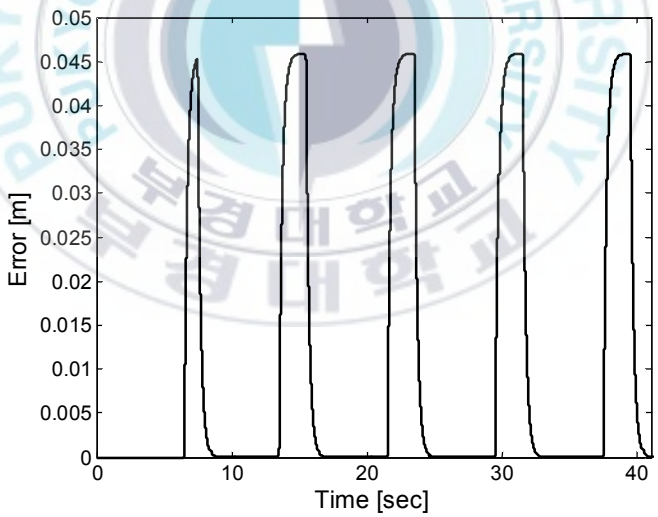

Fig. 3.35: *x* ZMP position error.

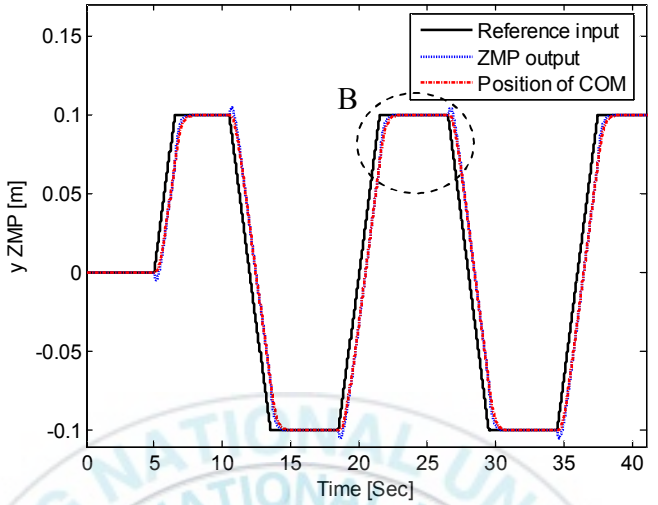

(a)

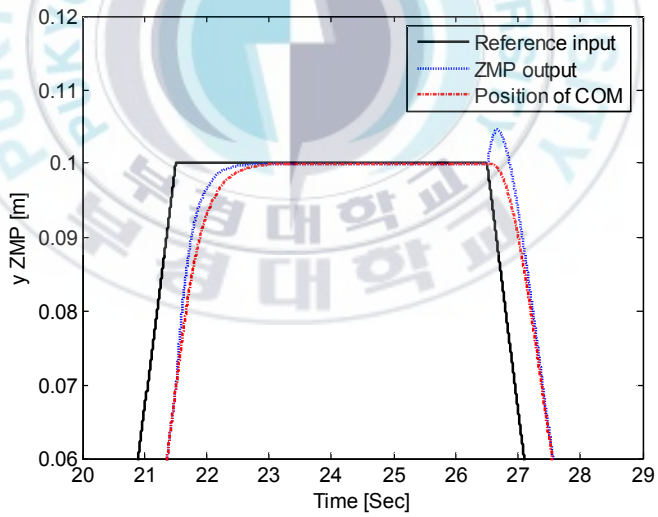

(b) B region.

Fig. 3.36: *y* ZMP reference input, *y* ZMP output and position of COM.

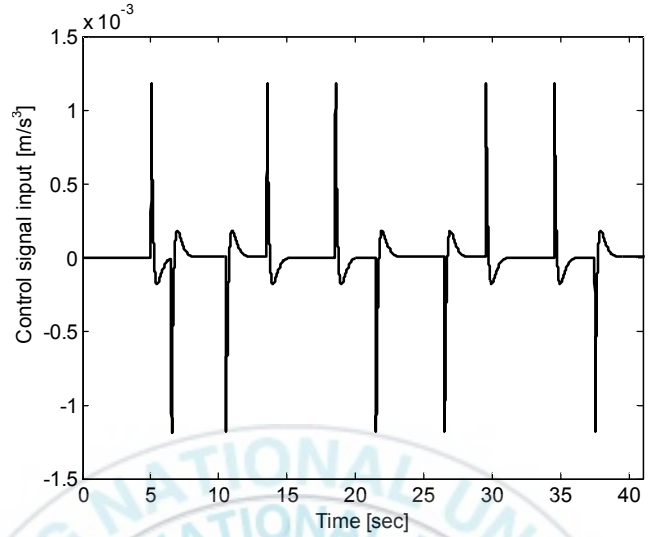

Fig. 3.37: Control signal input u_y.

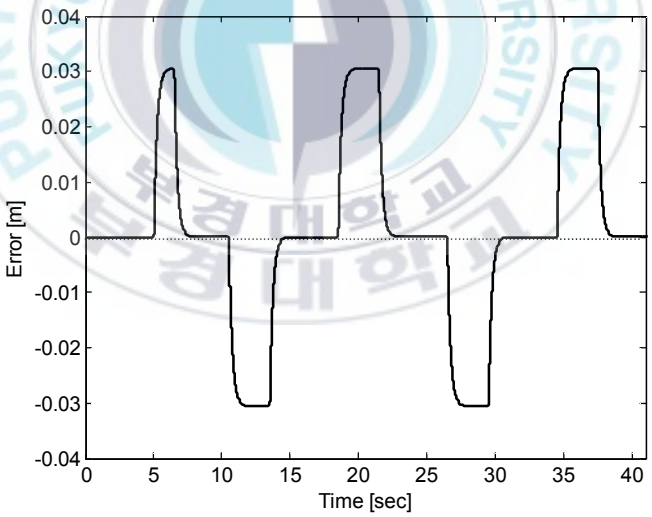

Fig. 3.38: *y* ZMP position error.

❖ **Simulation results with** $N = 10$ **:**

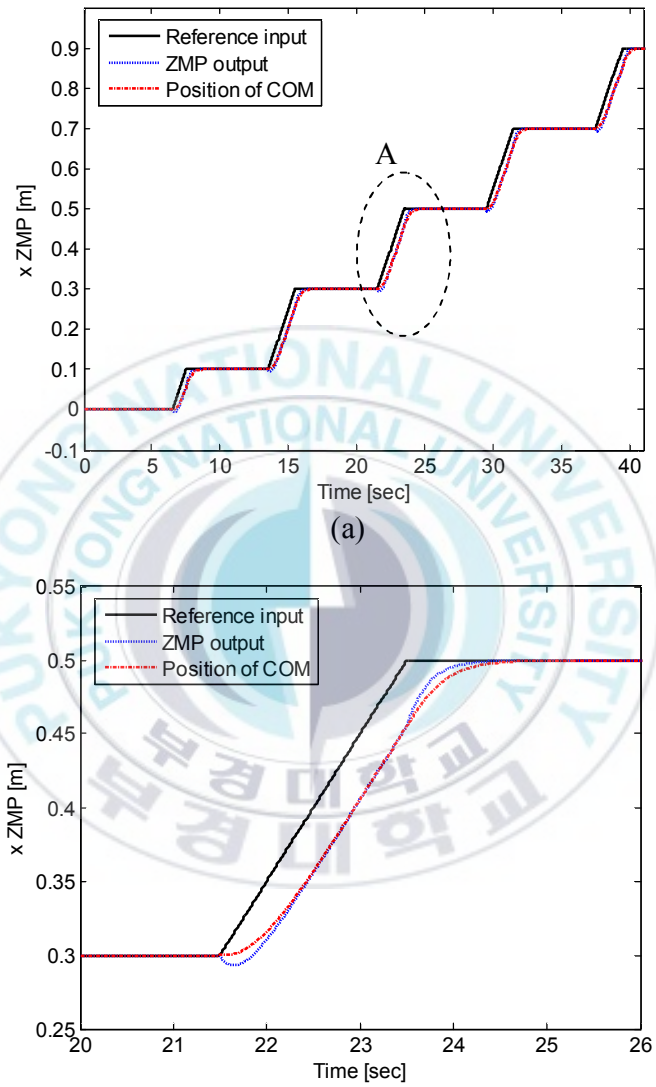

(b) A region.

Fig. 3.39: *x* ZMP reference input, *x* ZMP output and position of COM.

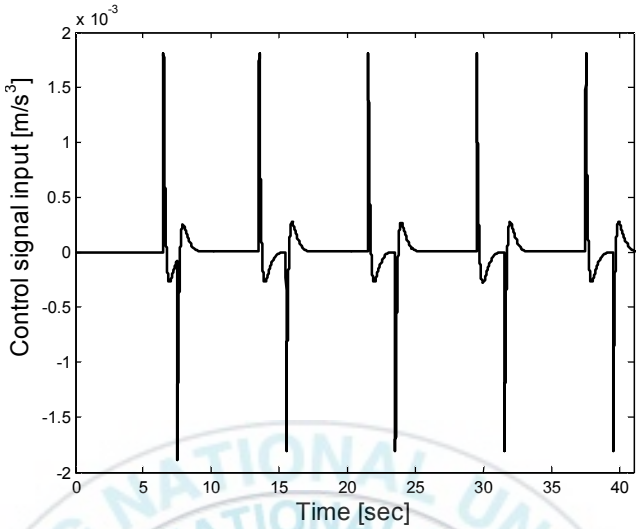

Fig. 3.40: Control signal input u_x.

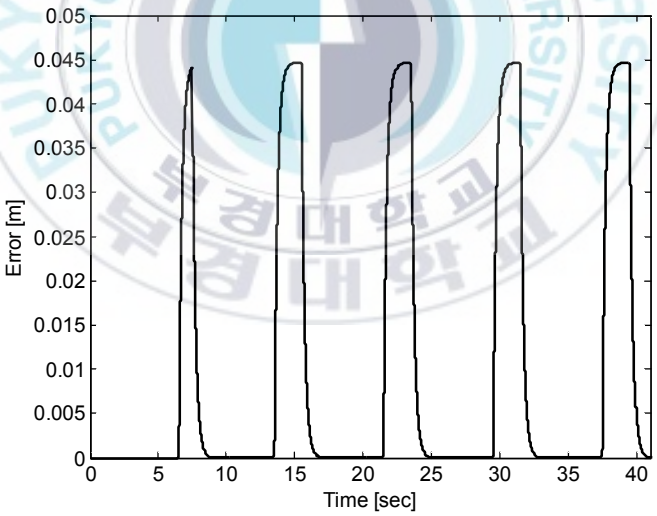

Fig. 3.41: *x* ZMP position error.

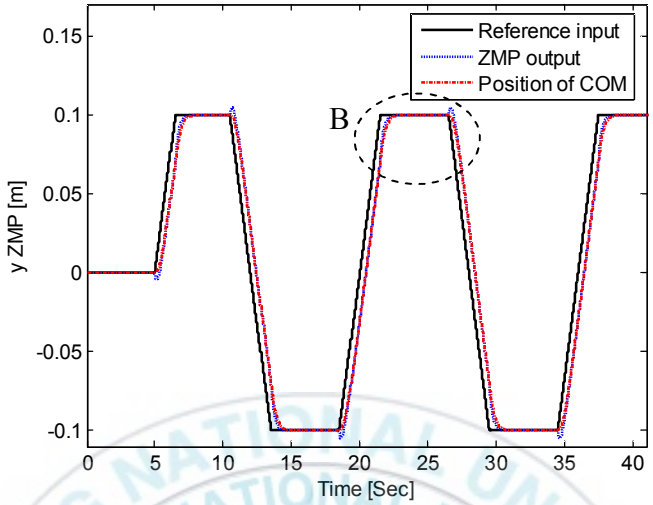

(a)

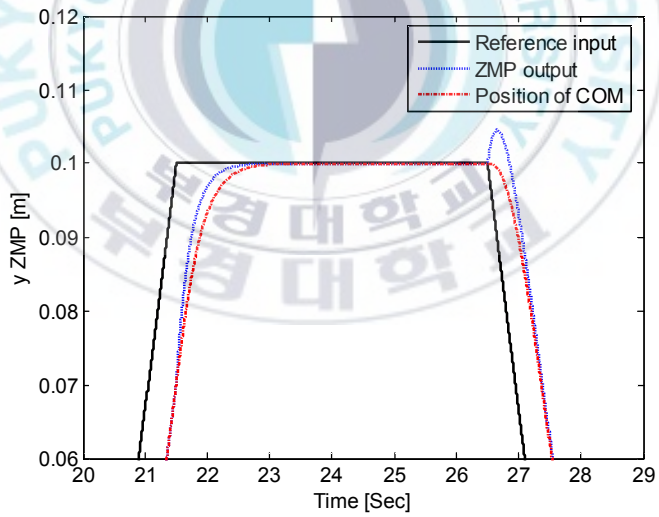

(b) B region.

Fig. 3.42: *y* ZMP reference input, *y* ZMP output and position of COM.

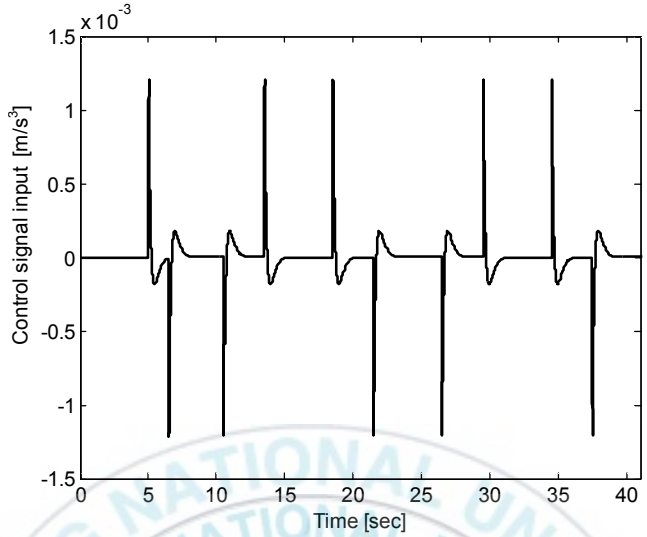

Fig. 3.43: Control signal input u_y.

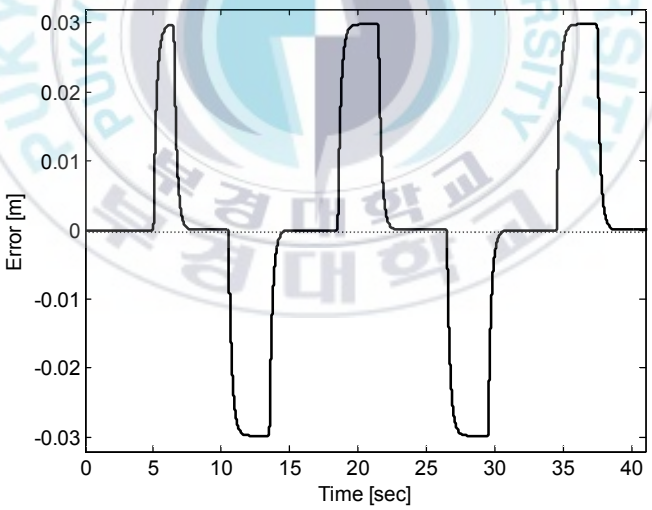

Fig. 3.44: *y* ZMP position error.

❖ **Simulation results with** $N = 500$ **:**

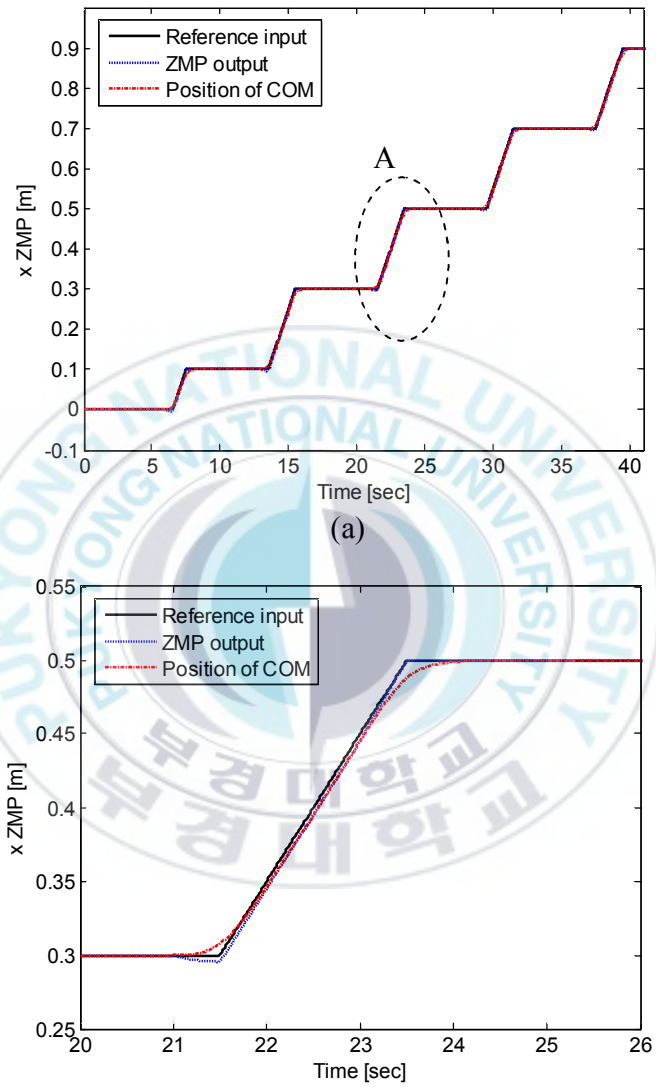

(b) A region.

Fig. 3.45: *x* ZMP reference input, *x* ZMP output and position of COM.

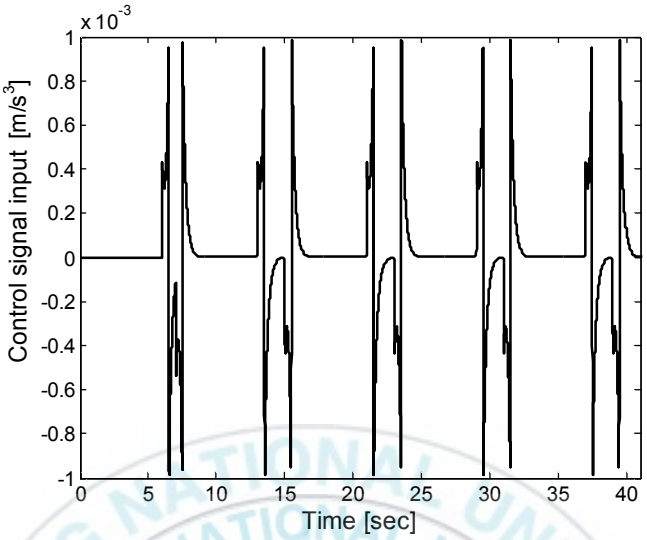

Fig. 3.46: Control signal input u_x.

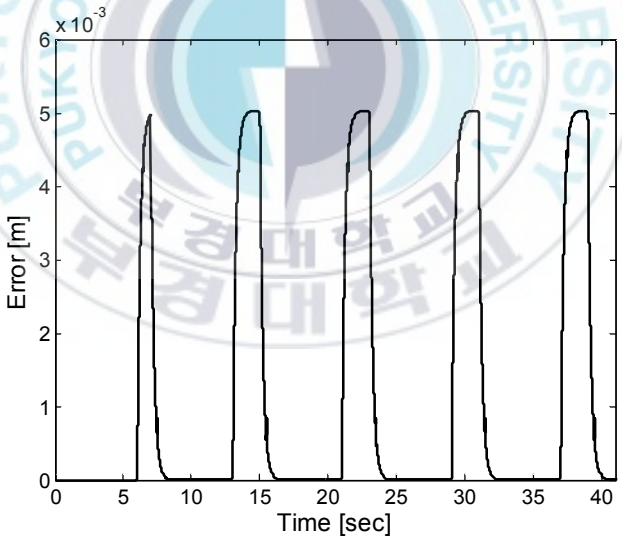

Fig. 3.47: *x* ZMP position error.

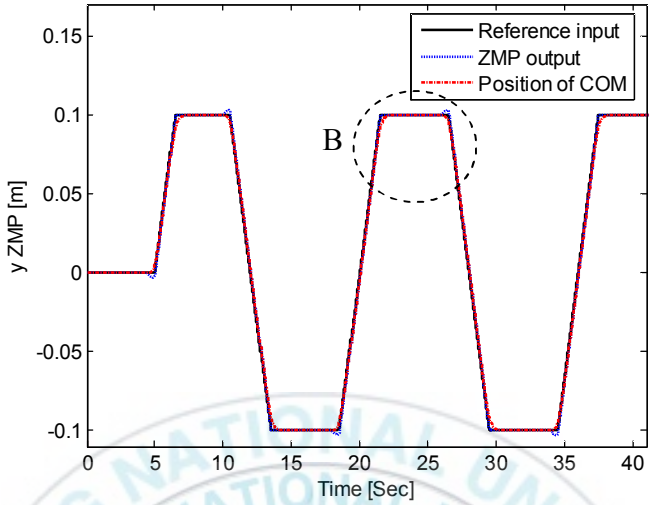

(a)

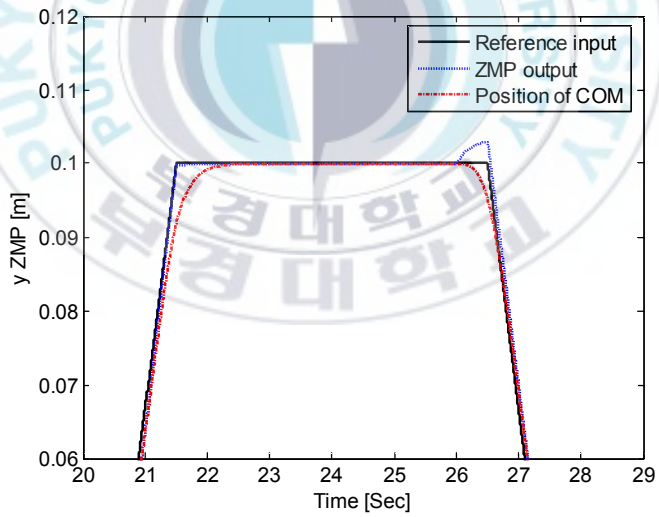

(b) B region.

Fig. 3.48: *y* ZMP reference input, *y* ZMP output and position of COM.

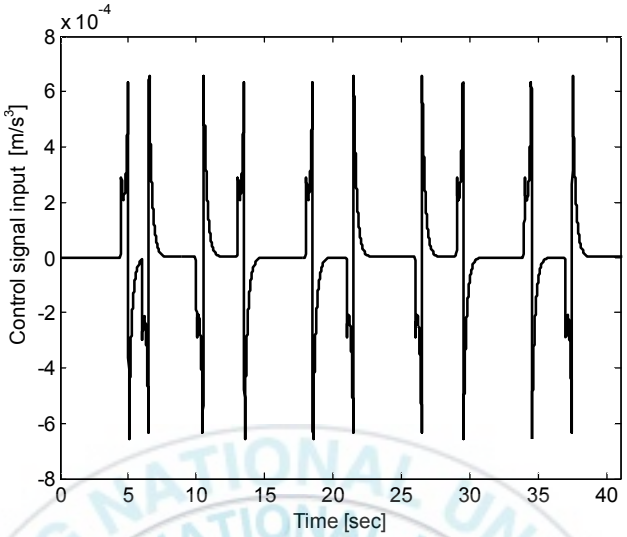

Fig. 3.49: Control signal input u_y.

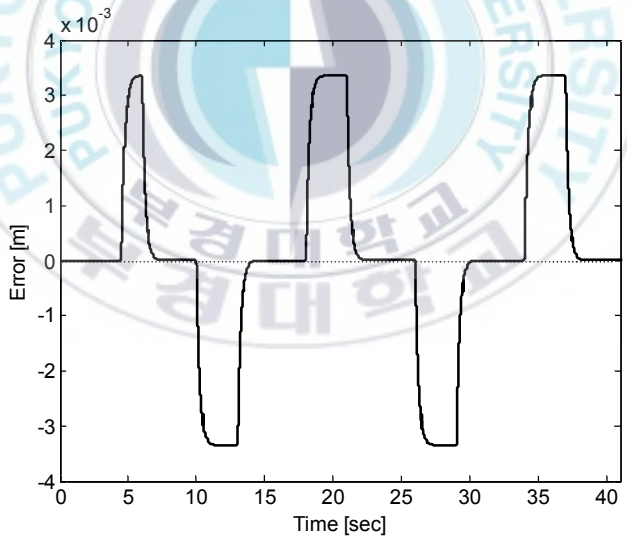

Fig. 3.50: *y* ZMP position error.

❖ **Simulation results with** $N = 1000$ **:**

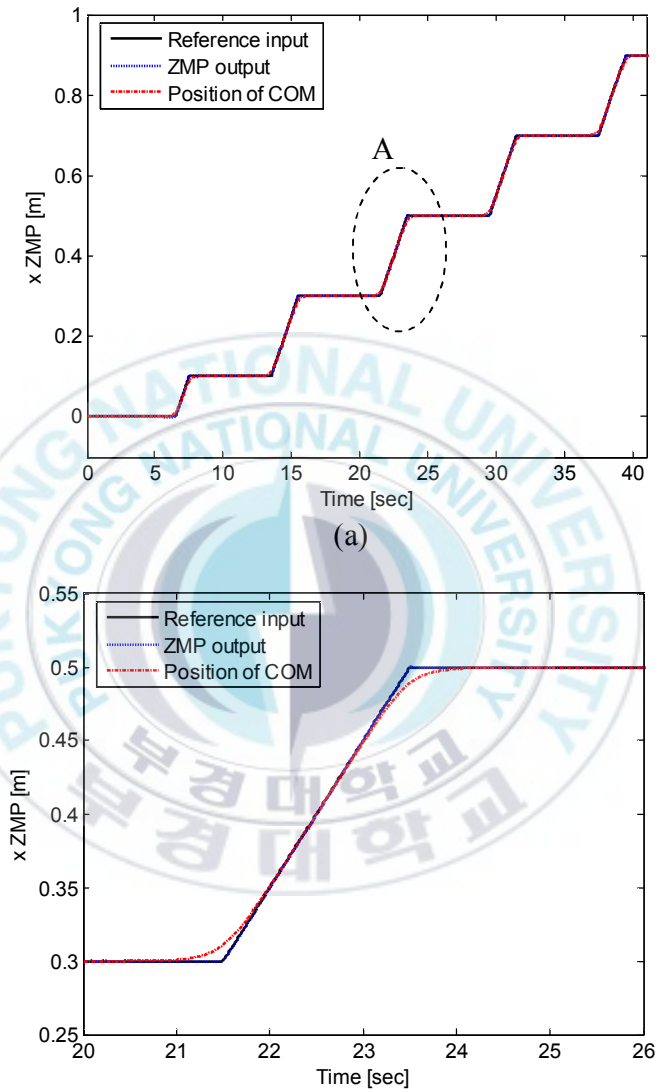

(b) A region.

Fig. 3.51: *x* ZMP reference input, *x* ZMP output and position of COM.

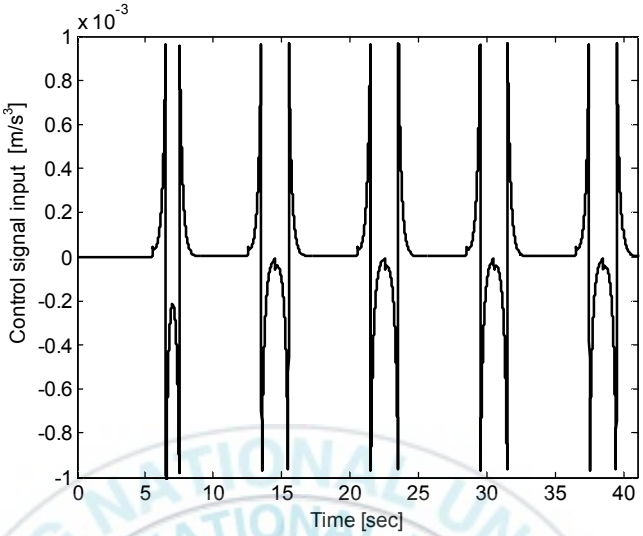

Fig. 3.52: Control signal input u_x.

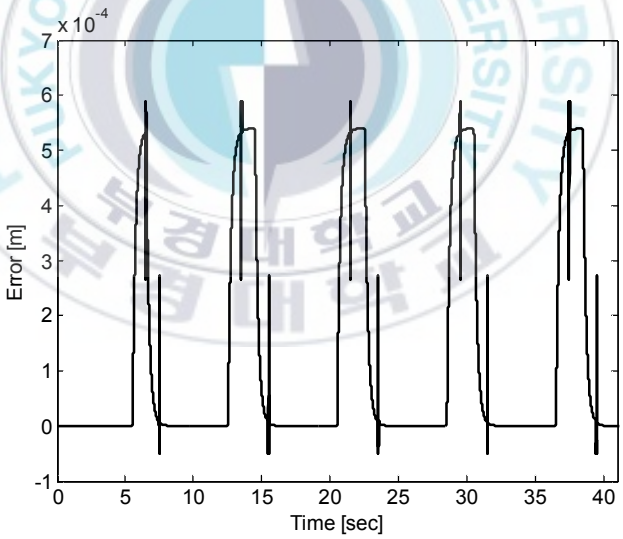

Fig. 3.53: *x* ZMP position error.

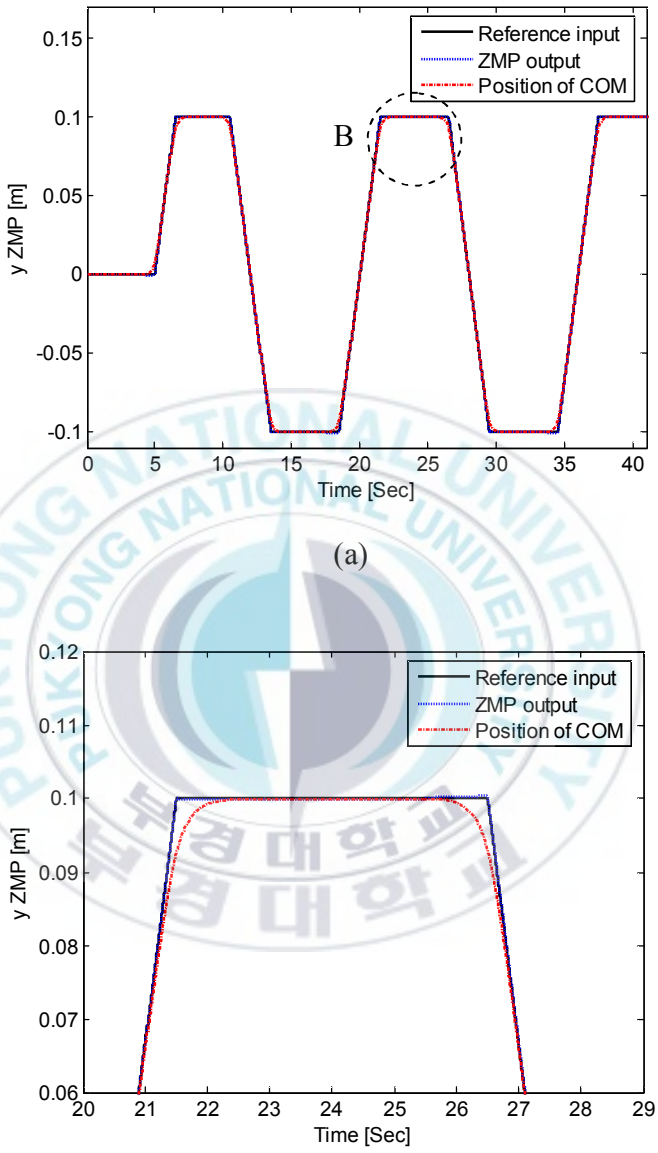

(a)

(b) B region.

Fig. 3.54: *y* ZMP reference input, *y* ZMP output and position of COM.

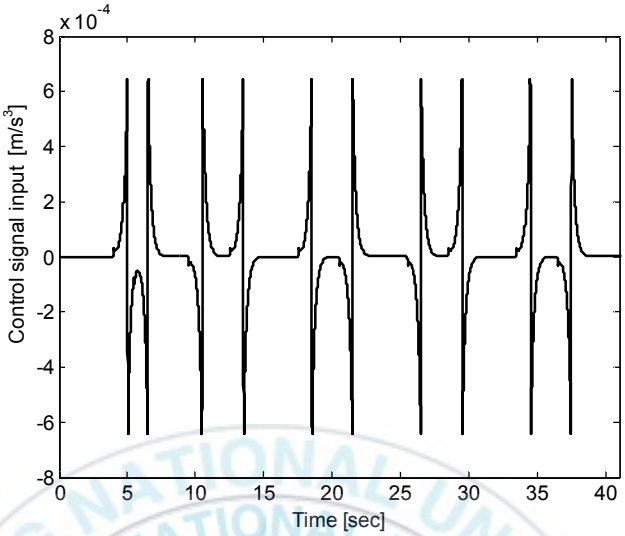

Fig. 3.55: Control signal input u_y.

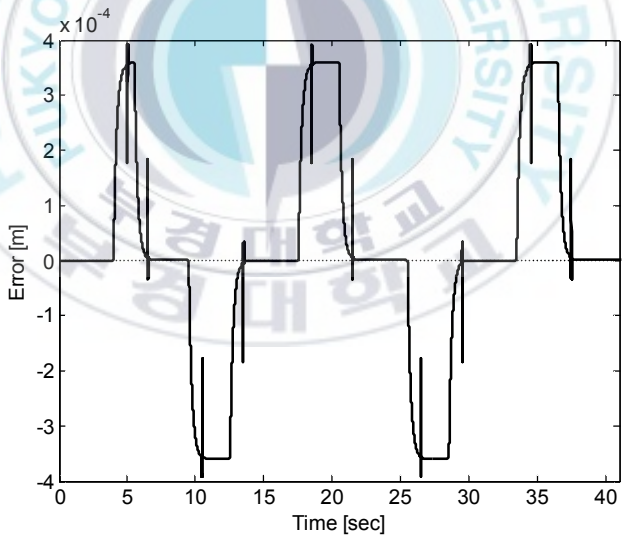

Fig. 3.56: *y* ZMP position error.

❖ **Simulation results with** $N = 2000$ **:**

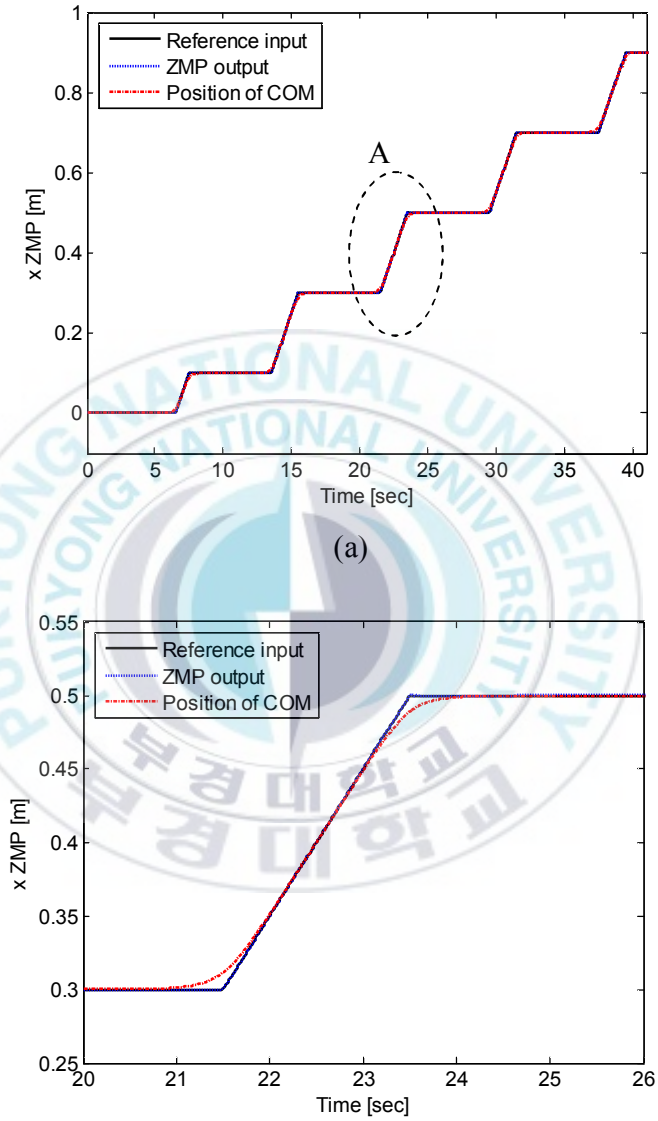

(b) A region.

Fig. 3.57: *x* ZMP reference input, *x* ZMP output and position of COM.

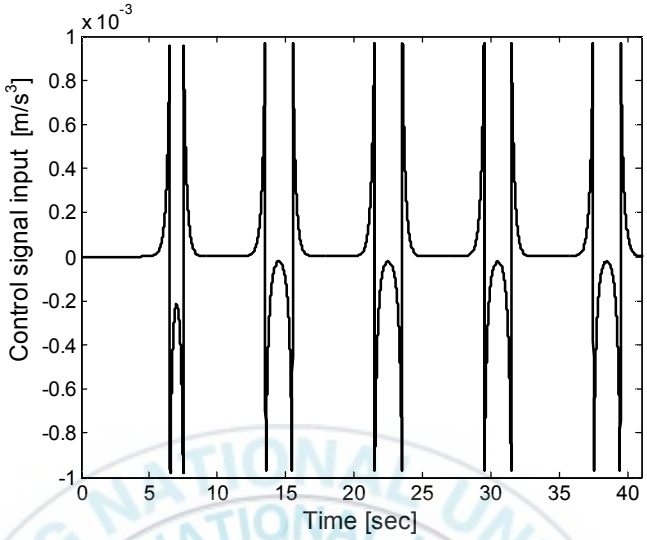

Fig. 3.58: Control signal input u_x.

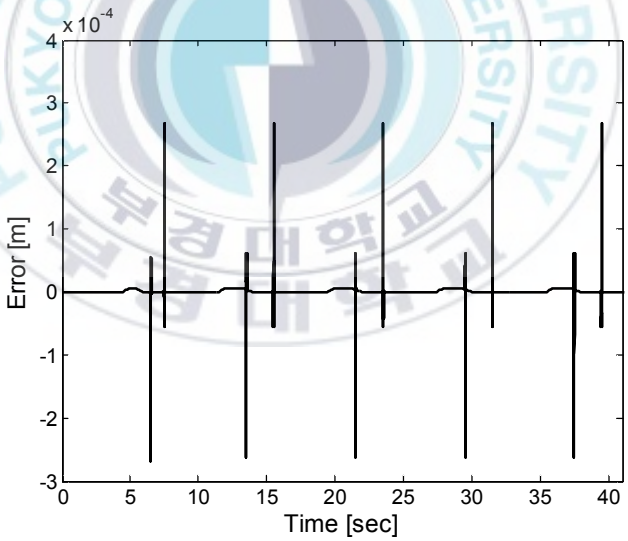

Fig. 3.59: *x* ZMP position error.

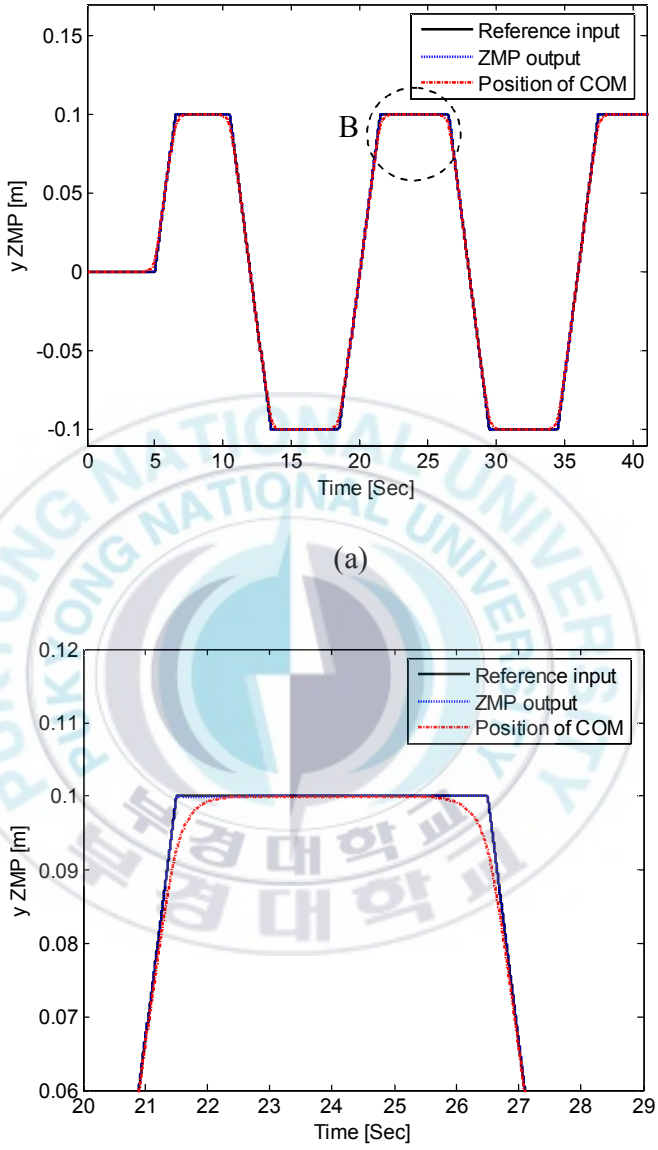

(a)

(b) region.

Fig. 3.60: *y* ZMP reference input, *y* ZMP output and position of COM.

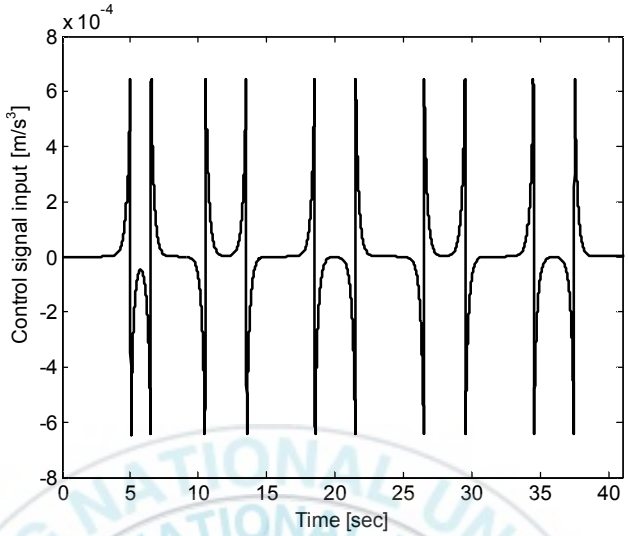

Fig. 3.61: Control signal input u_y.

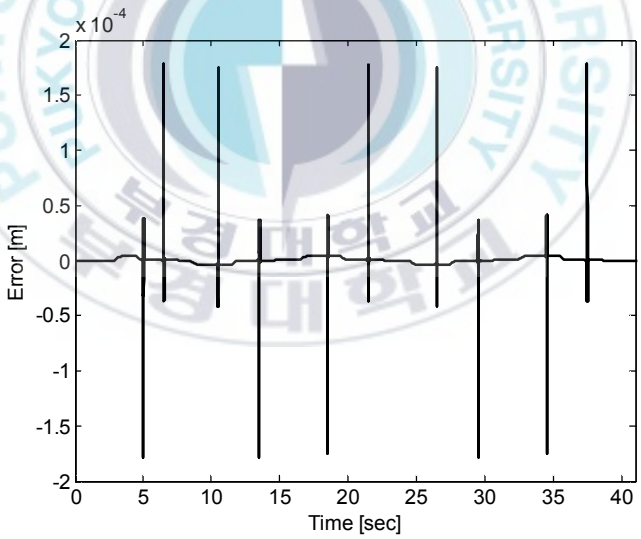

Fig. 3.62: *y* ZMP position error.

3.5.3 Comparison of designed optimal tracking control systems and discussion:

The comparison between the designed continuous time optimal tracking control system and the discrete time optimal tracking control system utilizing the future values of the reference input is summarized as shown in Table 3.3.

Table 3.3 Comparison of designed optimal tracking control systems

Specific characteristics	Designed continuous time	Designed discrete time
Steady state error between the reference and the output	Zero	Zero
Error between the reference and the output at the singular points of the reference input	Large	Very small
Overshoot	Large	Very small
Tracking performance	Good	Very good
Calculation time	Short	Long
Structure of controller	Double-integration	One-summation
Utilizing the future values of the reference	Difficult	Easy

The output of the continuous time control system is similar or better than that of the discrete time control system when the controllers have the same structure because the continuous time system is the discrete time system sampled with the sampling time $T = 0$ and is continuously controlled by the controller.

In the case that the future values of the reference input are not utilized, the controllers are obtained only from state variables and one-integration of the error in the case of continuous time and from state variables and one-summation of the error

in the case of discrete time. This means that the continuous time and discrete time controllers have the same structure and these controllers are designed to track the step reference input. In this case, the tracking performance of the outputs of the systems using these controllers to the ramp reference input can not be guaranteed because the internal model principle is not satisfied. As shown in Figs. 3.33 and 3.36, the output of the discrete time ZMP tracking control system using the discrete time controller obtained only from state variables and one summation of the error tracks the step segments of the reference input and has no overshoot but this output cannot track the ramp segments of the reference input. The output of the continuous time ZMP tracking control system using the same structure controller also tracks the step segments of the reference input, has no overshoot and cannot track the ramp segments of the reference input.

Because the future values of the reference input are difficult to be utilized in the continuous time ZMP tracking control system. To solve the tracking performance of the output of the continuous time ZMP tracking control system to the ramp segments of the reference input, the continuous time optimal tracking controller is designed under the assumption that the reference input is the ramp input. This controller includes double-integration of the error. In the case that the reference input is chosen as Fig. 3.4, the ZMP tracking control system using the designed continuous time optimal tracking controller satisfies the internal model principle. Consequently, its output tracks ramp and step segments of the reference input. As shown in the simulation results, when the designed optimal tracking controller is used to control the ZMP tracking control systems, their outputs track the ramp and step segments of the reference input and have overshoot.

In the case of the discrete time ZMP tracking control system, because the future values of the reference input are easy to be utilized, the tracking problem of the output of the ZMP tracking control system to the ramp segments of the reference input is solved by utilizing the future values of the reference input. The designed discrete time optimal tracking controller is obtained from the state variables, one-summation of the error and the future values of the reference input. As shown in the simulation results, the outputs of the ZMP tracking control systems that are controlled by the designed discrete time optimal tracking controller using the future values of the reference input track both the ramp and step segments of the reference input. These outputs have very small overshoot.

As shown in Figs. 3.3 and 3.4, the singular points of the reference input are very important points especially at the end of moving of the ZMP points shown in Fig. 3.4. The overshoot occurred at these points makes the ZMP of the biped robot to move outside the stable region if the maximum value of the overshoot is larger than the chosen value of stability margin. In this case, the biped robot becomes unstable.

From the above mentioned, for controlling the ZMP tracking control system to keep the good tracking performance of the outputs of the ZMP tracking control system to the reference input and small overshoot, the designed discrete time optimal tracking controller utilizing the future values of the reference input is better than the designed continuous time optimal tracking controller. Moreover, the designed discrete time controller is more adequate to implement in the Micro-Controller or Digital-Computer than the designed continuous time controller in the practical system. From the advantages of the designed discrete time controller in the practical

system, the designed discrete time controller is chosen to control the ZMP tracking control systems.

3.5 Summary:

This chapter introduces the relation between the ZMP and the stable walking of the biped robot. The ZMP tracking control systems are constructed to generate the stable walking pattern for the biped robot. A continuous time optimal tracking controller and a discrete time optimal tracking controller using the future values of the reference input are designed to control the ZMP tracking control systems. From the advantages of the designed discrete time optimal tracking controller in the practical system compared with the designed continuous time optimal tracking controller, this controller is chosen to control the ZMP tracking control systems. The simulation results show the effectiveness of the controllers.

Chapter 4: Walking Control of Biped Robot

Based on the stable walking pattern generation discussed in chapter 3, a trajectory of COM of the biped robot is generated by the ZMP tracking control system. The ZMP reference trajectory of the ZMP system is chosen to satisfy the stable condition of the biped robot. The control objective for the stable walking of the biped robot is to track the center of the pelvis link to the COM trajectory. The inverse kinematics of the biped robot is solved to obtain the angle of each joint of the biped robot. The walking control of the biped robot is performed based on the solutions of the inverse kinematics which is solved by the solid geometry method.

4.1 Inverse Kinematics of the Biped Robot:

The configuration of a 10 DOF biped robot is shown in Fig. 2.1. The relationship between the biped robot and the 3D inverted pendulum is shown in Fig. 4.1. Solving the inverse kinematics problems directly from kinematics models is complex. An inverse kinematics based on the solid geometry method is presented in this section.

During the walking of the biped robot, the following assumptions are supposed

- Trunk of robot is always located on the sagittal plane: when the trunk of the biped robot is located on the sagittal plane, from the geometric structure of the biped robot, it is easy to obtain the following equation.

$$\theta_2 = -\theta_4 \text{ and } \theta_9 = -\theta_6 \tag{4.1}$$

- The feet of the biped robot are always parallel with floor: when the trunk of the biped robot is on the sagittal plane, the feet of the biped robot are parallel with floor if the following conditions are satisfied

$$\begin{aligned} \theta_3 &= \theta_1 + \theta_5 \\ \theta_8 &= \theta_7 + \theta_{10} \end{aligned} . \tag{4.2}$$

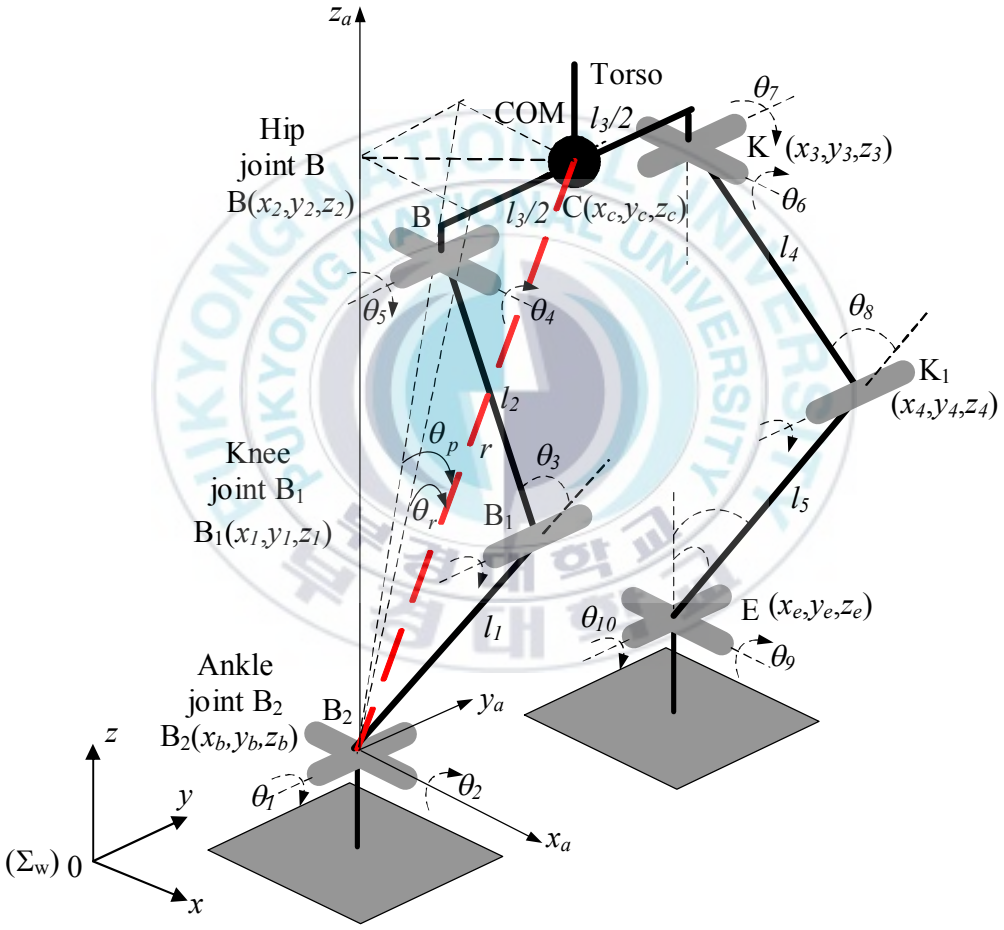

Fig. 4.1: Biped robot and 3D inverted pendulum.

- The walking of the biped robot is divided into three phases: Two-legs supported, right-leg supported and left-leg supported. When the biped robot is supported by one leg, another leg swings.

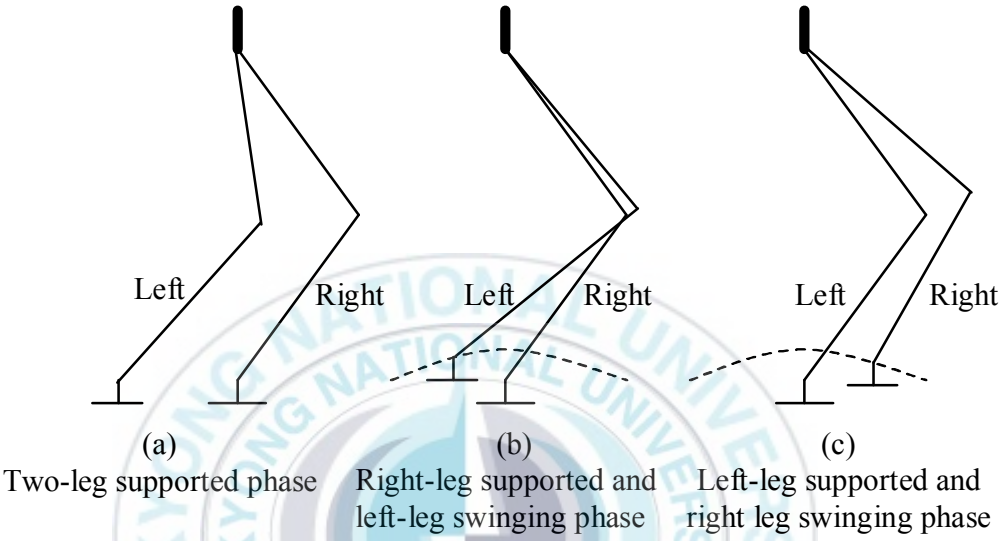

Fig. 4.2: Three walking phases of the biped robot.

- The origin of the 3D inverted pendulum is located at the center of the ankle joint of the supported leg.

4.1.1 Inverse kinematics of biped robot in one-leg supported phase:

It is supposed that biped robot is with the right-leg supported and left-leg swinging. The coordinate of the COM in coordinate system Σ_a whose origin is taken at the center of the ankle joint of the supported leg can be obtained as

$$x_{ca} = x - x_b \tag{4.3}$$

$$y_{ca} = y - y_b \tag{4.4}$$

$$z_{ca} = z - z_b \tag{4.5}$$

where

(x,y,z) : Coordinate of the COM in the world coordinate

(x_b,y_b,z_b) : Coordinate of the center of the ankle joint of the supported leg in the world coordinate

(x_{ca},y_{ca},z_{ca}) : Coordinate of the COM in the coordinate Σ_a

Solving Eqs. (2.25)~(2.27) at the k^{th} sample time with $z_{ca} = z_{cd}$ yields

$$r(k) = \sqrt{z_{cd}^2(k) + x_{ca}^2(k) + y_{ca}^2(k)} \tag{4.6}$$

Since the trunk of the biped robot is always located on the sagittal plane, the pelvis link is always on the horizontal plane □CBDC$_1$ as shown in Fig. 4.3. The line $\overline{\text{BC}}$ is perpendicular to the line $\overline{\text{OA}}$ at A, and it yields $\angle 0\text{CB} = \frac{\pi}{2} - \theta_r$. Using the cosine's law, the length of side $\overline{\text{OB}}$ of the triangle 0BC at the k^{th} sample time is obtained as follows:

$$h(k) = \sqrt{x_{ca}^2 + \left(y_{ca} - \frac{l_3}{2}\right)^2 + z_c^2} = \sqrt{\frac{l_3^2}{4} + r^2(k) - l_3 y_{ca}(k)} \tag{4.7}$$

The angle $\alpha(k)$ between sides l_2 and l_1 of the triangle 0BB$_1$ is calculated by the cosine's law as follows:

$$\alpha(k) = arccos\left(\frac{l_1^2 + l_2^2 - h^2(k)}{2l_1 l_2}\right). \tag{4.8}$$

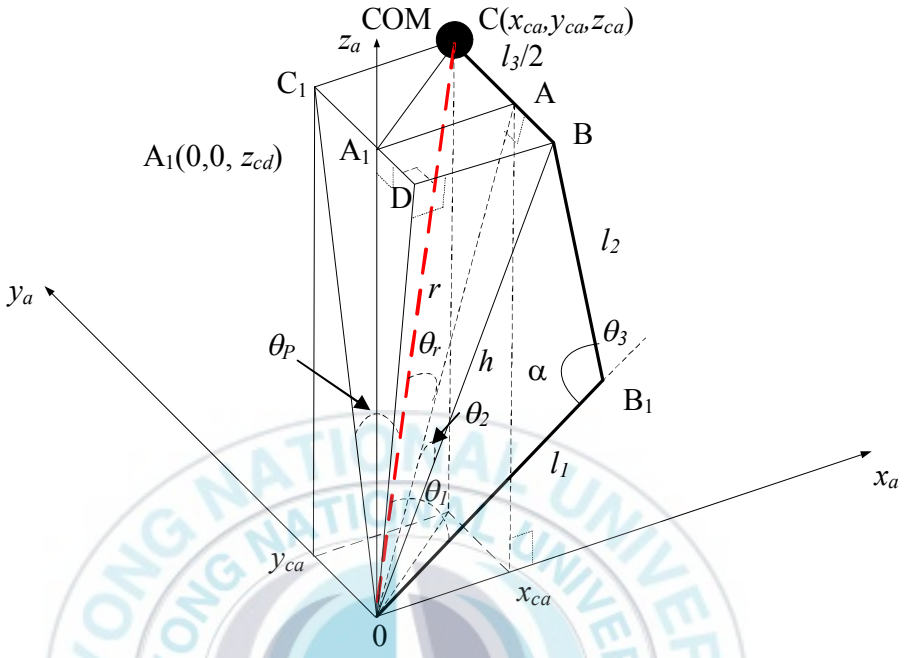

Fig. 4.3: Inverted pendulum and supported leg.

From $\alpha(k)$ in Eq. (4.8), the knee joint angle of the biped robot is gotten as Eq. (4.9).

$$\theta_3(k) = \pi - \alpha(k) \tag{4.9}$$

In Fig. 4.3, the line $\overline{\text{BC}}$ is perpendicular to the line $\overline{\text{OA}}$ at A. From the right-triangle 0AB, the ankle joint angle $\theta_2(k)$ can be obtained as

$$\theta_2(k) = \angle \text{A0B} = arcsin\left(\frac{y_{ca}(k) - \frac{l_3}{2}}{h(k)} \right). \tag{4.10}$$

Since the height of the COM of the biped robot is always kept equal to constant z_{cd} and is on the sagittal plane during walking of the biped robot, the line $\overline{\text{BD}}$ is perpendicular to $0y_a z_a$ plane. It means that the line $\overline{\text{BD}}$ is perpendicular to the line $\overline{\text{OD}}$. The triangles OBB_1 and ODB lie on the same plane which contains the links l_1 and l_2 of the biped robot as shown in Fig. 4.3. The angle $\theta_1(k)$ can be obtained as follows:

$$\theta_1(k) = \angle \text{D0B} + \angle \text{B0B}_1 = arcsin\left(\frac{x_{ca}(k)}{h(k)}\right) + arccos\left(\frac{h^2(k) + l_1^2 - l_2^2}{2h(k)l_1}\right). \quad (4.11)$$

4.1.2 Inverse kinematics of swinging leg:

It is assumed that the biped robot is supported by the right leg and is swung by the left leg as shown in Fig. 4.4.

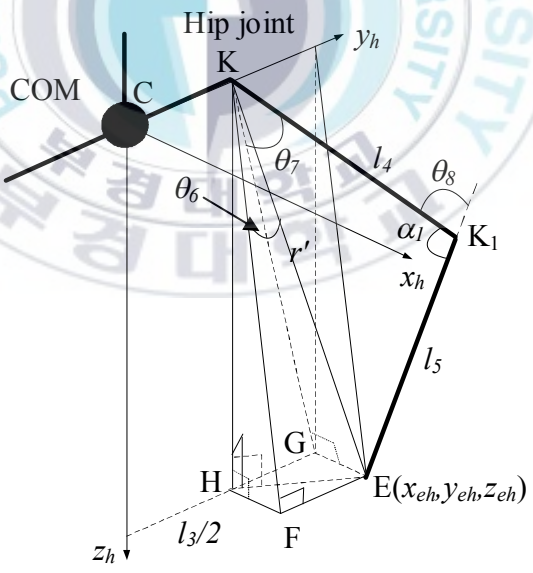

Fig. 4.4: Swinging leg of biped robot.

A coordinate system Σ_h with the origin taken at the middle of the pelvis link is defined as shown in Fig. 4.4. During the swing of this leg, the coordinate y_{eh} of the foot of the swinging leg is constant.

$r'(k)$ is defined as the distance between the ankle joint and the hip joint of the swinging leg at the k^{th} sample time. It is expressed in the coordinate system Σ_h as follows:

$$r'(k)^2 = x_{eh}^2(k) + \left(y_{eh}(k) - \frac{l_3}{2} \right)^2 + z_{eh}^2(k) \tag{4.12}$$

where $(x_{eh}(k), y_{eh}(k), z_{eh}(k))$ is coordinate of the ankle joint of the swinging leg in the coordinate Σ_h at the k^{th} sample time.

Since the line $\overline{\mathrm{EF}}$ is perpendicular to the line $\overline{\mathrm{KF}}$ at F, the hip angle $\theta_6(k)$ of the swinging leg is obtained based on the right-triangle KEF as

$$\theta_6(k) = -arcsin\left(\frac{y_{eh}(k) - l_3/2}{r'(k)} \right) \tag{4.13}$$

The minus sign in (4.13) means counterclockwise.

The links l_4 and l_5 lie on the plane which contains right-triangle KGE. The hip angle $\theta_7(k)$ is equal to the angle between link l_4 and Cy_hz_h plane. It is can be expressed as

$$\theta_7(k) = \angle \mathrm{GKE} + \angle \mathrm{EKK}_1 = arcsin\left(\frac{x_{eh}(k)}{r'(k)} \right) + arccos\left(\frac{r'^2(k) + l_4^2 - l_5^2}{2r'(k)l_4} \right) \tag{4.14}$$

Using the cosine's law, the angle of the knee of the swinging leg can be obtained as

$$\theta_8(k) = \pi - \alpha_1 = \pi - arccos\left(\frac{l_5^2 + l_4^2 - r'^2(k)}{2l_5 l_4}\right). \quad (4.15)$$

Similarly, when the biped robot is supported by the left leg and is swung by the right leg. The angles of the right leg are calculated from Eqs. (4.13)~(4.15).

4.1.3 Inverse kinematics of biped robot in two-leg supported phase:

It is assumed that the swinging leg of the biped robot contacts the ground after swinging phase as shown in Fig. 4.5. The biped robot is supported by two legs.

The coordinate of the COM is expressed in coordinate system Σ_f whose origin is taken at the ankle joint of new supported leg as

$$x_{cf}(k) = x_{ca}(k) - x_{ea}(k) \quad (4.16)$$

$$y_{cf}(k) = y_{ca}(k) - y_{ea}(k) \quad (4.17)$$

$$z_{cf}(k) = z_{ca}(k) \quad (4.18)$$

where (x_{ea}, y_{ea}, z_{ea}) is coordinate of the ankle joint of the new supported leg in coordinate system Σ_a, (x_{ca}, y_{ca}, z_{ca}) is coordinate of the COM in coordinate system Σ_a and (x_{cf}, y_{cf}, z_{cf}) is coordinate of the COM in coordinate system Σ_f.

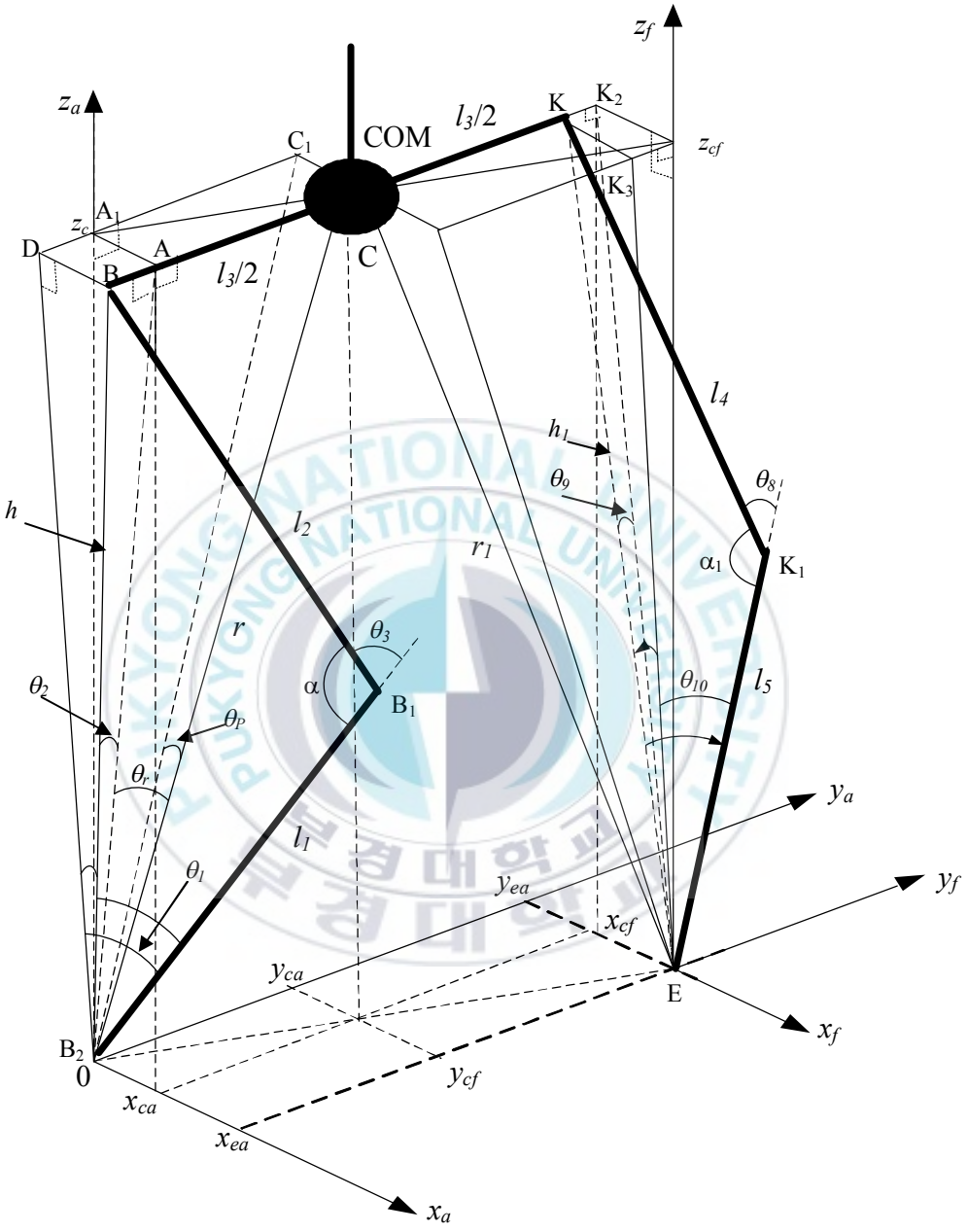

Fig. 4.5: Biped robot with two legs supported.

$r_1(k)$ is defined as distance between the COM and the ankle joint of the left leg. It is calculated based on the coordinate of the COM in coordinate system Σ_f as

$$r_1^2(k) = x_{cf}^2(k) + y_{cf}^2(k) + z_{cf}^2(k) \tag{4.19}$$

Similarly to the procedure in one-leg supported phase, the inverse kinematics of the biped robot in two-leg supported phase can be obtained. It can be expressed as following equations.

❖ Right-leg case:

$$h(k) = \sqrt{\frac{l_3^2}{4} + r^2(k) - l_3 y_{ca}(k)} \tag{4.20}$$

$$\alpha(k) = \angle \mathrm{BB_1B_2} = arccos\left(\frac{l_1^2 + l_2^2 - h^2(k)}{2l_1 l_2}\right) \tag{4.21}$$

$$\theta_3(k) = \pi - \alpha(k) \tag{4.22}$$

$$\theta_2(k) = \angle \mathrm{BB_2A} = arcsin\left(\frac{y_{ca}(k) - \frac{l_3}{2}}{h(k)}\right) \tag{4.23}$$

$$\theta_1(k) = \angle \mathrm{DB_2B} + \angle \mathrm{BB_2B_1} = arcsin\left(\frac{x_{ca}(k)}{h(k)}\right) + arccos\left(\frac{h^2(k) + l_1^2 - l_2^2}{2h(k)l_1}\right) \tag{4.24}$$

❖ Left-leg case:

$$h_1(k) = \sqrt{\frac{l_3^2}{4} + r_1^2(k) - l_3 \left| y_{cf}(k) \right|} \tag{4.25}$$

$$\alpha_1(k) = \angle \mathrm{KK_1E} = arccos\left(\frac{l_5^2 + l_4^2 - h_1^2(k)}{2 l_5 l_4} \right) \tag{4.26}$$

$$\theta_8(k) = \pi - \alpha_1(k) \tag{4.27}$$

$$\theta_9(k) = \angle \mathrm{KEK_2} = arcsin\left(\frac{y_{cf}(k) + \frac{l_3}{2}}{h_1(k)} \right) \tag{4.28}$$

$$\theta_{10}(k) = \angle \mathrm{KEK_1} + \angle \mathrm{KEK_3} = arccos\left(\frac{h_1^2(k) + l_5^2 - l_4^2}{2 h_1(k) l_5} \right) + arcsin\left(\frac{x_{cf}(k)}{h_1(k)} \right) \tag{4.29}$$

where

h : Distance between the right hip joint and the ankle of the right leg

h_1 : Distance between the left hip joint and the ankle joint of the left leg.

4.2 Control of the Biped Robot:

Considering one step walking of the biped robot is illustrated by consequent movement as shown in Fig. 4.6.

At the beginning of walking step, the left leg leaves from the ground to start swinging. This leg swings with following a reference trajectory. During the swing of the left leg, the ZMP of the biped robot exists at the geometry center of the right foot.

At the end of swinging, the left leg is contacted on the ground, and the biped robot is supported by two legs.

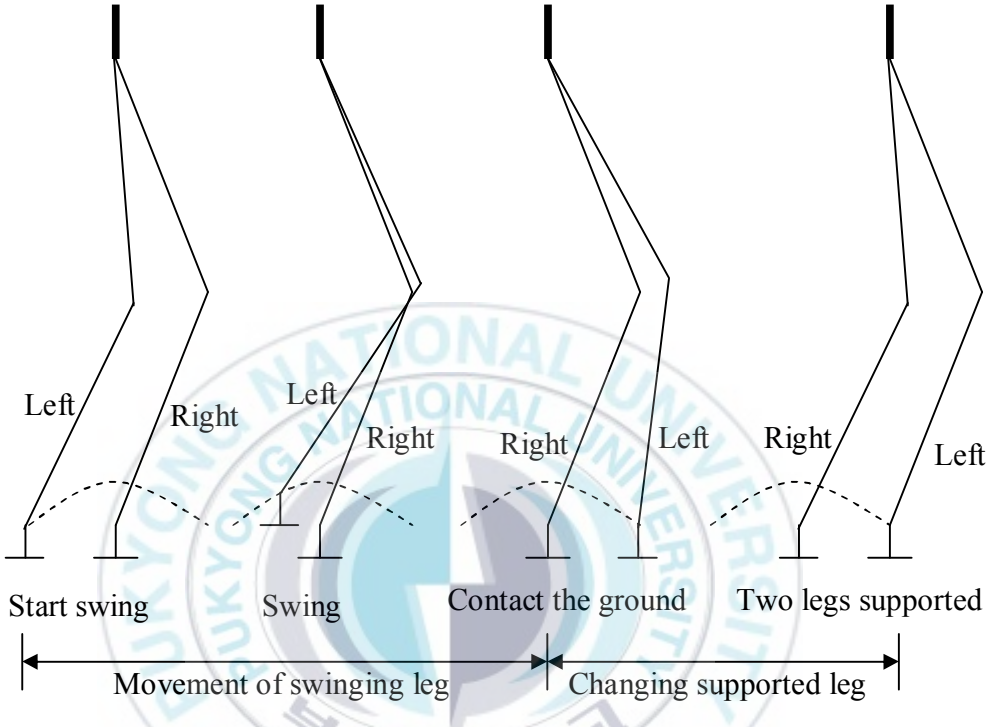

Fig. 4.6: One step walking of biped robot.

During two-leg supported phase, the ZMP of the biped robot moves from geometry center of the right foot to that of the left foot. The left leg becomes new supported leg and the right leg becomes swinging leg for next step. Based on the reference trajectory of the swinging leg and the trajectory of the COM which is generated by the ZMP tracking control system, the inverse kinematics is solved to obtain the angle of each joint of the biped robot. The control problem of the biped

robot becomes tracking control problem of DC motors of joints. The block diagram of the biped robot control system is shown in Fig. 4.7.

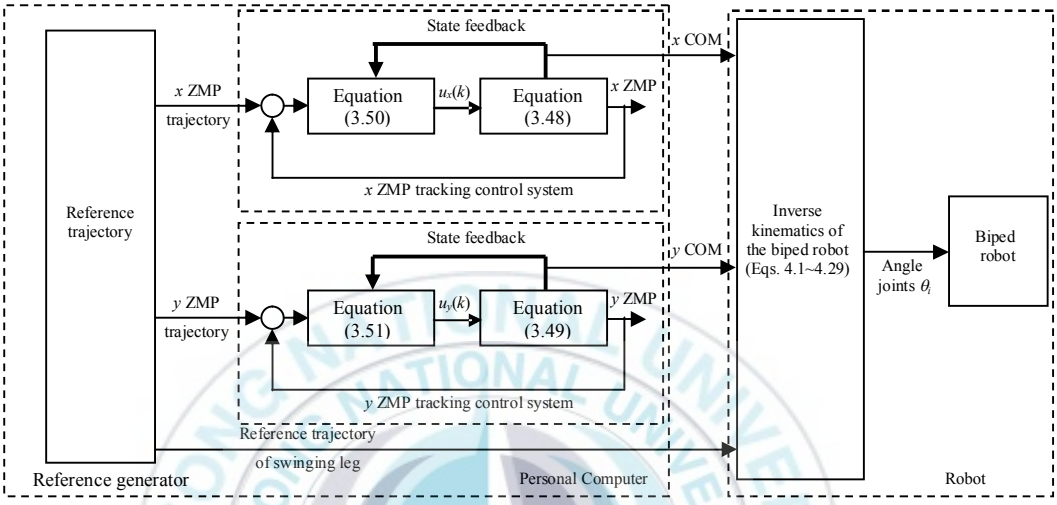

Fig. 4.7: Block diagram of the biped robot control system.

4.3 Simulation Results:

The parameters values of the biped robot used in the simulation are given in Table 4.1.

Table 4.1 Numerical values of the biped robot' parameters used in simulation

Parameters	Description	Values	Units
$l_1 = l_5$	Length of lower leg links	0.28	[m]
$l_2 = l_4$	Length of upper leg links	0.28	[m]
l_3	Length of pelvis link	0.2	[m]
a	Width of foot	0.18	[m]
b	Length of foot	0.24	[m]
z_{cd}	Height of center of pelvis link	0.5	[m]
θ_{01}	Initial value of θ_1	26.75	[deg]
θ_{02}	Initial value of θ_2	0	[deg]
θ_{03}	Initial value of θ_3	53.5	[deg]
θ_{04}	Initial value of θ_4	0	[deg]
θ_{05}	Initial value of θ_5	26.75	[deg]
θ_{06}	Initial value of θ_6	0	[deg]
θ_{07}	Initial value of θ_7	26.75	[deg]
θ_{08}	Initial value of θ_8	53.5	[deg]
θ_{09}	Initial value of θ_9	0	[deg]
θ_{010}	Initial value of θ_{10}	26.75	[deg]

To demonstrate the performance of the biped walking based on the ZMP walking pattern generation combined with the inverse kinematics, the simulation results for walking on the flat floor of the biped robot using Matlab are shown. The period of step is 10 seconds: changing supported leg time is 5 seconds and swinging leg time is 5 seconds. The length of step is 20 cm. During the moving of the biped robot, the height of the center of the pelvis link is constant. In the one-leg supported phase, the ZMP is located at the center of the supported foot. When two legs of the biped robot are contacted on the ground, the ZMP moves from the center of the foot of the current supported leg to the center of the foot of the new supported leg.

The footprint and the Zigzag reference trajectory of the ZMP are shown in Fig. 4.8.

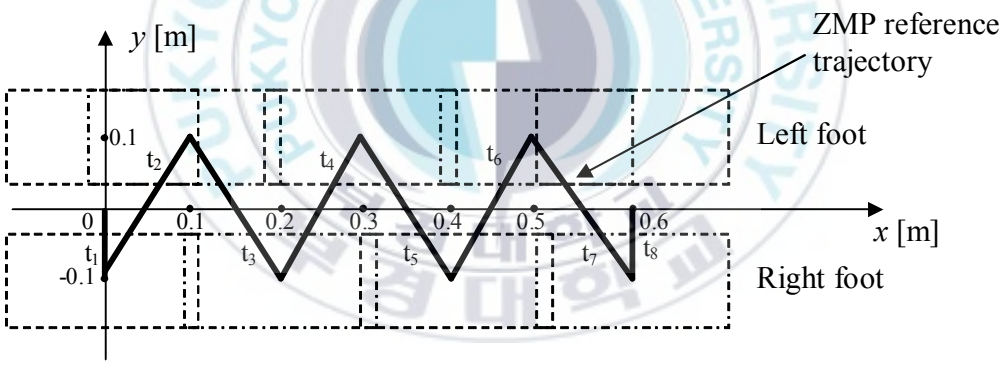

Fig. 4.8: Footprint and zigzag reference trajectory of ZMP.

The *x* and *y* ZMP reference trajectories versus times corresponding to the zigzag reference trajectory of the ZMP in Fig. 4.8 can be obtained as shown in Fig. 4.9.

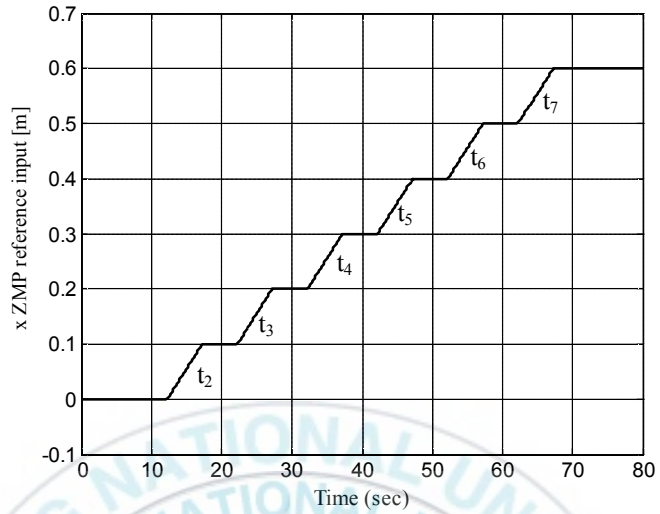

(a) *x* ZMP reference input versus time.

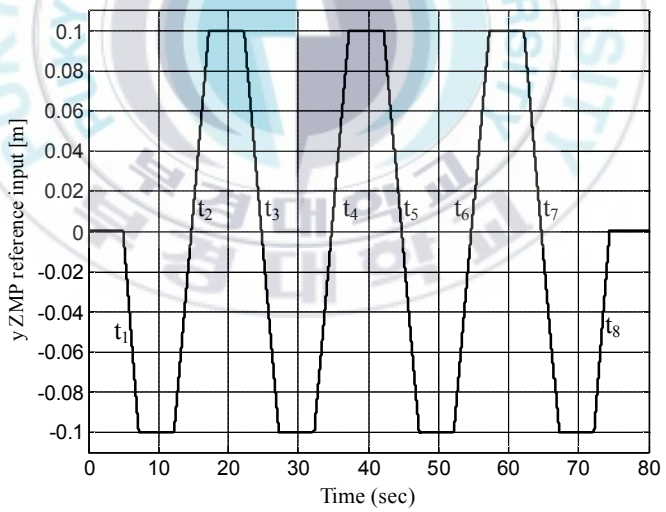

(a) *y* ZMP reference input versus time.

Fig. 4.9: Zigzag ZMP reference input trajectory versus time.

The reference input trajectory of the ankle joint of the swinging leg is an arc which has radius equal to 0.1 [m]. The reference input trajectory equations of the arc are expressed as Eq. (4.30) for the left leg and Eq. (4.31) for the right leg.

$$\begin{cases} x_{aa}^2 + z_{aa}^2 = 0.01 \\ y_{aa} = l_3 \end{cases} \quad for \quad -0.1 \le x_{aa} \le 0.1 \tag{4.30}$$

$$\begin{cases} x_{af}^2 + z_{af}^2 = 0.01 \\ y_{af} = l_3 \end{cases} \quad for \quad -0.1 \le x_{af} \le 0.1 \tag{4.31}$$

where (x_{aa}, y_{aa}, z_{aa}) is coordinate of one point on the arc in the coordinate system Σ_a, and (x_{af}, y_{af}, z_{af}) is coordinate of one point on the arc in the coordinate system Σ_f.

The *x*, *y* ZMP tracking control systems are controlled by the designed discrete time optimal tracking controller with $R = 1$, $Q = \begin{bmatrix} 0.12 & 0 & 0 & 0 \\ 0 & 0 & 0 & 0 \\ 0 & 0 & 0 & 0 \\ 0 & 0 & 0 & 0 \end{bmatrix}$ and number of the future of the reference input $N = 1200$. The simulation results are shown in Figs. 4.10~ 4.26.

Fig. 4.10 and Fig. 4.13 show the reference inputs, the ZMP outputs and the positions of the COM of the ZMP discrete time optimal tracking control systems. In these figures, the good tracking performance of the ZMP outputs to all segments of the reference input is shown. The ZMP outputs of the ZMP discrete time optimal tracking control systems have no overshoot and undercut.

Fig. 4.12 and Fig. 4.15 show that the tracking errors of the x and y ZMP tracking control systems converge to zeros and the errors occur at the singular points of the reference inputs. The absolute value of the maximum values of the error are very small with about 0.06 [mm] and about 0.1 [mm] for the x and y ZMP tracking control system.

Fig. 4.11 and Fig. 4.14 show that the control signals inputs of the x and y ZMP tracking control systems are bounded.

Figs. 4.16~4.25 show the angles of each joint of the biped robot. In these figures, the sharp points occur at the transient states of the biped robot where the joints of the biped robot change their direction of rotation.

The movement of the COM of the biped robot on the horizontal constraint plane and the ZMP reference trajectory are shown in Fig. 4.26. This figure shows that the projection of the COM on the ground of the biped robot is always on the ZMP reference trajectory.

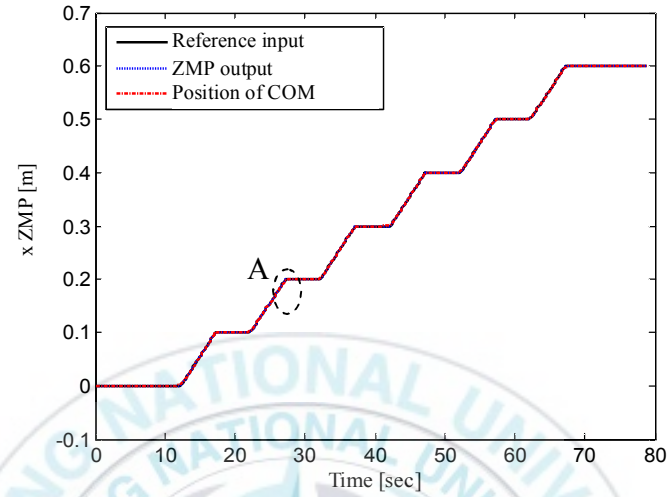

(a)

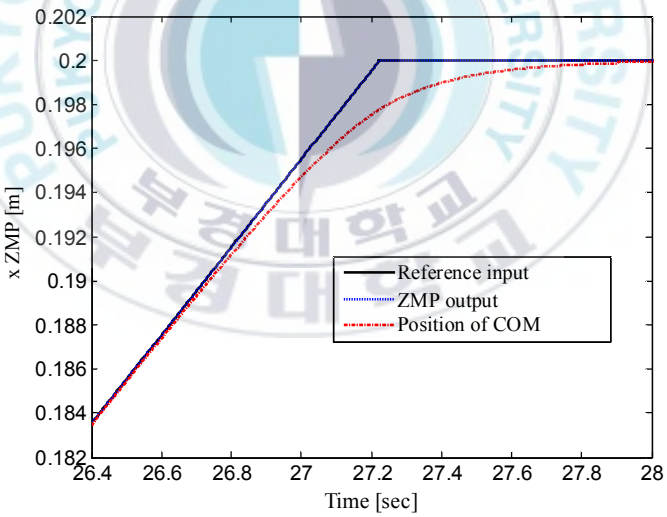

(b) A region.

Fig. 4.10: *x* ZMP reference input, *x* ZMP output and position of COM.

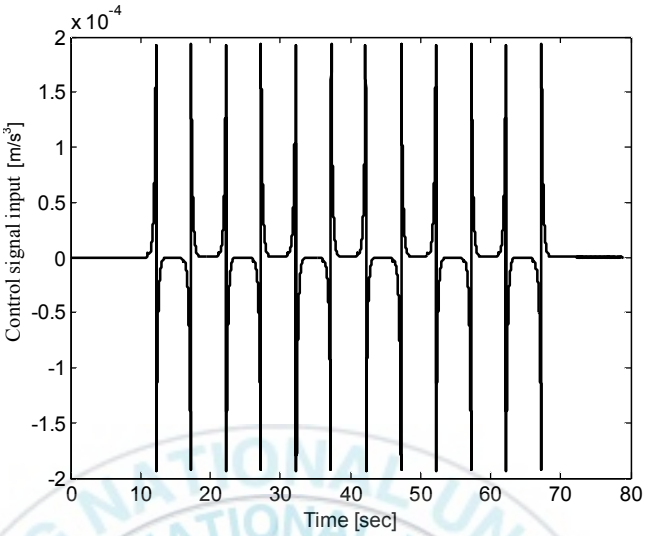

Fig. 4.11: Control signal u_x.

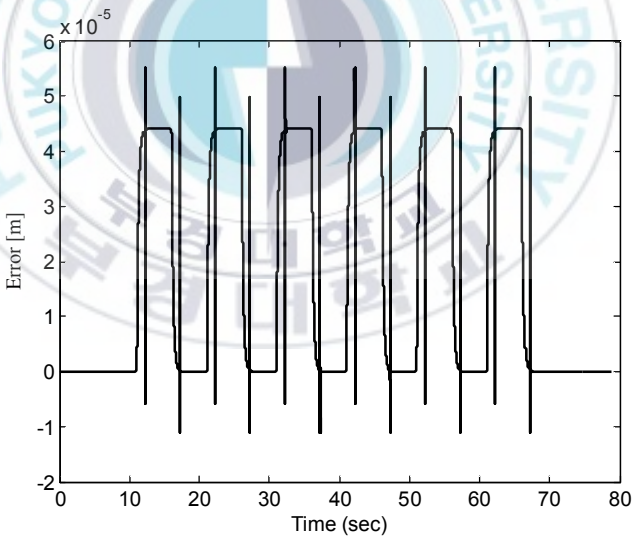

Fig. 4.12: *x* ZMP position error.

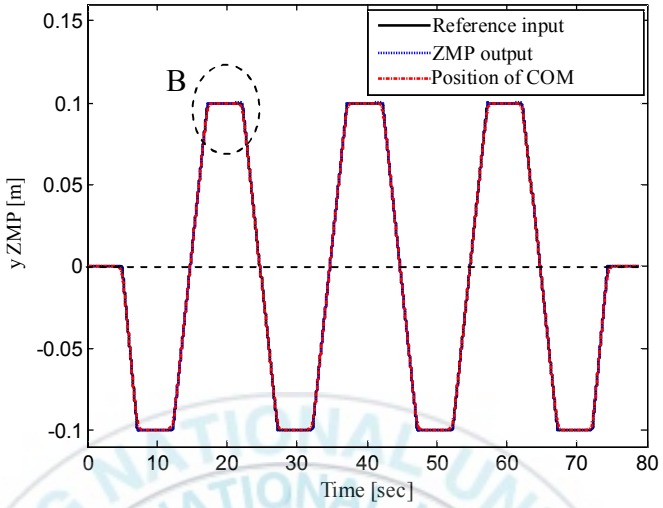

(a)

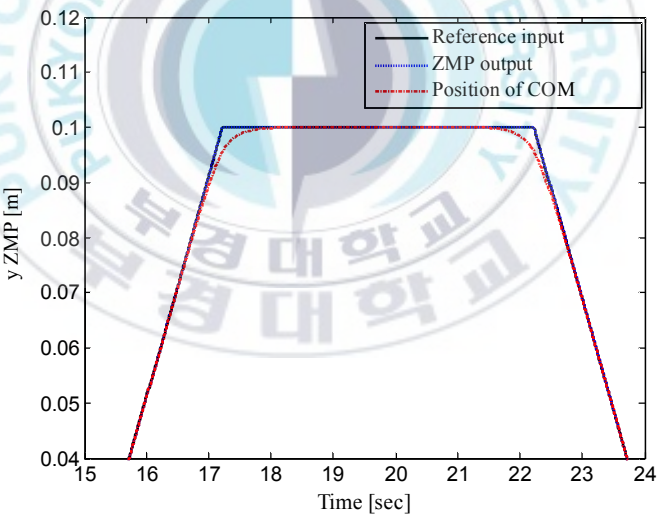

(b) B region.

Fig. 4.13: *y* ZMP reference input, *y* ZMP output and position of COM.

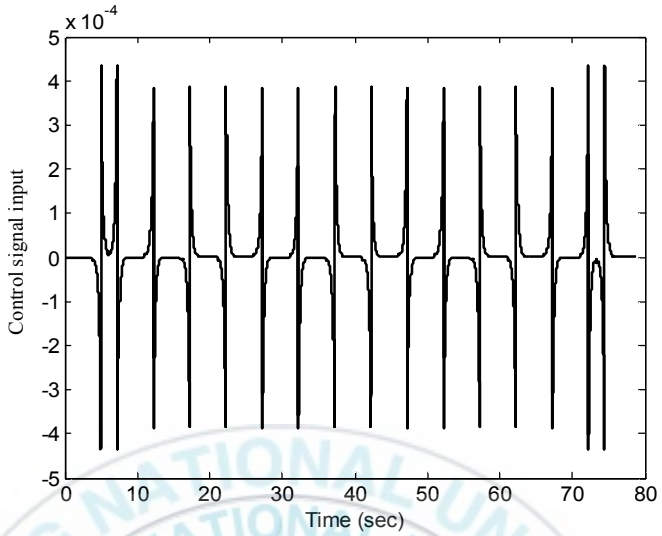

Fig. 4.14: Control signal input u_y.

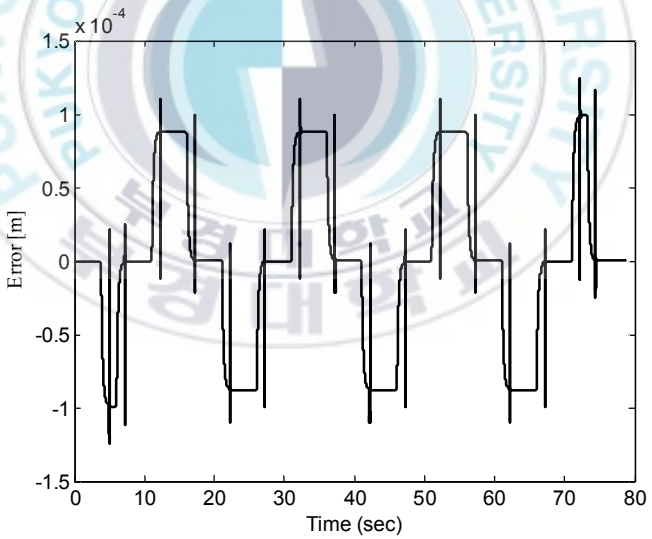

Fig. 4.15: *y* ZMP position error.

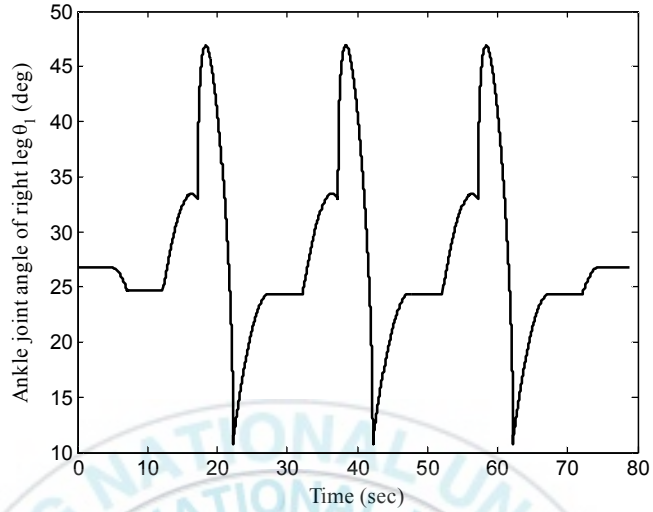

Fig. 4.16: Ankle joint angle θ_1.

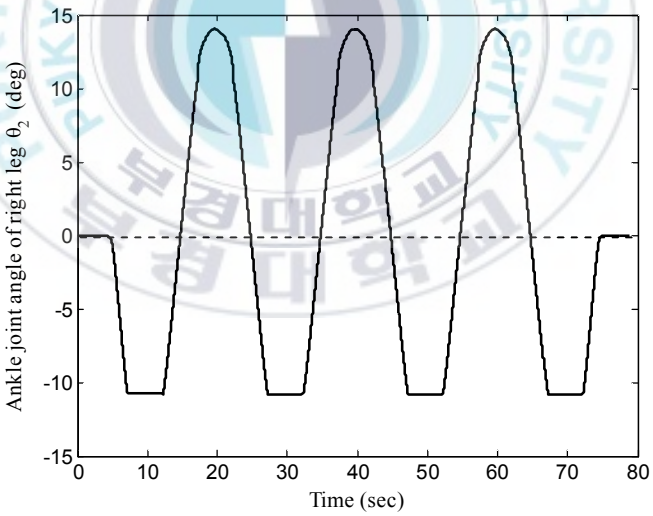

Fig. 4.17: Ankle joint angle θ_2.

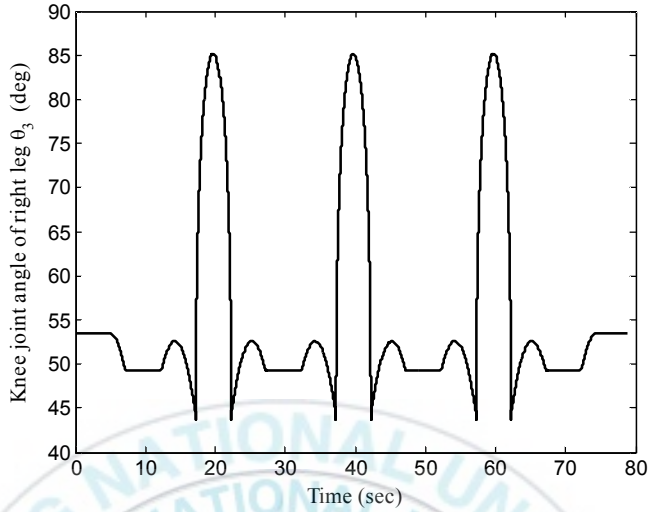

Fig. 4.18: Knee joint angle θ_3.

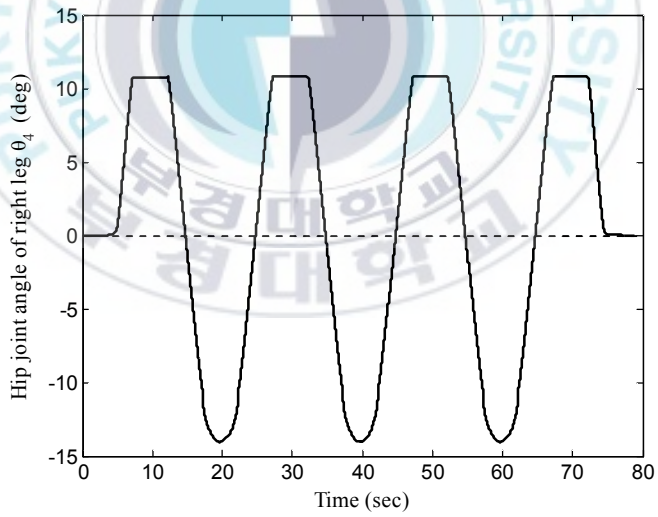

Fig. 4.19: Hip joint angle θ_4.

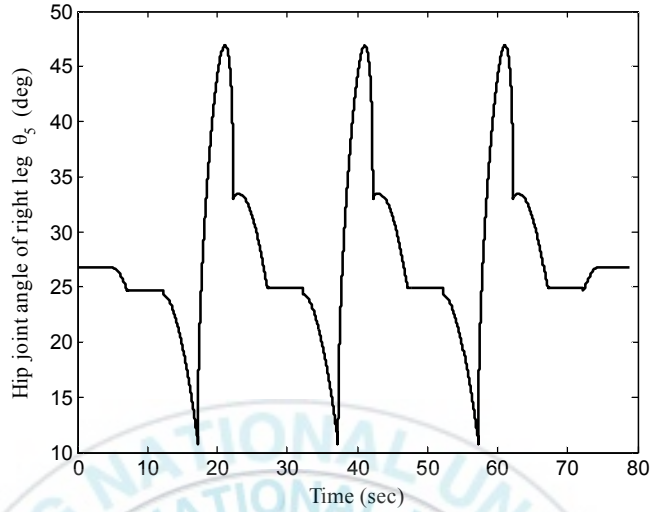

Fig. 4.20: Hip joint angle θ_5.

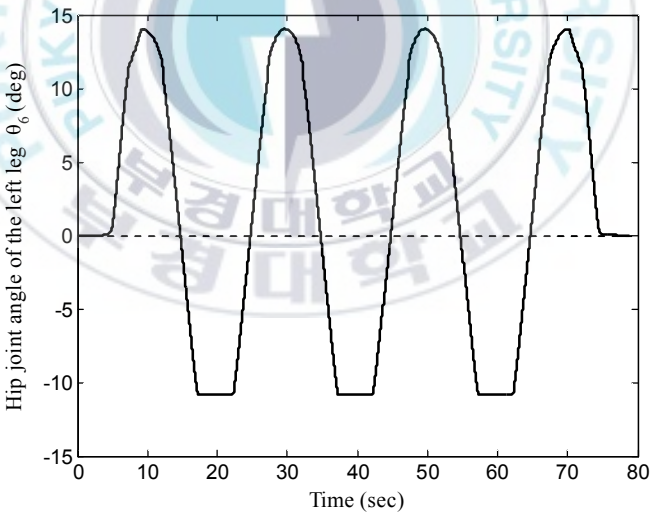

Fig. 4.21: Hip joint angle θ_6.

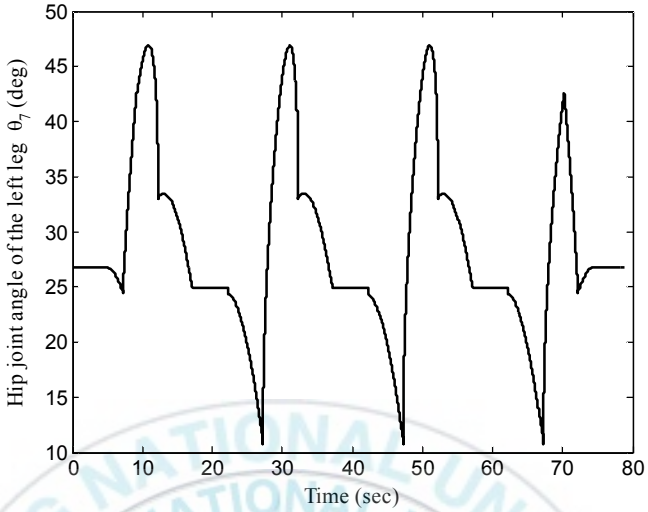

Fig. 4.22: Hip joint angle θ_7.

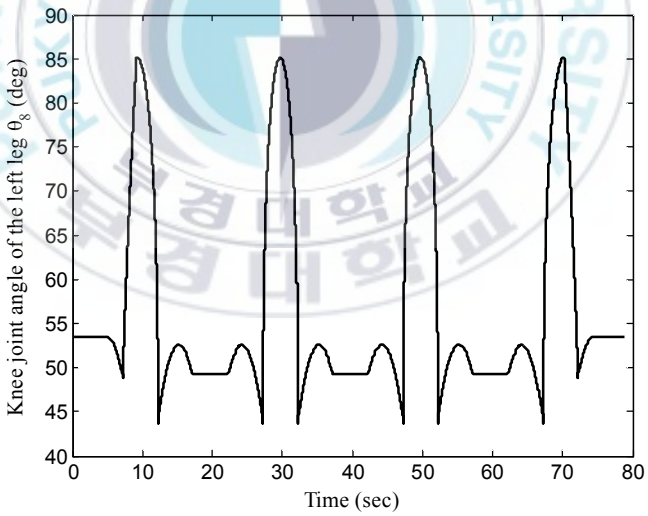

Fig. 4.23: Knee joint angle θ_8.

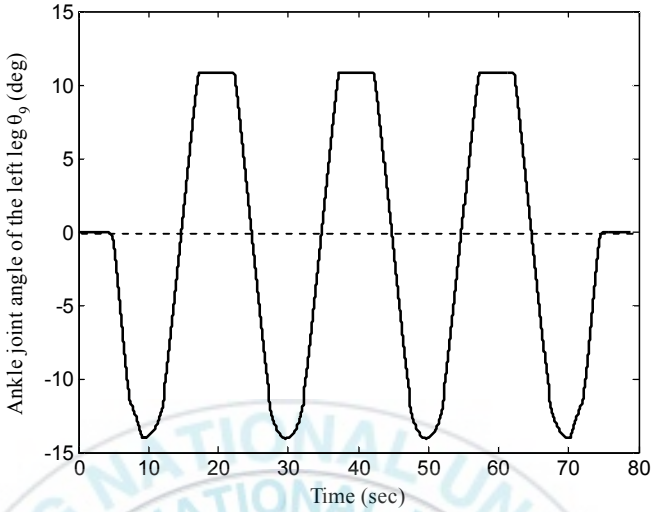

Fig. 4.24: Ankle joint angle θ_9.

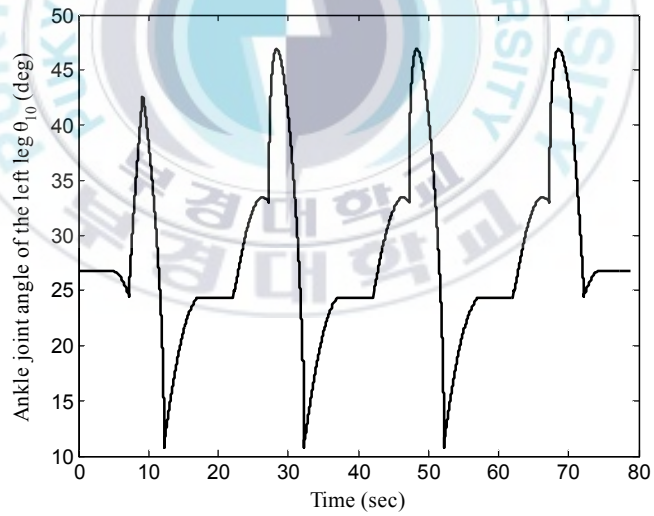

Fig. 4.25: Ankle joint angle θ_{10}.

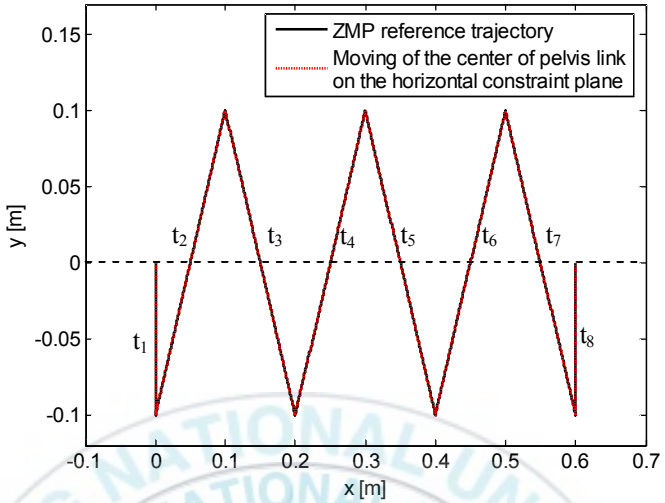

Fig. 4.26: Movement of the center of pelvis link on the horizontal constraint plane and the ZMP reference trajectory.

4.4 Summary:

In this chapter, an inverse kinematics using the solid geometry is presented to solve inverse kinematics problem. Based on the stable walking pattern generation and solution of the inverse kinematics, the control method for the biped robot with stable walking is proposed. The simulation results are shown to prove effectiveness of the proposed control method.

Chapter 5: Optimal Tracking Control for Motion of the Biped Robot and Experiment Results

As discussed in previous chapters, the configuration of the 10 DOF biped robot was introduced. Each rotating joint is driven by one DC motor. All DC motors used in this thesis are assumed to have the same parameters. The motion of the biped robot depends on the motion of the DC motors at the joints. To control the position of the center of the pelvis link of the biped robot tracked the COM trajectory which is generated by the ZMP tracking control system, the angle of rotor of the DC motors at joints of the biped robot should track the reference angle which is obtained by solving the inverse kinematics problem. In this chapter, modeling of the DC motor is expressed in state equation. A discrete time full-order state observer is also designed. Feedback gain matrix of the observer is obtained by pole assignment method using Ackermann formulation with observability matrix. The state feedback variables are given by the state observer. A discrete time LQ optimal tracking control of the DC motor system is constructed to track the angle of rotor of the DC motor to the reference angle based on the designed observer.

5.1 Discrete Time Optimal Tracking Control of DC Motor:

5.1.1 Modeling of DC motor:

DC motor is an actuator which directly provides rotary motion. The electric circuit of the armature and the free body diagram of the rotor are shown in Fig. 5.1.

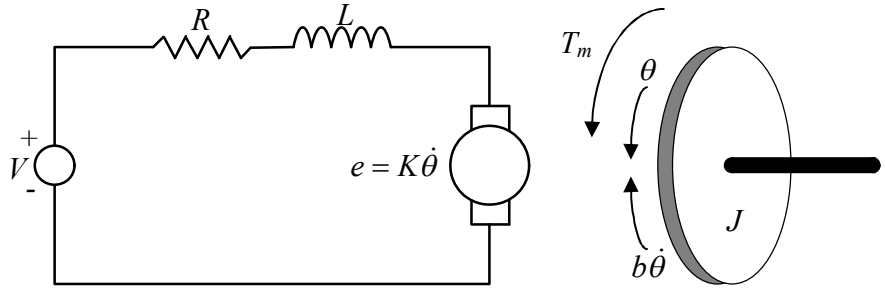

Fig. 5.1: Diagram of the DC motor.

where

R : Armature resistance [Ω].

L : Armature inductance [H].

K : Electromotive force constant [Nm/A].

K_t : Torque constant [Nm/A].

K_e : Voltage constant [Vs/rad].

V : Source voltage [V].

$\dot{\theta}$: Angular velocity of rotor [rad/s].

J : Moment of inertia of the rotor [kgm^2].

b : Damping ratio of the mechanical system [Nms].

The electromagnetic torque of the motor T_m has the relationship to the armature current i and a torque constant K_t as follows:

$$T_m = K_t i \tag{5.1}$$

The relationship between the back-electromotive force of the motor E and the angular velocity can be obtained as follows:

$$E = K_e \dot{\theta} \tag{5.2}$$

It is assumed that load of the DC motor is negligible. In SI unit system, K_t is equal to K_e. Using the Newton's law combined with Kirchhoff's law, the dynamic equations of the DC motor can be written as follows:

$$J\ddot{\theta} + b\dot{\theta} = T_m = Ki \tag{5.3}$$

$$L\frac{di}{dt} + Ri = V - K\dot{\theta} \tag{5.4}$$

where $K = K_t = K_e$

Combining (5.3) and (5.4) yields

$$LJ\dddot{\theta} + (Lb + RJ)\,\ddot{\theta} + (Rb + K^2)\,\dot{\theta} = KV \tag{5.5}$$

$\boldsymbol{x_m} = \begin{bmatrix}\theta & \dot{\theta} & \ddot{\theta}\end{bmatrix}^T$ is defined as state vector of the DC motor. Eq. (5.5) can be written as

$$\underbrace{\begin{bmatrix}\dot{\theta}\\ \ddot{\theta}\\ \dddot{\theta}\end{bmatrix}}_{\dot{x}_m} = \underbrace{\begin{bmatrix}0 & 1 & 0\\ 0 & 0 & 1\\ 0 & -\dfrac{Rb+K^2}{LJ} & -\dfrac{Lb+RJ}{LJ}\end{bmatrix}}_{A_m}\underbrace{\begin{bmatrix}\theta\\ \dot{\theta}\\ \ddot{\theta}\end{bmatrix}}_{x_m} + \underbrace{\begin{bmatrix}0\\ 0\\ \dfrac{K}{LJ}\end{bmatrix}}_{B_m}V$$
$$y_m = \underbrace{\begin{bmatrix}1 & 0 & 0\end{bmatrix}}_{C_m}\underbrace{\begin{bmatrix}\theta\\ \dot{\theta}\\ \ddot{\theta}\end{bmatrix}}_{x_m} \tag{5.6}$$

where y_m is rotational angle of the rotor of the DC motor.

A discrete time controller is designed based on discrete time model of the DC motor. The discrete time system equations of the DC motor can be obtained as

$$\begin{aligned} \boldsymbol{x_m}(k+1) &= \boldsymbol{\Phi_m}(T)\boldsymbol{x_m}(k) + \boldsymbol{\theta_m}(T)V(k) \\ y_m(k) &= \boldsymbol{C_m}(T)\boldsymbol{x_m}(k) \end{aligned} \tag{5.7}$$

where

$\boldsymbol{x_m}(k) \in \Re^{3\times 1}$ is state vector of the DC motor at the k^{th} sample time,

$y_m(k) \in \Re$ is rotational angle of the rotor of the DC motor at the k^{th} sample time,

$\boldsymbol{\Phi_m}(T) = e^{\boldsymbol{A_m}T} = \boldsymbol{I_3} + A_m T + \frac{1}{2!}\boldsymbol{A_m^2}T^2 + \frac{1}{3!}\boldsymbol{A_m^3}T^3 + \cdots \quad \in \Re^{3\times 3}$,

$\boldsymbol{\theta_m}(T) = \int_0^T \boldsymbol{\Phi_m}(T-\tau)\boldsymbol{B}d\tau \quad \in \Re^{3\times 1}$, and

$\boldsymbol{C_m}(T) = \boldsymbol{C_m} \quad \in \Re^{1\times 3}$

5.1.2 Discrete time full-order state observer design:

To implement the discrete time optimal tracking controller, the information of all state variables of the system is needed. However, all state variables are not accessible in practical systems [5]. Furthermore, in the system that all state variables are accessible, the hardware configuration of the system becomes complex and the cost to implement this system is very high because sensors to measure all states are needed. Because of these reasons, a discrete time observer is needed to estimate the information of all states of the system. In the case that the output of the system is

measurable and the system is full-observable, a discrete time full-order state observer can be designed to observe information of all state variables of the system.

It is assumed that the system (5.7) is full-observable. The system equations of the discrete time closed loop observer are proposed as follows:

$$\begin{aligned} \hat{\boldsymbol{x}}_{\boldsymbol{m}}(k+1) &= \boldsymbol{\Phi}_{\boldsymbol{m}}(T)\hat{\boldsymbol{x}}_{\boldsymbol{m}}(k) + \boldsymbol{\theta}_{\boldsymbol{m}}(T)V(k) - \boldsymbol{L}(\hat{y}_m(k) - y_m(k)) \\ \hat{y}_m(k) &= \boldsymbol{C}_{\boldsymbol{m}}(T)\hat{\boldsymbol{x}}_{\boldsymbol{m}}(k) \end{aligned} \tag{5.8}$$

where $\hat{\boldsymbol{x}}_{\boldsymbol{m}}(k) \in \Re^{3\times 1}$ is state vector of the observer at the k^{th} sample time, $\hat{y}_m(k) \in \Re$ is the rotational angle of rotor of the observer at the k^{th} sample time, and $\boldsymbol{L} \in \Re^{3\times 1}$ is the feedback gain matrix.

$\tilde{\boldsymbol{x}}_{\boldsymbol{m}}(k) = \boldsymbol{x}_{\boldsymbol{m}}(k) - \hat{\boldsymbol{x}}_{\boldsymbol{m}}(k)$ is defined as the estimated error state vector between the motor and the observer. Subtracting Eq. (5.8) from Eq. (5.7), the error state equation can be obtained as

$$\tilde{\boldsymbol{x}}_{\boldsymbol{m}}(k+1) = \left[\boldsymbol{\Phi}_{\boldsymbol{m}}(T) - \boldsymbol{L}\boldsymbol{C}_{\boldsymbol{m}}(T)\right]\tilde{\boldsymbol{x}}_{\boldsymbol{m}}(k) = \boldsymbol{A}_{\boldsymbol{cd}}\tilde{\boldsymbol{x}}_{\boldsymbol{m}}(k) \tag{5.9}$$

The design objective of the observer is to obtain a feedback gain matrix $\boldsymbol{L}$ such that the estimated error states approach to zero as fast as possible. That is, the feedback gain matrix $\boldsymbol{L}$ must be designed such that eigenvalues of $\boldsymbol{A}_{\boldsymbol{cd}}$ exist in unit circle for the system (5.9) to be stable. By pole assignment method using Ackermann formulation with observability matrix $\boldsymbol{O}_{\boldsymbol{m}}$, the feedback gain matrix $\boldsymbol{L}$ is obtained as follows [5]:

$$\boldsymbol{L} = \Delta'(\boldsymbol{\Phi}_m)\, \boldsymbol{O}_m^{-1} \boldsymbol{e}_3^T = \Delta'(\boldsymbol{\Phi}_m) \begin{bmatrix} \boldsymbol{C}_m \\ \boldsymbol{C}_m \boldsymbol{\Phi}_m \\ \boldsymbol{C}_m \boldsymbol{\Phi}_m^2 \end{bmatrix}^{-1} \begin{bmatrix} 0 \\ 0 \\ 1 \end{bmatrix} \tag{5.10}$$

where $\Delta'(\boldsymbol{\Phi}_m)$ is desired characteristic equation of the observer, $\boldsymbol{O}_m = \begin{bmatrix} \boldsymbol{C}_m & \boldsymbol{C}_m \boldsymbol{\Phi}_m & \boldsymbol{C}_m \boldsymbol{\Phi}_m^2 \end{bmatrix}^T$ is observability matrix, and $\boldsymbol{e}_3 = \begin{bmatrix} 0 & 0 & 1 \end{bmatrix}$ is unit vector.

Block diagram of this observer is shown in Fig. 5.2.

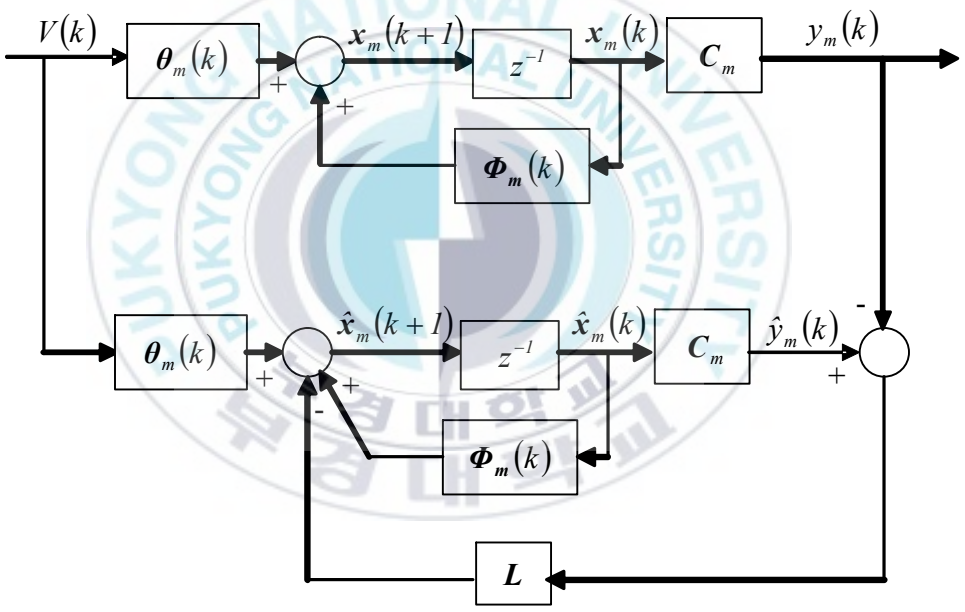

Fig. 5.2: Block diagram of the system with observer.

5.1.3 Discrete time optimal tracking controller design based on discrete time full-order state observer:

It is assumed that future values of the reference input $\boldsymbol{r}(k+1), \boldsymbol{r}(k+2), \cdots,$ cannot be utilized. The future values of the reference input beyond the k^{th} sample time are approximated as $\boldsymbol{r}(k)$. It means that the following is satisfied.

$$\Delta \boldsymbol{r}(k+i) = 0 \quad \text{for} \quad i = 1,2,\ldots \tag{5.11}$$

Based on the proposed observer (5.8) and the condition (5.11), the controller can be given from (3.47) as follows:

$$V(k) = K_{1e} \frac{z}{z-1} e(k) + \boldsymbol{K}_{1x} \hat{\boldsymbol{x}}_m(k) \tag{5.12}$$

where

$$\boldsymbol{K}_1 = \begin{bmatrix} K_{1e} & \boldsymbol{K}_{1x} \end{bmatrix} = -\left[\boldsymbol{R} + \boldsymbol{G}^T \boldsymbol{P}_1 \boldsymbol{G}\right]^{-1} \boldsymbol{G}^T \boldsymbol{P}_1 \boldsymbol{A}_E \in \Re^{1\times 4},\ \boldsymbol{G} = \begin{bmatrix} -\boldsymbol{C}_m \boldsymbol{\theta}_m \\ \boldsymbol{\theta}_m \end{bmatrix} \in \Re^{1\times 4}$$

$$\boldsymbol{A}_E = \begin{bmatrix} 1 & -\boldsymbol{C}_m \boldsymbol{\Phi}_m \\ \boldsymbol{0}_{3\times 1} & \boldsymbol{\Phi}_m \end{bmatrix} \in \Re^{4\times 4} \text{ and } \boldsymbol{P}_1 = \in \Re^{4\times 4} \text{ is positive definite matrix.}$$

$\boldsymbol{P}_1$ is solution of the following Ricatti equation.

$$\boldsymbol{P}_1 = \boldsymbol{Q} + \boldsymbol{A}_E^T \boldsymbol{P}_1 \boldsymbol{A}_E - \boldsymbol{A}_E^T \boldsymbol{P}_1 \boldsymbol{G}\left[R + \boldsymbol{G}^T \boldsymbol{P}_1 \boldsymbol{G}\right]^{-1} \boldsymbol{G}^T \boldsymbol{P}_1 \boldsymbol{A}_E \tag{5.13}$$

where $\boldsymbol{Q} \in \Re^{4\times 4}$ is semi-positive definite matrix, and $R \in \Re$ is positive scalar.

The discrete time optimal tracking control system of the DC motor (5.12) designed based on the information of states of the system obtained from discrete time closed loop observer (5.8) is shown in Fig. 5.3.

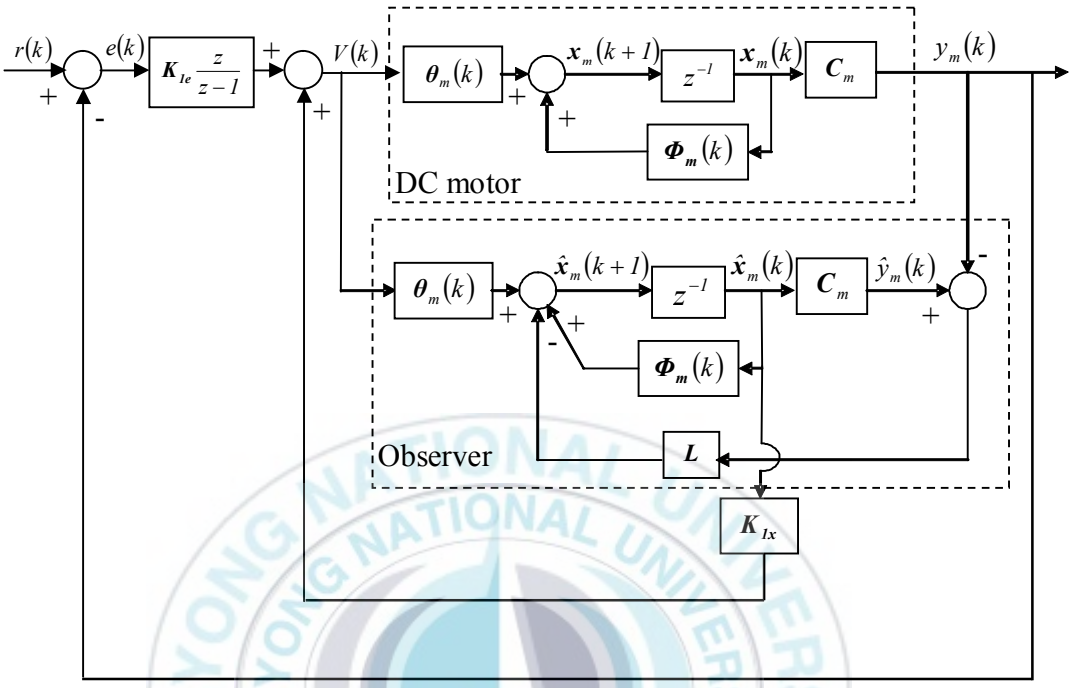

Fig. 5.3: Block diagram of the optimal control of the DC motor.

5.1.4 Traditional Discrete Time PID controller:

The traditional discrete time PID controller using forward-rectangular integration is proposed as follows [5]:

$$V(z) = \frac{(k_p T + k_d + k_i T^2) z^2 - (k_p T + 2k_d) z + k_d}{Tz(z-1)} \tag{5.14}$$

where T is sampling time, and k_p, k_i and k_d are proportional, derivative and integral gains with positive constants, respectively.

It is used to compare with the controller designed in section 5.1.3

5.1.5 Simulation results:

The effectiveness of the controller (5.12) as shown in Fig. 5.3 is verified by the simulation results. The values of the motor's parameters used in the simulation are given in Table 5.1 as shown below:

Table 5.1 Numerical values of the DC motor's parameters

Parameters	Description	Values	Units
R	Armature resistance	2.7	[Ω]
L	Armature inductance	1.4	[mH]
K	Electromotive force constant	$5.3\text{x}10^{-2}$	[Nm/A]
V	Rated voltage	24	[V]
J	Moment of inertia of rotor	$0.049\text{x}10^{-4}$	[kgm^2]
b	Damping ratio of the mechanical system	$0.025\text{x}10^{-3}$	[Nms]

The DC motor is controlled by the optimal tracking controller (5.12) which is obtained by choosing $R = 1$ and $\boldsymbol{Q} = \begin{bmatrix} 0.2 & 0 & 0 & 0 \\ 0 & 0 & 0 & 0 \\ 0 & 0 & 0 & 0 \\ 0 & 0 & 0 & 0 \end{bmatrix}$. The poles of the system (5.9) are chosen as $\boldsymbol{\lambda} = [0.5 \quad 0.375 + j0.32 \quad 0.375 - j0.32]$ for fast response. The feedback gain matrix $\boldsymbol{L} = [-0.153 \quad 0.00009 \quad 0.00000012]^T$ is obtained from (5.10). The simulation results of the observer are shown in Figs. 5.4~5.6. And the simulation results of the designed discrete time optimal tracking controller of the DC motor designed based on the discrete time full-order state observer are shown in Figs. 5.7~5.10.

Figs. 5.4~5.7 show that even with the different initial conditions between the observer and the system, all states and the output of the designed observer converge to those of the system after about 0.01 second.

Fig. 5.8 shows that discrete time optimal tracking controller of the DC motor designed based on the discrete time full-order state observer has good performance. The output of the system converges to the reference input after about 0.08 second, and its overshoot is about 4.5%. The tracking error of the system is shown in Fig. 5.9. The control signal input is shown in Fig. 5.10.

Figs. 5.11~5.16 show the simulation results of the tracking angle of the DC motor control system using the traditional PID controller with two cases: unbounded control signal and bounded control signal. The traditional PID controller is designed based on the flat criterion. The parameters of the traditional PID controller are k_p = 417.7, k_i = 21915.4 and k_d = 0.6. When control signal V is unbounded, the overshoot of the output is about 11.5% as shown in Fig. 5.11, and the tracking error converges to zero after about 0.07 second as shown in Fig. 5.12. However, the control signal V changes from -2000 to 4100 as shown in Fig. 5.13, and it is too big value to be implemented for the real system. When the control signal V is bounded as shown in Fig. 5.16, the overshoot of the output is about 40% as shown in Fig. 5.14, and the tracking error converges to zero after about 0.08 second as shown in Fig. 5.15.

In comparing the simulation results of the discrete time optimal tracking controller designed based on the discrete time full-order state observer with those of the traditional PID controller, it is shown that the designed discrete time optimal tracking controller has better performance than the traditional PID controller.

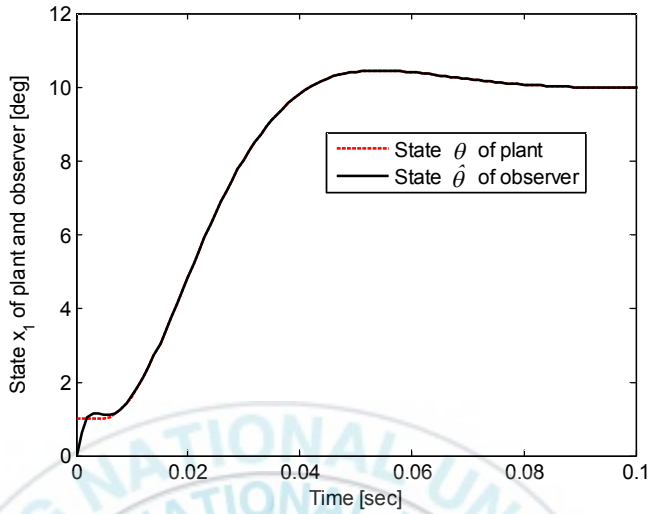

Fig. 5.4: State $\hat{\theta}$ of observer and state θ of the DC motor.

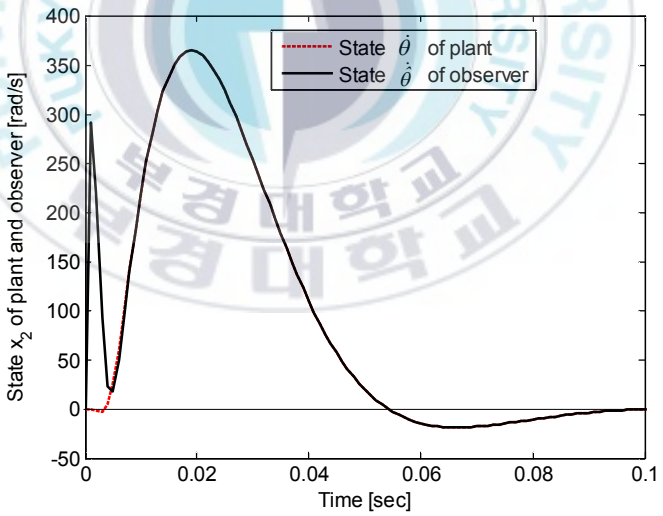

Fig. 5.5: State $\dot{\hat{\theta}}$ of observer and state $\dot{\theta}$ of the DC motor.

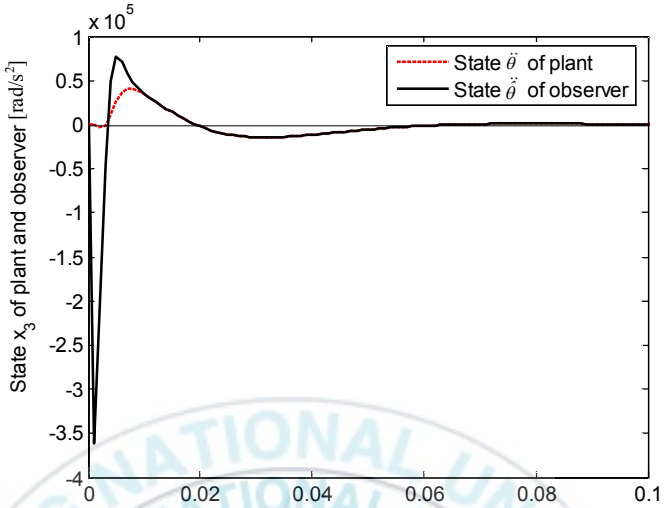

Fig. 5.6: State $\ddot{\hat{\theta}}$ of observer and state $\ddot{\theta}$ of the DC motor.

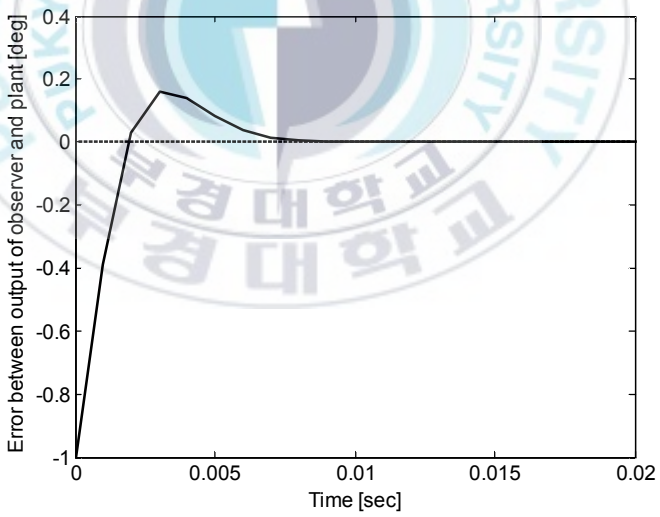

Fig. 5.7: Error between estimated output of observer and output of the DC motor.

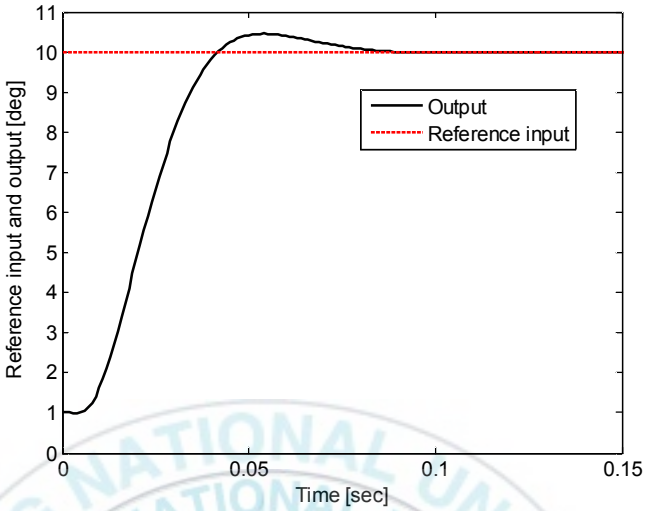

Fig. 5.8: Reference input and output of system using the discrete time optimal tracking controller.

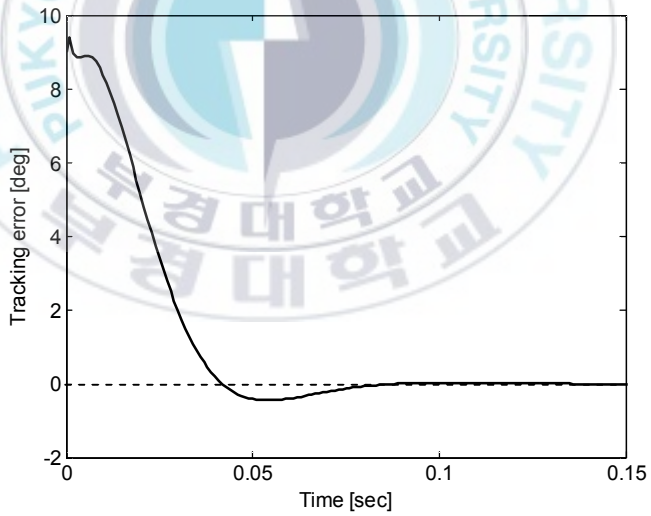

Fig. 5.9: Tracking error of system using the discrete time optimal tracking controller.

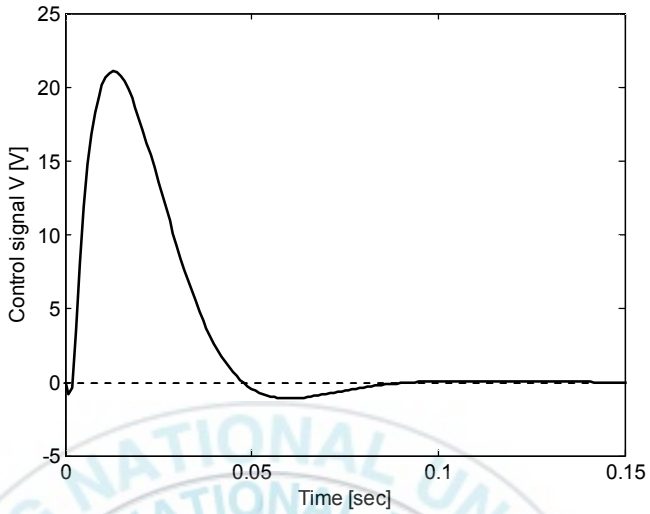

Fig. 5.10: Control signal input using the discrete time optimal tracking controller.

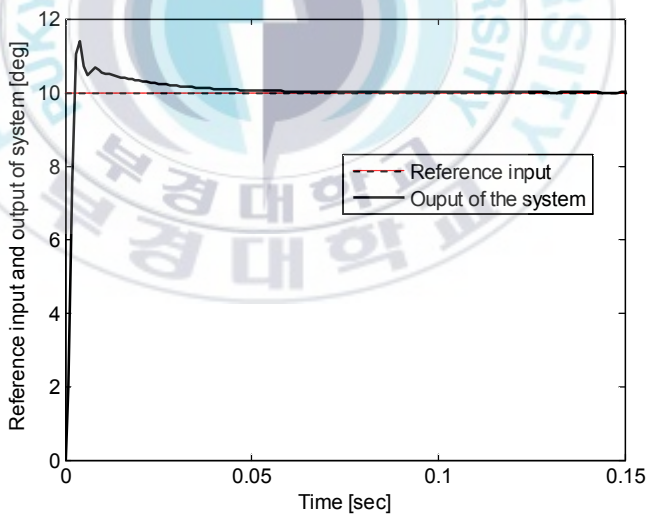

Fig. 5.11: Reference and output of system using traditional PID controller with unbounded control signal *V*.

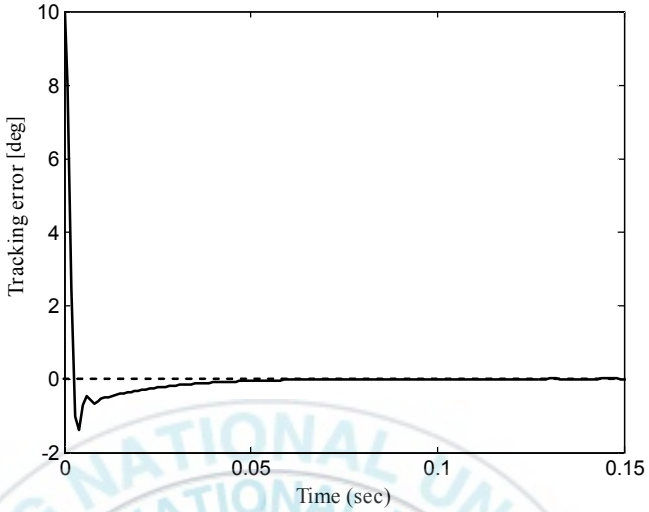

Fig. 5.12: Tracking error of system using traditional PID controller with unbounded control signal *V*.

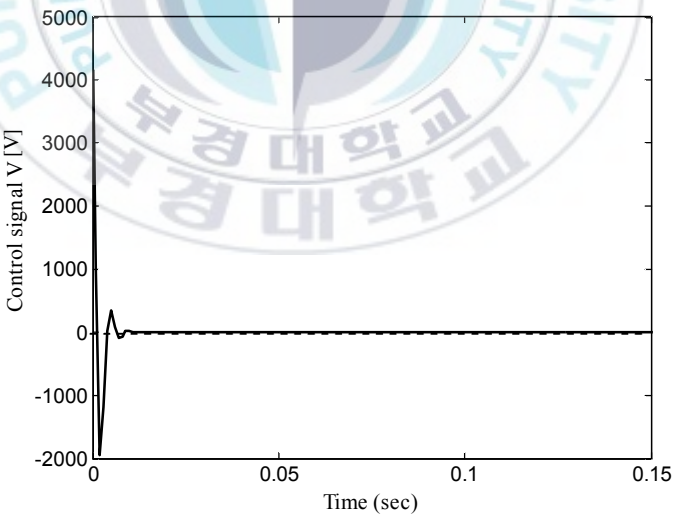

Fig. 5.13: Unbounded control signal *V* of traditional PID controller.

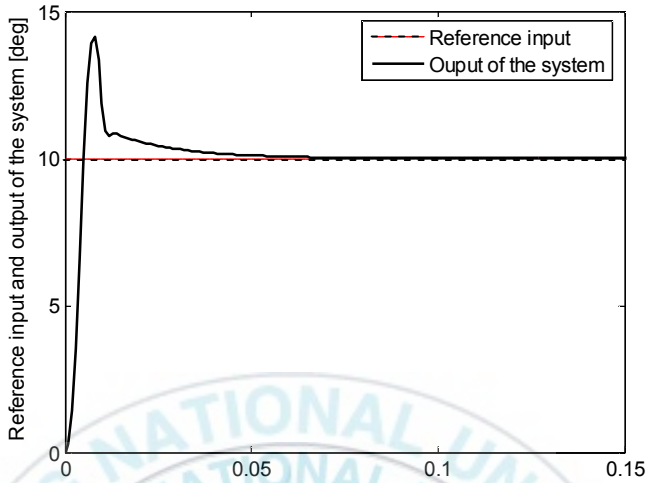

Fig. 5.14: Reference and output of system using traditional PID controller with bounded control signal *V*.

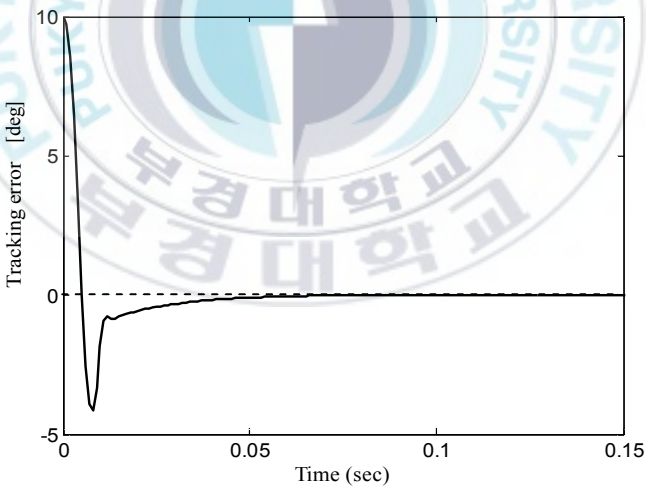

Fig. 5.15: Tracking error of system using traditional PID controller with bounded control signal *V*.

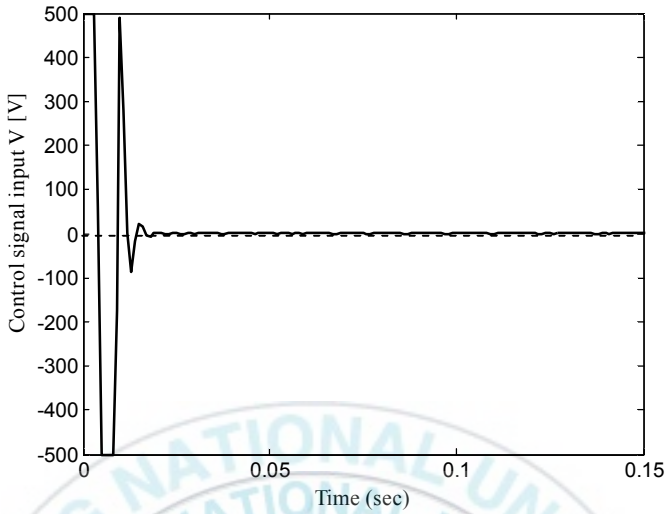

Fig. 5.16: Bounded control signal *V* of traditional PID controller.

5.2 Hardware of the Biped Robot:

The walking control method proposed in chapter 3 and 4 is implemented in CIMEC-1 biped robot developed for this thesis as shown in Fig. 5.17. A simple hardware configuration using three PIC18F4431 and one dsPIC30F6014 for the CIMEC-1 is shown in Fig. 5.18. The dsPIC30F6014 is used as mater unit, and PIC18F4431 is used as slave unit. The master unit and the slave units communicate each other via I2C communication. The control algorithm designed in section 5.1 is implemented in PIC18F4431 to control the DC motors at the joints of the biped robot. The angles of joints of the biped robot are measured by potentiometers. The dsPIC30F6014 is used to solve the inverse kinematics problem based on the trajectory of the center of the pelvis of biped robot and the trajectory of the ankle of the swinging leg which are contained in its memory. It can also communicate

personal computer via RS-232 communication. The angles at the k^{th} sample time obtained from inverse kinematics are sent to PIC18F4431 as reference signals.

Fig. 5.17: CIMEC-1 biped robot.

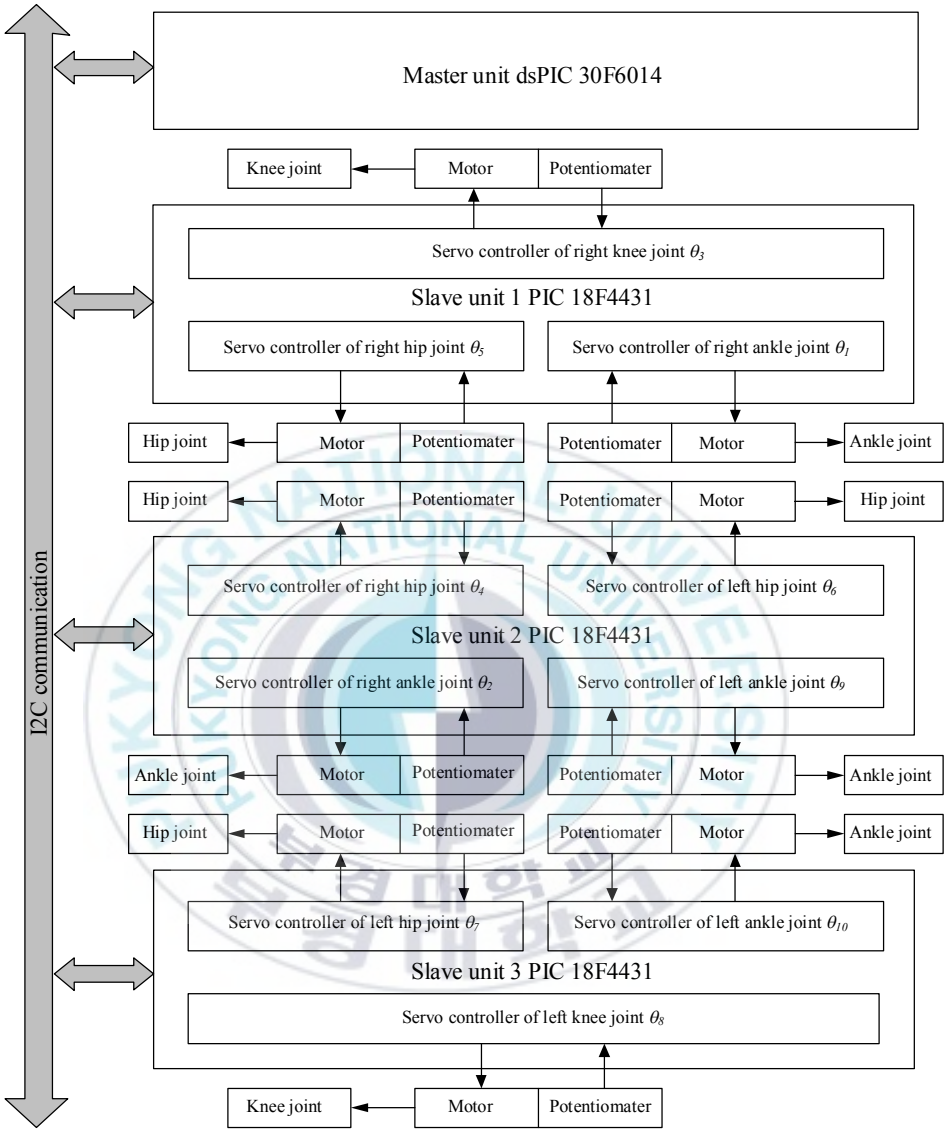

Fig. 5.18: Hardware configuration of the CIMEC-1.

5.3 Experimental Results:

In this section, the experimental results of the motion of the CIMEC-1 are shown. The discrete time optimal tracking controller designed in section 5.1 is implemented with the PIC18F4431 to control the DC motor of the joints of the CIMEC-1. The effectiveness of the controller presented in section 5.1 is proved by the experiment results as shown in Figs. 5.19~5.28. The experiment results of the angles of the joints of the CIMEC-1 are vibrated around their simulation results and reference inputs. These several vibrations are created by the backlash of the gear box of the motor, the disturbances from the electronic circuit, the resolution of the ADC of the PIC, the sensitivity of the sensors, etc. The experimental results of the angles of the joints of the CIMEC-1 are shifted-time to be compared with their simulation results although the shifted-time is small. This shifted-time occurs in data acquisition to be displayed on screen of personal computer because transmission and receipt data of computer cannot occur in the same time. The receipt data time is delayed compared with transmission data time. It means that without data acquisition to be displayed on screen of personal computer, the experimental results are vibrated around the simulation results. The simulation and experiment results show that the motion of CIMEC-1 is stable.

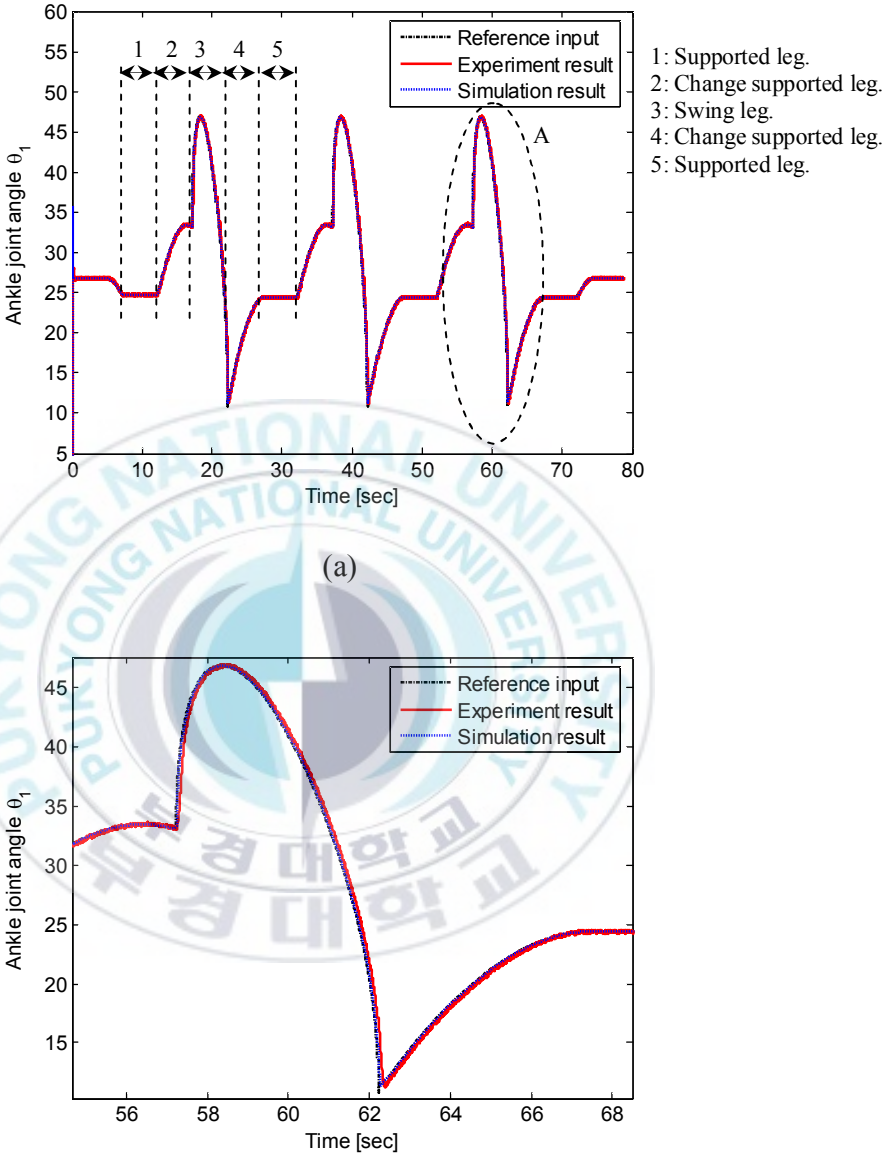

Fig. 5.19: Simulation and experimental results of the ankle joint θ_1.

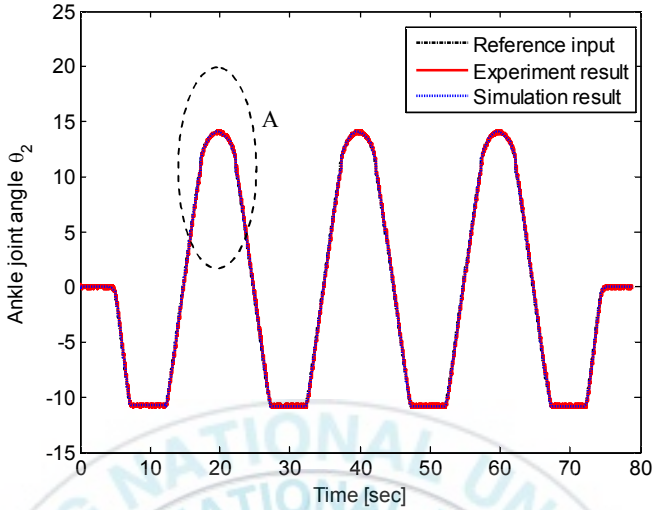

(a)

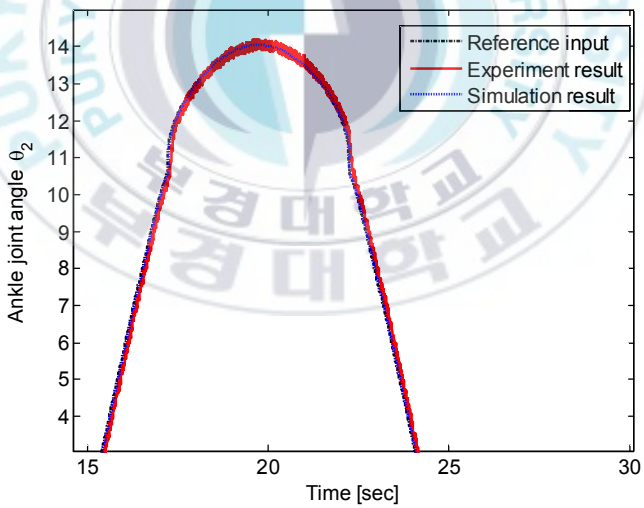

(b) A region

Fig. 5.20: Simulation and experimental results of the ankle joint θ_2.

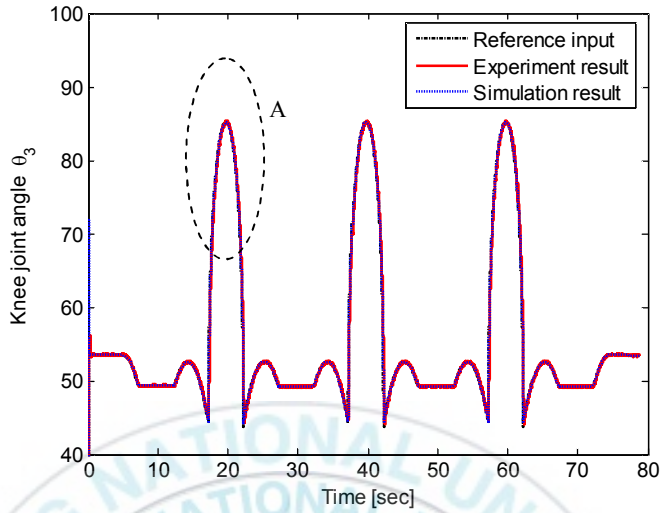

(a)

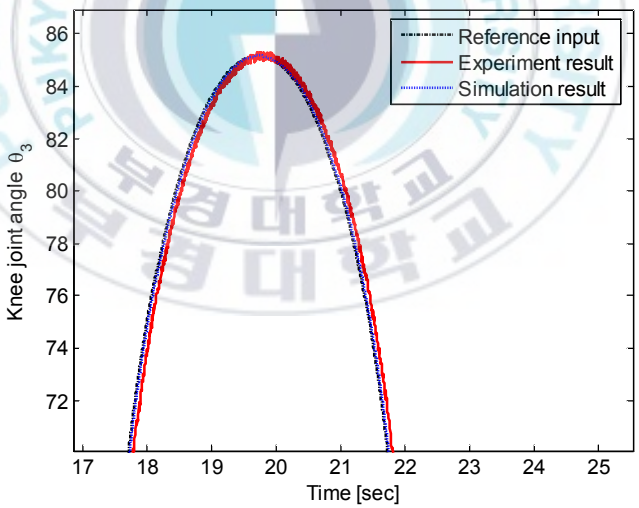

(b) A region

Fig. 5.21: Simulation and experimental results of the ankle joint θ_3.

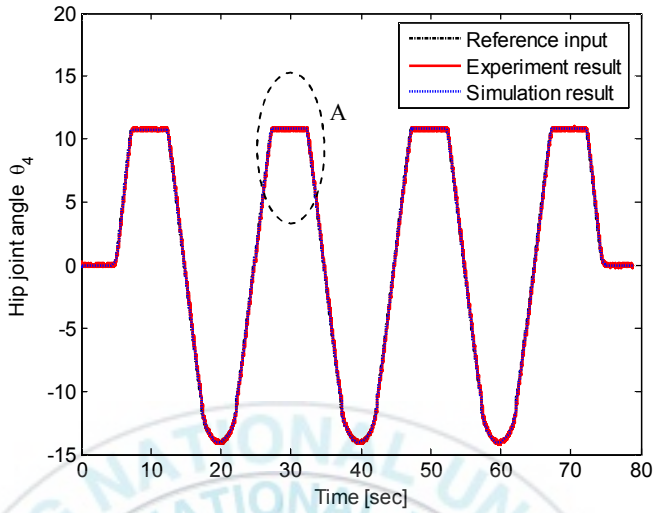

(a)

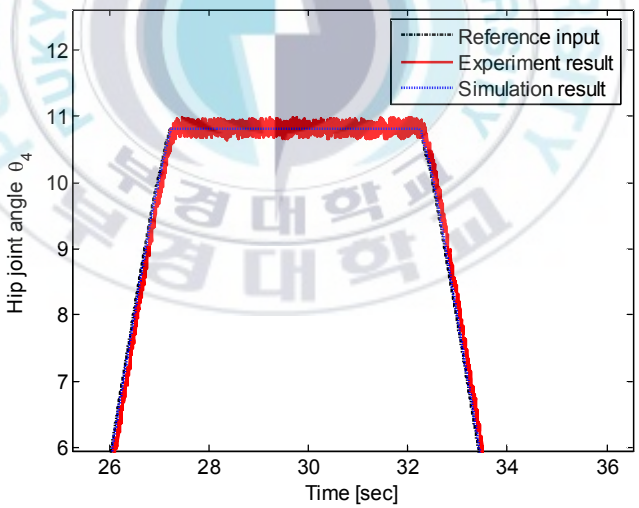

(b) A region

Fig. 5.22: Simulation and experimental results of the ankle joint θ_4.

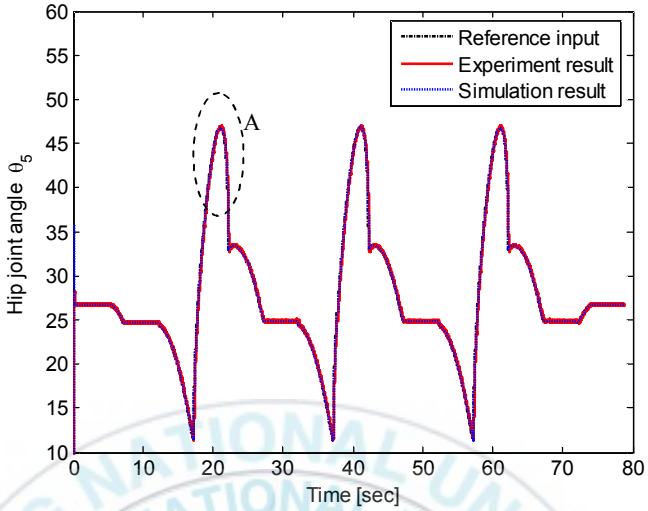

(a)

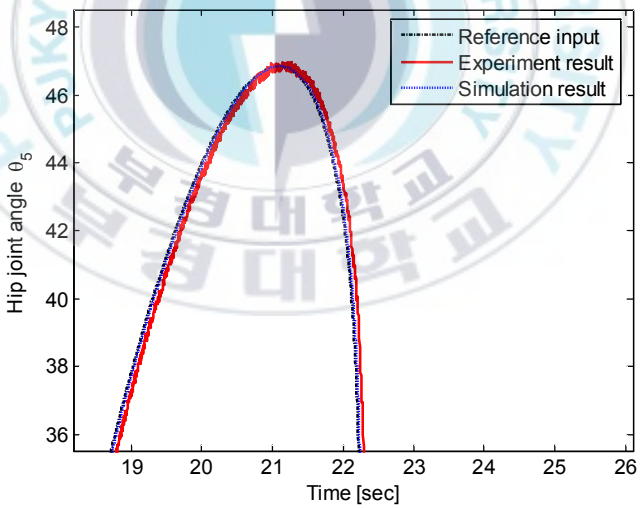

(b) A region

Fig. 5.23: Simulation and experimental results of the ankle joint θ_5.

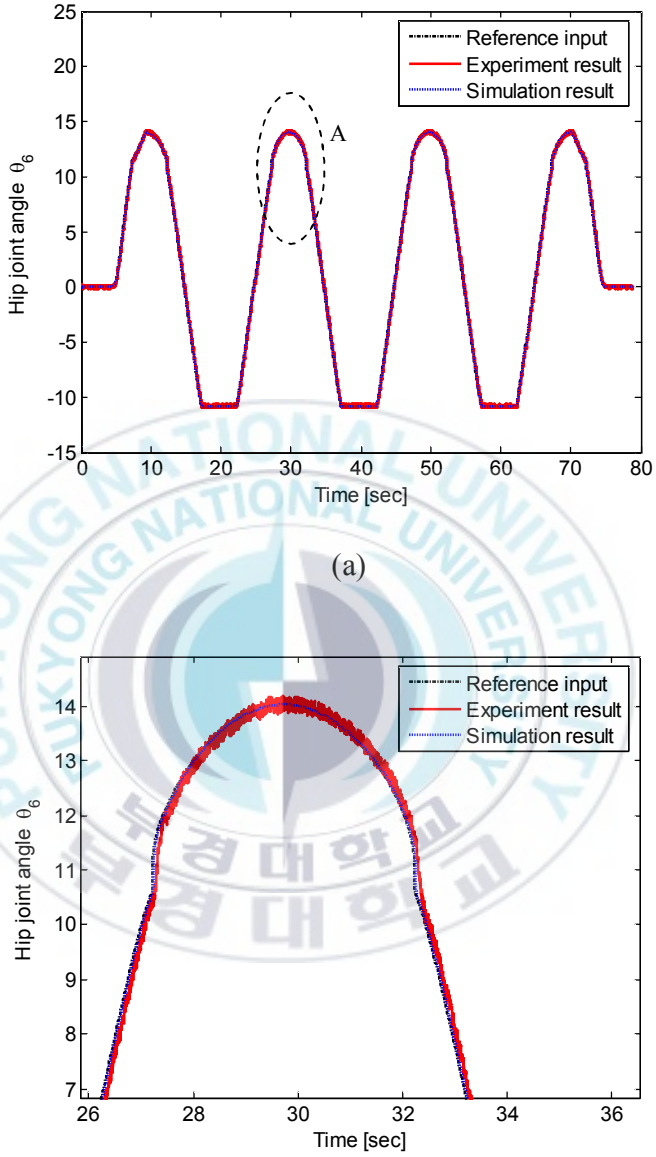

(b) A region

Fig. 5.24: Simulation and experimental results of the ankle joint θ_6.

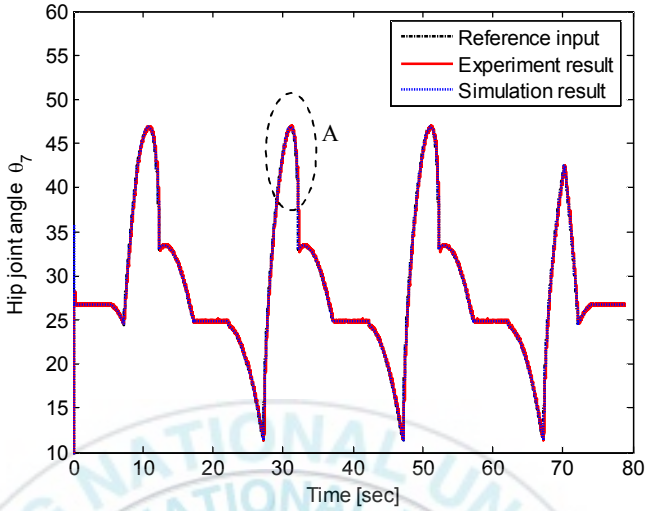

(a)

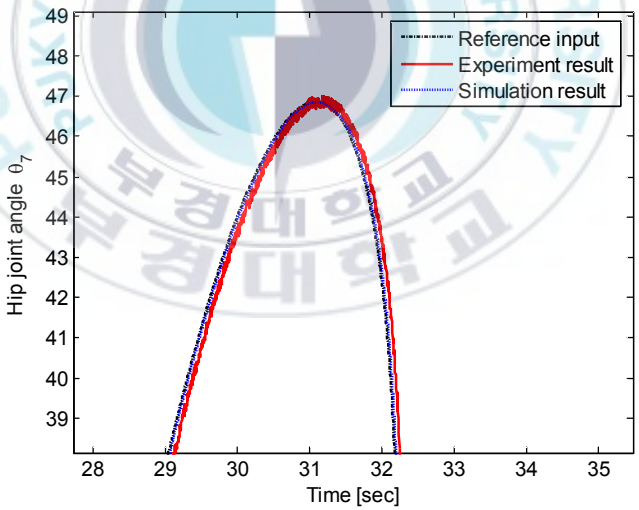

(b) A region

Fig. 5.25: Simulation and experimental results of the ankle joint θ_7.

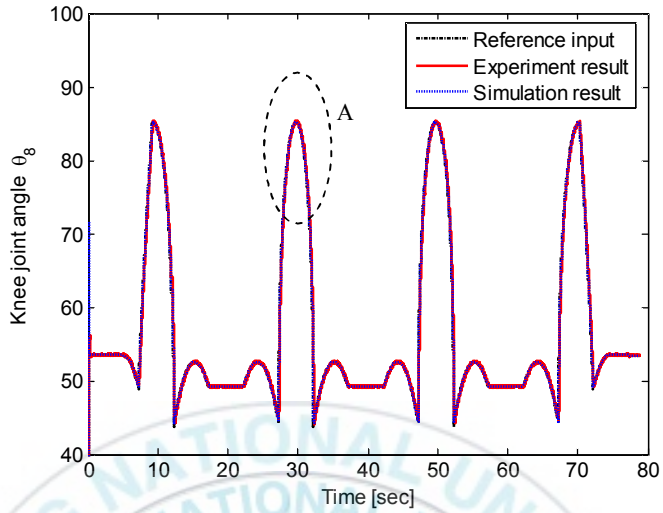

(a)

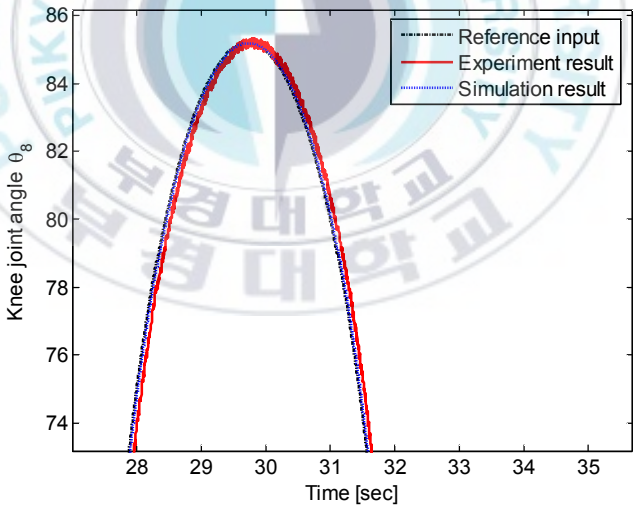

(b) A region

Fig. 5.26: Simulation and experimental results of the ankle joint θ_8.

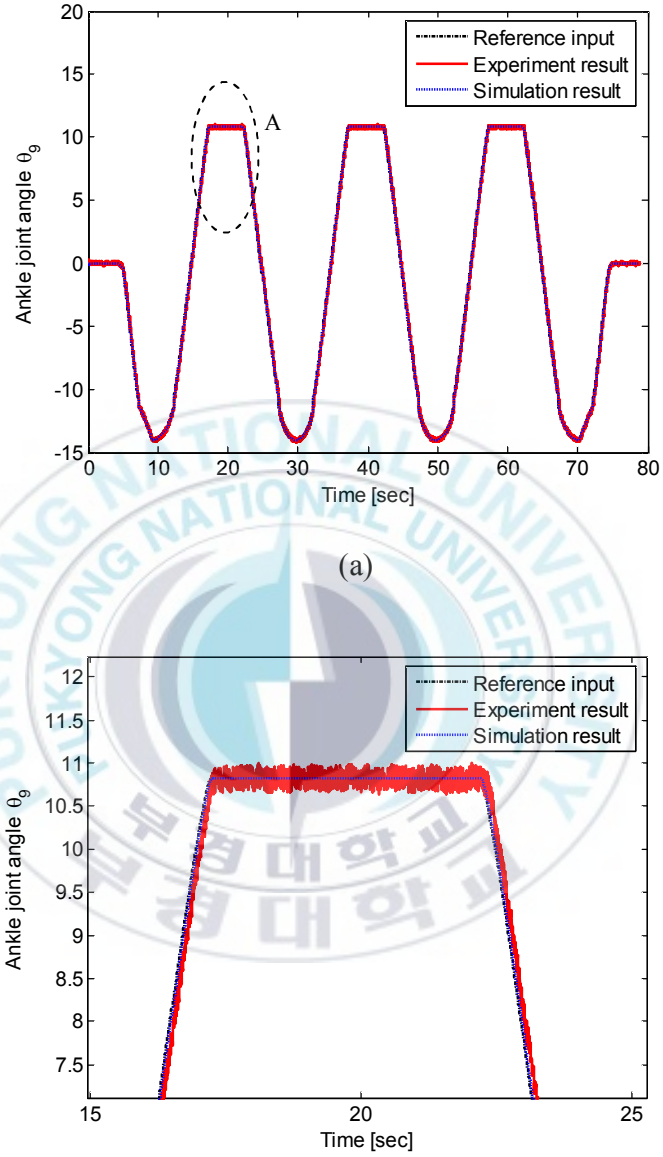

(b) A region

Fig. 5.27: Simulation and experimental results of the ankle joint θ_9.

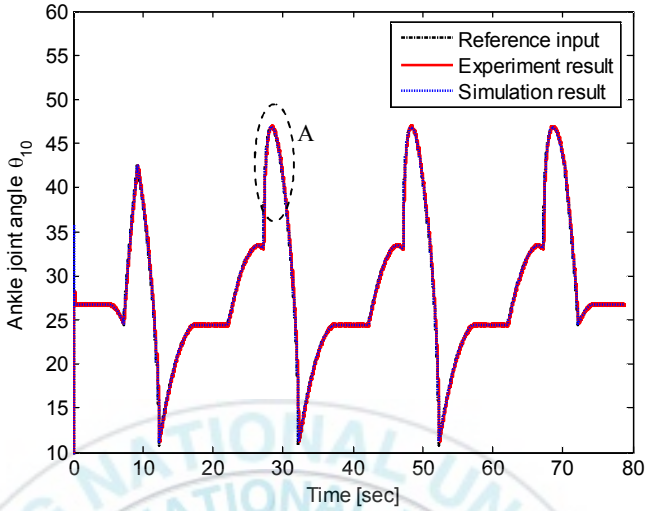

(a)

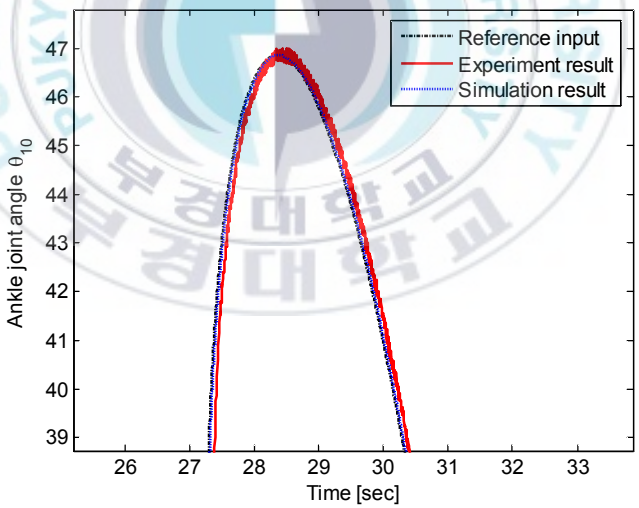

(b) A region

Fig. 5.28: Simulation and experimental results of the ankle joint θ_{10}.

5.4 Summary:

This chapter presents a discrete time optimal tracking control system for the motion of the biped robot based on a full-order observer. A closed loop observer is designed based on poles assignment method using Ackermann formulation to estimate feedback states of the DC motor. A discrete time optimal tracking controller designed based on the discrete time full-order state observer is proposed. The effectiveness of the proposed controller is shown by the simulation and experiment results. Moreover, the simulation results of the discrete time optimal tracking controller designed based on the discrete time full-order state observer are compared with those of the traditional PID controller. It is shown that the designed discrete time optimal tracking controller has better performance than the traditional PID controller.

Chapter 6: Conclusions and Future Works

6.1 Conclusions:

This thesis presents the development results of the 10 DOF biped robot with stable and human-like walking using the simple hardware configuration. The conclusions of this thesis are summarized as follows:

- Kinematics model of the 10 DOF biped robot and its dynamic model based on the 3D inverted pendulum are presented.
- ZMP equations of the biped robot depending on the coordinate of the center of the pelvis link obtained from the dynamic model of the biped robot are given.
- The continuous time and the discrete time model of the ZMP systems are presented.
- A continuous time and a discrete time optimal tracking controllers are designed to control the ZMP tracking control system. From the advantage of the designed discrete time optimal tracking controller using the future values of the reference input in the practical system compared with the designed continuous time optimal tracking controller, the designed discrete time optimal tracking controller using the future values of the reference input is chosen to control the ZMP tracking control systems.

- A stable walking pattern generation method of the biped robot based on the discrete time ZMP tracking control system is proposed.
- A solving method inverse kinematics of the biped robot based on the solid geometry method is presented.
- A simple control method for the stable walking of the biped robot is also presented.
- A discrete time full-order state observer of the DC motor is designed to estimate the information of the full states of the DC motor. Feedback gain matrix of the closed loop observer is obtained by pole assignment method using Ackermann formulation with observability matrix.
- A discrete time optimal tracking control of the DC motor system with state feedback of the information of states obtained by the designed discrete time full-order state observer is designed to control actuator at the joints of the biped robot.
- A traditional discrete time PID controller using forward-rectangular integration is proposed to compare with the designed discrete time optimal tracking controller.
- Hardware to implement the biped robot controller using dsPIC30F6014 and PIC18F4431 is developed.
- The simulation and experiment results are shown to prove the effectiveness of the proposed walking control method of the biped robot.

With the proposed walking control method using rectangular reference trajectory and zigzag reference trajectory of the ZMP, the biped robot can walk not only with stable gait but also with human-like gait. Furthermore, the hardware configuration is simple so that it can easy to implement for the low cost biped robot.

6.2 Future Works:

This thesis only takes the focus on the stable walking of the biped robot. There are some future works as follows:

- ❖ Consideration of the uneven terrain and arbitrary reference trajectory of the ZMP,
- ❖ Climbing up and down stair,
- ❖ Equipping arms and head and development humanoid robot.

References

[1] A. Farooq and D. J. N. Limebeer, "Path Following of Optimal Trajectories Using Preview Control", Proc. of IEEE Conference on Decision and Control, and The European Control Conference, pp. 2787~2792, 2005.

[2] A. Takanishi, M. Ishida, Y, Yamazaki and I. Kato, "The Realization of Dynamic Walking by the Biped Walking Robot WL-10RD", International Conference on Advanced Robotics, pp. 459~466, 1985.

[3] ASIMO Humanoid Robot: http://asimo.honda.com/index.asp?bhcp=1.

[4] A. Goswami, B. Espiau and A. Keramane, "Limit cycles and their stability in a passive bipedal gait", Proc. of the IEEE International Conference on Robotics and Automation, pp. 246-251, 1996.

[5] B. C. Kou, "Digital Control Systems", International Edition, 1992.

[6] C. Shih and W. Gruver, "Control of a Biped Robot in the Double Support Phase", IEEE Trans. Systems, Man and Cybernetics, Vol. 22 , No. 4, pp. 729~735, 1992.

[7] C. Zhu and A. Kawamara, "Walking Principle Analysis for Biped Robot with ZMP Concept, Friction Constraint, and Inverted Pendulum Model", Proc. of IEEE/RSJ International conference on Intelligent Robots and Systems, pp. 364~369, 2003.

[8] D. Li, D. Zhou, Z. Hu and H. Hu, "Optimal Priview Control Applied to Terrain Following Flight", Proc. of IEEE Conference on Decision and Control, pp. 211~216, 2001.

[9] D. Plestan, J. W. Grizzle, E. R. Westervelt and G. Abba, "Stable Walking of A 7-DOF Biped Robot", IEEE Trans. on Robotics and Automation, Vol. 19, No. 4, pp. 653-668, 2003.

[10] E. Mosca and A. Casavola, "Deterministic LQ Preview Tracking Design", IEEE Trans. Automatic Control, Vol. 40, pp. 1278~1281, 1995.

[11] F. L. Lewis, C. T. Abdallah and D.M. Dawson, "Control of Robot Manipulator", Prentice Hall International Edition, 1993.

[12] G. F. Franklin, J. D. Powell and A. E. Naeini, “Feedback Control of Dynamic System”, Prentice Hall Upper Saddle River, New Jersey 07458.

[13] G. Kinoshita, C. Oota, H. Osumi and M. Shimojo, “Acquisition of Reaction Force Distributions for a Walking Humanoid Robot”, Proc. of IEEE/RSJ International conference on Intelligent Robots and Systems, pp. 3859~3864, 2004.

[14] G. A. Bekey, “Autonomous Robots From Biological Inspiration to Implementation and Control”, The MIT Press, 2005.

[15] H. K. Lum, M. Zribi and Y. C. Soh, “Planning and Control of a Biped Robot”, Int. Journal of Engineering Science ELSEVIER, Vol. 37, pp. 1319~1349, 1999.

[16] H. Hirukawa, S. Kajita, F. Kanehiro, K. Kaneko and T. Isozumi, “The Human-size Humanoid Robot That Can Walk, Lie Down and Get Up”, International Journal of Robotics Research, Vol. 24, No. 9, pp. 755~769, 2005.

[17] H. Inoue, K. Tachi, K. Tanie, S. Yokoi and H. Hirai, “HPR: Humanoid Robotics Project of MIT”, First IEEE/RAS International Conference on Humanoid Robots, Massachusetts Institute of Technology, Cambridge, Mass, 2000.

[18] HUBO Lab Site: http://ohzlab.kaist.ac.kr/.

[19] J. H. Part, “Impedance Control for Biped Robot Locomotion”, IEEE Trans. Robotics and Automation, Vol. 17, No. 3, pp. 870~882, 2001.

[20] J. Perry, “Gait Analysis: Normal and Pathological Function”, Thorofare N. J Slack Inc, 1992.

[21] J. Perry and J. K. Gronley, “Observation Gait Analysis Handbook”, Downey California Rancho Los Amigos Medical Center, 1989.

[22] J. Hu, J. Pratt and G. Pratt, “Adaptive Dynamic Control of a Bipedal Walking Robot With Radial Basic Function Neuron Networks ”, Proc. of IEEE International conference on Intelligent Robots and Systems, pp. 400~405, 1998..

[23] J. Golden and Y. Zheng, “Gait Synthesis for the SD-2 Biped Robot to Climb Stairs”, International Journal of Robotics and Automations, Vol. 5, No. 4, pp. 149~159, 1990.

[24] K. Hazawa, J. Shin, D. Fujirawa and K. Igarashi, “Autonomous Flight Control of Hobby-Class Small Unmanned Helicopter”, Proc. of IEEE/RSJ International conference on Intelligent Robots and Systems, pp. 754~760, 2004.

[25] K. Mitobe, G. Capi and Y. Nasu, “A New Control Method for Walking Robots Based on Angular Momentum”, Journal of Mechatronics ELSEVIER, Vol. 14, pp. 164~165, 2004.

[26] K. Kato, A. Katanishi, H. Jishikawa and I. Kato, “The Realization of Quasi-Dunamic Walking by the Biped Walking Machine”, The Fourth Symposium on Theory and Practice of Robots and Manipulators, pp. 341~351, 1983.

[27] K. Hirai, M. Hirose and T. Takenaka, “The Development of Honda Humanoid Robot”, Proc. of the 1998 IEEE International Conference on Robotics & Automation, pp. 1321-1326, 1998.

[28] K. Yokoyoma, H. Handa, T. Isozumi, Y. Fukase, K. Kaneko, F. Kanehira, Y. Kawai, F. Tomita and H. Hirukawa, “Cooperative Works by a Humanoid and a Humanoid Robot”, Proc. of the IEEE International Conference on Robotics and Automation, pp. 14-19, 2003.

[29] K. Harada, S. Kajita, K. Kaneko and H. Hirukawa, “Walking Motion for Pushing Manipulation by a Humanoid Robot”, Journal of the Robotics Society of Japan, Vol. 22, No. 3, pp. 392–399, 2004.

[30] K. Yokoyoma, H. Handa, T. Isozumi, Y. Fukase, K. Kaneko, F. Kanehira, Y. Kawai, F. Tomita and H. Hirukawa, “Cooperative Works by a Humanoid and a Humanoid Robot”, in Proceedings of the IEEE International Conference on Robotics and Automation,pp. 14-19, 2003.

[31] K. Harada, S. Kajita, K. Kaneko and H. Hirukawa, “Walking Motion for Pushing Manipulation by a Humanoid Robot”, Journal of the Robotics Society of Japan, Vol. 22, No. 3, pp. 392–399, 2004.

[32] L. Jalics, H. Hemami, and B. Clymer, “A Control Strategy for Terrain Adaptive Bipedal Locomotion”, Autonomous Robots, Vol. 5, No. 3, pp. 243-257, 1997.

[33] M. E. Halpern, “Optimal Tracking with Previewed Commands”, Proc. of IEE, Vol. 138, pp. 237~241, 1991.

[34] M. Wisse, A. L. Schwab, R. Q. van der Linde and F. C. T. van der Helm, “How to Keep From Falling Forward : Elementary Swing Leg Action for Passive Dynamic Walkers”, IEEE Transactions on Robotics, Vol. 21, No. 3, 2005.

[35] N. E. Sian, K. Yokoi, S. Kajita, F. Kanchiro and K. Tanie, “Whole Body Teleoperation of a Humanoid Robot – A Method of Integrating Operator’s Intention and Robot’s Autonomy”, Proc. of IEEE International conference on Robotics and Automations, pp. 1613~1619, 2003.

[36] P. Sardain and G. Bessonnet, “Zero Moment Point-Measurments From a Human Walker Wearing Robot Feet as Shoes”, IEEE Trans. Systems, Man and Cybernetics, Vol. 34 , No. 5, pp. 638~648, 2004.

[37] P. J. McKerrow, “Introduction to Robotics”, Addivision Wesley Longman China Ltd., VVP, 1998.

[38] Q. Huang, S. Kajita, N. Koyachi, K. Kaneko, K. Yokoi, H. Arai, K. Komoriya and K. Tanie, “A High Stability, Smooth Walking Pattern for a Biped Robot”, Proc. of IEEE International conference on Robotics and Automation, pp. 65~71, 1999.

[39] Q. Huang and Y. Nakamura, “Sensor Reflex Control for Humanoid Walking”, IEEE Trans. Robotics, Vol. 21, No. 5, pp. 977~984, 2005.

[40] QRIO Official Site: http://www.sony.net/SonyInfo/QRIO/.

[41] R. K. Mehra, J. N. Amin, K. J. Hedrick, C. Osorio and S. Gopalasamy, “Active Suspension Using Preview Information and Model Predictive Control”, Proc. of IEEE International conference on Control Apllications, pp. 860~865, 1997.

[42] S. Kajita, F. Kanehiro. K. Kaneko, K. Yokoi and H. Hirukawa, “The 3D Linear Inverted Pendulum Mode: A Simple Modeling for a Biped Walking

Pattern Generation", Proc. of IEEE/RSJ International conference on Intelligent Robots and Systems, pp. 239~246, 2001.

[43] S. Aramaki, H. Shirouzu, S. Kurono, M. Mino, Y. Uno, K. Hara, H. Tanaka and T. Tsuruoka, "Development od Autonomous Mobile Humanoid Robot", Proc. of the IEEE International Conference on Industrial Electronics Society, pp. 529-534, 1999.

[44] S. K. Agrawal and A. Fattah, "Motion Control of a Novel Planar Biped with Nearly Linear Dynamics", IEEE/ASME Trans. Mechatronics, Vol. 11, No. 2, pp. 162~168, 2006.

[45] S. Kajita, F. Kanehiro, K. Kaneko, K. Fujiwara, K. Harada, K. Yokoi and H. Hirukawa, "Biped Walking Pattern Generation by using Preview Control of Zero-Moment Point", Proc. of the 2003 IEEE International Conference on Robotics and Automation, pp. 1620-1626, 2003.

[46] T. Suzuki and K. Ohnishi, "Trajectory Planning of the Biped Robot with Two Kind of Inverted Pendulums", Proc. of IEEE/RSJ International conference on Intelligent Robots and Systems, pp. 396~401, 2006.

[47] T. Tsuji and K. Ohnishi, "A Control of Biped Robot which Applied Inverted Pendulum Mode with Virtual Supporting Point", Proc. of IEEE/RSJ International conference on Intelligent Robots and Systems, pp. 478~483, 2002.

[48] T. Komura, H. Leung, S. Kudoh and J. Kuffner, "A Feedback Controller for Biped Humanoid that Can Counteract Large Perturbations During Gait", Proc. of IEEE International conference on Robotics and Automations, pp. 1989~1995, 2005.

[49] T. Furuta, Y. Okumura, T. Tawara and H. Kitano, "Morph: a small-size humanoid platform for behavior coordination research", Proc. of IEEE/RAS Int. Conference on Humanoid Robots, pp. 165–171, 2001.

[50] T. McGeer, "Passive Dynamic Walking", The International Journal of Robotics Research, Vol. 9, No. 2, pp. 62-82, 1990.

[51] V. G. Ivancevic and M. Snoswell, "Fuzzy-Stochastic Functor Machine gor General Humanoid-Robot Dynamics", IEEE Trans. Systems, Man and Cybernetics, Vol. 31 , No. 3, pp. 319~329, 2001.

[52] Y. Fujimoto, S. Obata and A. Kawamura, “Robust Biped Walking with Active Interaction Control between Foot and Ground”, Proc. of IEEE Int. conference on Robotics and Automations, pp. 2030~2035, 1998.

[53] K. Zhou, J. C. Doyle and K. Glover, “Robust and Optimal Control”, Prentice Hall, Englewood Cliffs, New Jersey 07632.

[54] K. Furuta, A. Sano and D. Atherton, “State variable methods in Automatic Control”, John Wiley and Son 1988.

[55] H. Jeyer, “Simple Models of Legged Locomotion based on Compliant Limb Behavior”, PhD Thesis 2005.

[56] J. E. Pratt, “Exploiting Inherent Robustness and Natural Dynamics in the Control of Bipedal Walking Robots”, PhD thesis 2000.

[57] T. Mita and H. Yoshida, “Undershooting Phenomenon and Its Control in Linear Multivariable Servomechanisms”, IEEE Trans. Automatic Control, Vol. AC-26 , No. 2, pp. 402~407, 1981.

[58] K. Furuta and K. Komiya, “ Design of Model – Following Servo Controller”, IEEE Trans. Automatic Control, Vol. AC-27 , No. 3, pp. 725~727, 1982.

Publications and Conferences

A. Publications

[1] M. D. Ngo, V. H. Duy, N. T. Phuong, S. B. Kim and M. S. Oh, "Two Wheel Welding Mobile Robot for Tracking a Smooth Curved Welding Path Using Adaptive Sliding Mode Control Technique", *International Journal of Control, Automation and Systems (ICASE)*, Vol. 5, No. 3, pp. 1~12, 2007.

[2] M. D. Ngo, V. H. Duy, N. T. Phuong, H. K. Kim and S. B. Kim, "Development of Digital Gas Metal Arc Welding System", *ELSEVIER, Journal of Materials Processing Technology*, Vol. 189, No. 3, pp. 384~391, 2007.

[3] M. D. Ngo, V. H. Duy, N. T. Phuong and S. B. Kim, "Robust Control of Welding Robot for Tracking a Rectangular Welding Line", *International Journal of Advanced Robotic Systems*, Vol. 3, No. 3, pp. 239~249, September 2006.

[4] M. D. Ngo, N. T. Phuong, V. H. Duy, H. K. Kim and S. B. Kim, "Control of Two Wheel Welding Mobile Manipulator", *International Journal of Advanced Robotic Systems*, Vol. 4, No. 3, pp. 293~302, September 2007.

B. Submitted papers

[1] V. H. Duy, N. T. Phuong, S. M. Yoon, H. K. Kim and S. B. Kim, "A New Approach for Development of the Quadruped Walking Robot Based on Biological Concepts", *International Journal of Advanced Robotic Systems*, July 2007.

[2] V. H. Duy, N. T. Phuong, S. M. Yoon, H. K. Kim and S. B. Kim, "A Novel Approach for Developing Quadruped Robot", *ELSEVIER, Robotics and Autonomous Systems*, May 2007.

[3] V. H. Duy, N. T. Phuong, H. K. Kim and S. B. Kim, "Design of a Mixed H_2/H_∞ PID Controller for Speed Control of Brushless DC Motor by Genetic Algorithm", *Control and Cybernetics*, Warszawa, Poland, Aug. 2006.

[4] M. T. Kang, N. T. Phuong, H. K. Kim and S. B. Kim, "Stabilizing Control for Nonlinear Mobile Inverted Pendulum via Sliding Mode Technique", *ELSEVIER, Mechatronics*, Juny, 2007.

[5] N. T. Phuong, N. Hung, Sang Kwun Jeong, H. K. Kim and S. B. Kim, "Control of Biped Robot with Stable Walking", *ELSEVIER, Mechatronics*, January, 2008.

[6] N. T. Phuong, N. Hung, Sang Kwun Jeong, H. K. Kim and S. B. Kim, "A Simple Walking Control Method for Biped Robot with Stable Gait", *International Journal of Control, Automation and Systems*, January 2008.

C. Conferences

[1] V. H. Duy, N. T. Phuong, S. M. Yoon, H. K. Kim and S. B. Kim, "A New Approach for Designing Quadruped Robot", *IEEE International Conference on Mechatronics*, Japan, May 2007.

[2] N. T. Phuong, V. H. Duy, J. H. Jeong, H. K. Kim and S. B. Kim, "Adaptive Control for Welding Mobile Manipulator with Unknown Dimensional Parameters", *IEEE International Conference on Mechatronics*, Japan, May 2007.

[4] M. D. Ngo, N. T. Phuong, V. H. Duy, H. K. Kim and S. B. Kim, "Control of Gas Metal Arc Welding System Using Decentralized Method", *International Workshops of the 20th Anniversary of the Korean Society of Ocean Engineers*, Busan, Korea, pp. 60-66, Nov. 2006.

[5] V. H. Duy, N. T. Phuong, H. K. Kim and S. B. Kim, "Design of a Mixed H_2/H_∞ PID Controller for Speed Control of Brushless DC Motor by Genetic Algorithm", *KOSME*, Korea, 2006.

[6] M. D. Ngo, N. T. Phuong, H. K. Kim and S. B. Kim, "Control of Two-Wheeled Welding Mobile Robot For Tracking a Smooth Curved Welding Path", Proceeding of the Korean Society of Marine Engineering (KSOME) 2006 first conference, Thong-Yong City, Korea, June 2006.

[7] M. D. Ngo, V. H. Duy, N. T. Phuong, B. Y. Kim, H. K. Kim and S. B. Kim, "Adaptive Sliding-Mode Control for Two-Wheeled Welding Mobile Robot for Tracking a Smooth Curved Welding Path", The International Symposium on Advanced Mechatronics, Cybernetics and Automation, HCMC University of Technology, HoChiMinh City, Vietnam, February 2006.

[8] N. T. Phuong, V. H. Duy, M. D. Ngo, B. D. Park, H. K. Kim and S. B. Kim, "Current Control Using Fuzzy Logic Controller for DC Plasma Torch Power Supply", The International Symposium on Advanced Mechatronics, Cybernetics and Automation, HCMC University of Technology, HoChiMinh City, Vietnam, February 2006.

[9] V. H. Duy, N. T. Phuong, M. D. Ngo, L. H. Suk and S. B. Kim, "Design of An Optimal Robust PID for Speed Control of Brushless DC Motor", The International Symposium on Advanced Mechatronics, Cybernetics and Automation, HCMC University of Technology, HoChiMinh City, Vietnam, February 2006.

[10] J. W. Park, N. S. Choi, N. T. Phuong, T. T. Nguyen and S. B. Kim, "Motion Control of Animal Type Hybrid Quadruped Robot", The International Symposium on Mechatronics and Automation, HCMC University of Technology, HoChiMinh City, Vietnam, October 2007.

[11] N. T. Phuong, T. P. Tran, Y. J. An, H. K. Kim and S. B. Kim, "Control of Biped Robot with Stable Walking", The International Symposium on Mechatronics and Automation, HCMC University of Technology, HoChiMinh City, Vietnam, October 2007.

[12] S. M. Yoon, V. H. Duy, N. T. Phuong, S. B. Kim and M. S. Oh, "A New Approach for Development of the Quadruped Walking Robot", The International Symposium on Mechatronics and Automation, HCMC University of Technology, HoChiMinh City, Vietnam, October 2007.

Appendix A

Proof of Eq. 2.29:

The 3D inverted pendulum is shown in Fig. A.1

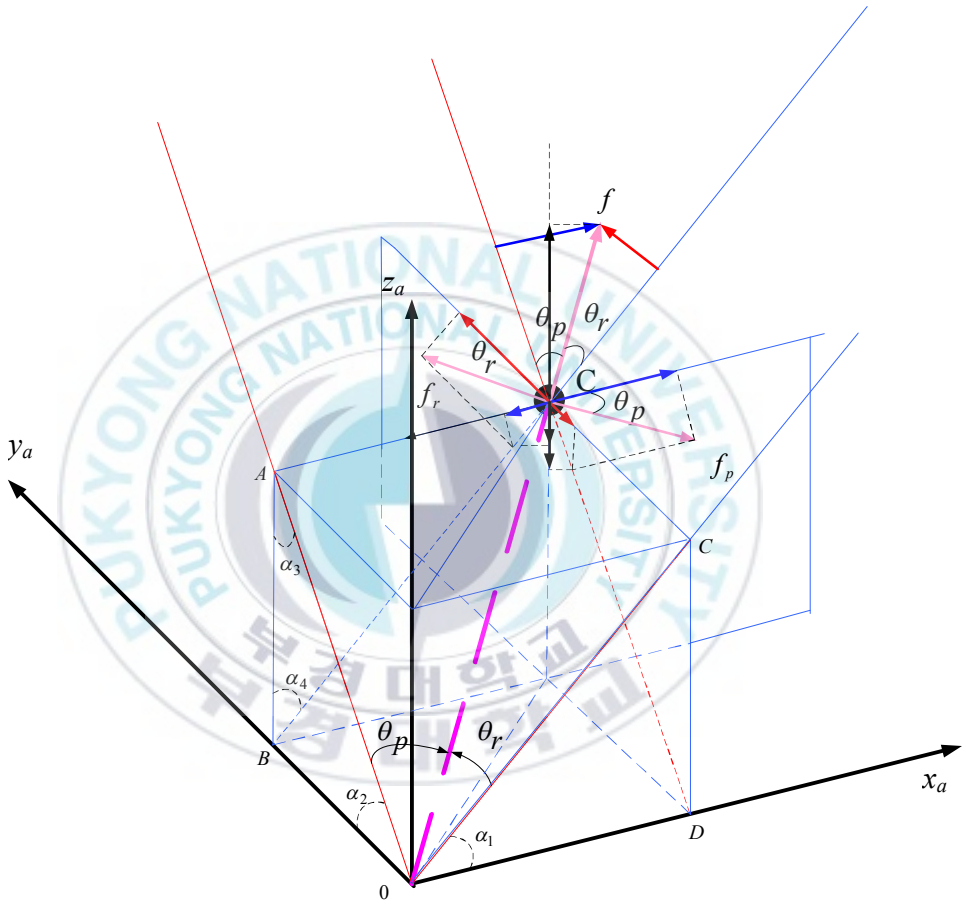

Fig. A.1: 3D Inverted pendulum.

The Lagrangian of the 3D inverted pendulum is given as Eq. (2.28).

$$L = \frac{1}{2} m(\dot{x}_{ca}^2 + \dot{y}_{ca}^2 + \dot{z}_{ca}^2) - mgz_{ca} \tag{2.28}$$

$\boldsymbol{q} = [x_{ca} \quad y_{ca} \quad z_{ca}]^T$ is defined as coordinate vector of the COM.

The Euler – Lagrange equation is given as follows:

$$\frac{d}{dt}\left(\frac{\partial L}{\partial \dot{\boldsymbol{q}}}\right) - \frac{\partial L}{\partial \boldsymbol{q}} = \boldsymbol{f} \tag{A.1}$$

where $\boldsymbol{f} = [f_{x_a} \quad f_{y_a} \quad f_{z_a}]^T$ is force vector.

Partial derivative of Eq. (2.28) is obtained as

$$\frac{\partial L}{\partial \dot{x}_{ca}} = m\dot{x}_{ca} \tag{A.2}$$

$$\frac{\partial L}{\partial \dot{y}_{ca}} = m\dot{y}_{ca} \tag{A.3}$$

$$\frac{\partial L}{\partial \dot{z}_{ca}} = m\dot{z}_{ca} \tag{A.4}$$

$$\frac{\partial L}{\partial x_{ca}} = 0 \tag{A.5}$$

$$\frac{\partial L}{\partial y_{ca}} = 0 \tag{A.6}$$

$$\frac{\partial L}{\partial z_{ca}} = -mg \tag{A.7}$$

The time derivative of Eqs. (A.2)~(A.4) are as follows:

$$\frac{d}{dt}\left(\frac{\partial L}{\partial \dot{x}_{ca}}\right) = m\ddot{x}_{ca} \tag{A.8}$$

$$\frac{d}{dt}\left(\frac{\partial L}{\partial \dot{y}_{ca}}\right) = m\ddot{y}_{ca} \tag{A.9}$$

$$\frac{d}{dt}\left(\frac{\partial L}{\partial \dot{z}_{ca}}\right) = m\ddot{z}_{ca} \tag{A.10}$$

From Fig. A.1 and Eq. (A.1), the followings can be obtained

$$m\ddot{x}_{ca} = f_{x_a} = -\frac{S_r S_p}{rC_r}\tau_r + \frac{C_p}{r}\tau_p + S_p f \tag{A.11}$$

$$m\ddot{y}_{ca} = f_{y_a} = -\frac{C_r}{r}\tau_r + \frac{S_p S_r}{rC_p}\tau_p - S_r f \tag{A.12}$$

$$m\ddot{z}_{ca} + mg = f_{z_a} = -\frac{S_r D}{rC_r}\tau_r - \frac{S_p D}{rC_p}\tau_p + Df \tag{A.13}$$

Eqs. (A.11)~(A.13) are rewritten in the matrix form as follows:

$$m\begin{bmatrix}\ddot{x}\\ \ddot{y}\\ \ddot{z}\end{bmatrix} = \begin{bmatrix}-S_r S_p / rC_r & C_p / r & S_p\\ -C_r / r & S_r S_p / rC_p & -S_r\\ -S_r D / rC_r & -S_p D / rC_p & D\end{bmatrix}\begin{bmatrix}\tau_r\\ \tau_p\\ f\end{bmatrix} + \begin{bmatrix}0\\ 0\\ -mg\end{bmatrix} \tag{2.29}$$